Conseil national de recherches Canada
Institut de génie des matériaux
Boucherville (Québec)

National Research Council Canada
Industrial Materials Research Institute
Boucherville, Quebec

IGM86D-000-584-G
CNRC 27860

POLYBLENDS 86

Polymer Engineering and Science

Vol. 27 • No. 5 MID-MARCH 1987

POLYMER TOPICS

Polyblends-'86

Contents

313
L.A. UTRACKI/Preamble

315
S. ROSTAMI and D.J. WALSH/The Simulation of Phase Diagrams for Polymer Blends at Various Pressures

324
P.R. COUCHMAN and K.E. VAN NESS/Surface Tension of Polymer Liquids

328
R. FAYT, R. JEROME, and Ph. TEYSSIÉ/Characterization and Control of Interfaces in Emulsified Incompatible Polymer Blends

335
S. WU/Formation of Dispersed Phase in Incompatible Polymer Blends: Interfacial and Rheological Effects

344
J. LYNGAAE-JØRGENSEN and K. SØNDERGAARD/Phase Transitions During Shear Flow of Two-Phase Polymer Blends. I. Theory. Transition to "Homogeneous" Melt State

351
J. LYNGAAE-JØRGENSEN and K. SØNDERGAARD/Phase Transitions During Shear Flow of Two-Phase Polymer Blends. II. Styrene-acrylonitrile/Poly(methylmethacrylate) Transition to "Homogeneous" Melt State

359
B. SCHLUND and L.A. UTRACKI/Linear Low Density Polyethylenes and Their Blends: Part 1. Molecular Characterization

367
L.A. UTRACKI and B. SCHLUND/Linear Low Density Polyethylenes and Their Blends: Part 2. Shear Flow of LLDPE's

380
B. SCHLUND and L.A. UTRACKI/Linear Low Density Polyethylenes and Their Blends: Part 3. Extensional Flow of LLDPE's

Published by Society of Plastics Engineers

Polymer Engineering and Science

Published by Society of Plastics Engineers

EDITOR—ROGER S. PORTER
Polymer Science and Engineering
University of Massachusetts
Amherst, Mass. 01003

GUEST EDITOR—L. A. UTRACKI
National Research Council Canada
Boucherville, Quebec

ASSOCIATE EDITOR—RICHARD E. BALL
Western New England College
Springfield, Mass. 01119

ADVISORY BOARD

K. B. ABBÅS
AB Nobel Plast

E. BAER
Case Institute of Technology

J. A. BIESENBERGER
Stevens Institute of Technology

D. M. BIGG
Battelle Columbus Laboratories

L. L. BLYLER, JR.
Bell Laboratories

L. J. BROUTMAN
Illinois Institute of Technology

E. S. CLARK
University of Tennessee

R. K. EBY
Johns Hopkins University

A. N. GENT
University of Akron

H. B. HOPFENBERG
North Carolina State University

J. F. JOHNSON
University of Connecticut

M. R. KAMAL
McGill University

R. P. KAMBOUR
General Electric Company

J. R. KNOX
Amoco Chemicals Corporation

S. MATSUOKA
Bell Telephone Laboratories

B. MAXWELL
Princeton University

C. L. MCCORMICK
University of Southern Mississippi

D. R. PAUL
University of Texas

D. H. RENEKER
National Bureau of Standards

C. E. ROGERS
Case Western Reserve University

R. SALOVEY
University of Southern California

N. S. SCHNEIDER
Army Materials and Mechanics Research Center

T. L. SMITH
IBM Research Center

M. TAKAYANAGI
Kyushu University

PUBLICATIONS COMMITTEE

E. W. ROWAN, JR., Chairman
Parkway Plastics, Inc.

R. P. BRADDICKS, JR.
Plastics Consultant

A. T. DIBENEDETTO
University of Connecticut

L. H. DREXLER
AT&T Consumer Products

H. FINKEL
Industrial Designer

R. D. FORGER
Society of Plastics Engineers

J. L. HULL
Hull Corporation

W. C. KUHLKE
DeWitt & Co., Inc.

M. A. MENDELSOHN
Westinghouse Electric Corp.

R. S. PORTER
University of Massachusetts

D. W. RILEY
Extrusion Engineers

A. A. SCHOENGOOD
Society of Plastics Engineers

A. E. WHITNEY, JR.
Plastics Consultant

Copyright by Society of Plastics Engineers, 1987. POSTMASTER: Send address changes to POLYMER ENGINEERING AND SCIENCE, 14 Fairfield Dr., Brookfield Center, CT 06805. Telephone (203) 775-0471, TELEX #643-712. Reproduction in whole or in part without written permission is strictly prohibited.

POLYMER ENGINEERING AND SCIENCE (ISSN 0032-3888) is printed at Waverly Press, Easton, MD 21601. Address changes, undeliverable copies, and orders for subscriptions should be sent to Circulation Manager, Society of Plastics Engineers, 14 Fairfield Dr., Brookfield Center, CT 06805. Published semimonthly except for June and December, when published monthly. Second-class postage paid at Brookfield Center, Conn., and additional entry offices. Accepted at special postal rate provided in P.M. Sec. 132.122.

Neither the Society of Plastics Engineers nor POLYMER ENGINEERING AND SCIENCE is responsible for the views expressed by individual contributors, either in articles published in POLYMER ENGINEERING AND SCIENCE or in technical papers presented at meetings of the Society.

Subscription rates for 1987. SPE members, 1 year—$95, 2 years—$175, 3 years—$225. Nonmembers (U.S. and North America), 1 year—$130, 2 years—$225, 3 years—$310. Corporate, Institutional, or Library, 1 year—$340. Postage charge for all subscriptions outside North America—$22 per year. Air delivery outside North America—$65 per year.

SOCIETY OF PLASTICS ENGINEERS
Business and Executive Offices, 14 Fairfield Dr., Brookfield Center, CT 06805

DANIEL J. DOMOFF
Managing Editor

MARIE J. BRUCKENTHAL
Production Manager

PAM ARSENAULT
Copy Editor

MICHAEL R. CAPPELLETTI
Circulation Manager

OFFICERS OF THE SOCIETY

GREG R. THOM
President

JOHN R. KRETZSCHMAR
President-elect

BRUCE A. PETERSEN
First Vice President

VIVIAN E. MALPASS
Second Vice President

JACQUES DE CRAENE
Vice President for International Affairs

LEONARD H. DREXLER
Secretary

KISHOR S. MEHTA
Treasurer

ROBERT D. FORGER
Executive Director and Publisher

POLYMER ENGINEERING AND SCIENCE is indexed by:—Chemical Abstracts—Engineering Index, Inc.

PREAMBLE

"Polyblends-'86" was the 7th annual symposium on polymer alloys and blends organized and sponsored by the Industrial Materials Research Institute of the National Research Council Canada (NRCC/IMRI). The previous six have also been published in *Polymer Engineering and Science*: **22** (2), **22** (17), **24** (2), **24** (17), and **26** (1). The symposium, held in Montreal, Canada, April 4th, 1986, was a part of the 2nd Annual Meeting of the Polymer Processing Society (International). The Institute also organizes two other symposia series on modeling of plastics processing and on polymer composites; these are published respectively in *Polymer Engineering and Science* and in *Polymer Composites*. The entire symposia are recorded and the tapes of the presentations and discussions are kept in the NRCC/IMRI library for a period of two years, available to anyone interested in the subject

"Polyblends-'86" was the largest symposium on polymer blends organized by IMRI. With speakers from nine countries it had a stimulating international character. This is reflected in the content of these special issues.

When organizing the "Polyblends-'86" we tried to encourage presentation of papers on three particularly important aspects of polymer blends: (i) interfacial properties, (ii) flow induced morphology, and (iii) engineering blends.

The effects of the interfacial properties are of increasing interest to researchers and to manufacturers. The existing methods of measurements are cumbersome and limited in scope. Better theories and test procedures are badly needed. Both these aspects have been discussed extensively during the meeting.

The performance of a pair of blended immiscible polymers depends on their chemical nature and blend composition. Within a low concentration region of the minor phase, say below 13 volume percent, only spherical particles are to be expected. The size of the spheres decreases to zero as miscibility is improved. Similar size reduction is observed at higher loading, where co-continuous structures predominate. Addition of a compatibilizer, which in principle does not change the polymer-polymer miscibility but modifies the interfacial properties, also improves dispersion as well as performance of the finished material. In short, the equilibrium morphology depends on the free energy of the system as given by equilibrium thermodynamics.

The equilibrium morphology can be drastically modified by rheological means. At least three different (but related) mechanisms can be identified: (i) mechanical deformation of dispersed phase, e.g., as in an extensional flow field, (ii) shear stress induced variation of the dynamic interfacial tension, and (iii) flow induced change of the free energy of the system which may affect blend miscibility and upon cooling, lead to either dispersed or interconnected morphology.

The possibilities of generation of nonequilibrium morphology can be commercially advantageous. Generation of polyamide fibrils in poly(ethylene terephthalate) matrix is known to improve the tensile and shrink properties of the fibers, even though the polymers are strongly incompatible. Generation of lamellar polyamide morphology in polyolefins has a profound effect on permeability. The reinforcing effect of liquid crystal polymers in thermoplastic polyesters can have major effects in anisotropic applications. Several papers presented at the meeting and published in this symposium issue deal with these problems.

Now, nearly all engineering resins are being modified by blending. A desire for better processability, decrease of cost, and adjustment of properties provide strong motivation for blending. The 1984 world market for engineering alloys, blends, and composites was 1.4Mt (3 billion lbs) or 14

percent of total plastics. With the three times higher growth rate than commodity resins and about three to four times higher price, the engineering blends evolve into a major factor in plastics industry. Several papers in this issue contribute to the knowledge of these important materials.

This issue contains the first of two sets of symposium papers. The second set will appear in *Polym. Eng. Sci.*, Vol. 27, No. 6 (March, 1987). As organizer of "Polyblends-'86," I want to thank all the authors for their excellent contributions and Professor Roger S. Porter, the Editor of this Journal, for his hospitality and help in publishing the proceedings.

L. A. Utracki
Guest Editor

The Simulation of Phase Diagrams for Polymer Blends at Various Pressures

SHAMSEDIN ROSTAMI* *and* DAVID J. WALSH**

Department of Chemical Engineering and Chemical Technology
Imperial College
London SW7, England

A procedure is described for the simultaneous prediction of the binodal and spinodal curves of polymer mixtures at various pressures using a form of the equation-of-state theory of Flory and co-workers. The results of the calculation are compared with experimental results for the effect of pressure on the cloud points of both oligomer mixtures showing upper critical behavior and polymer mixtures showing lower critical behavior. The procedure successfully predicts the sign of the effect and its magnitude within the experimental and theoretical uncertainties for the systems studied.

INTRODUCTION

The equation-of-state theory of Flory and co-workers (1–4) has been widely used in describing the miscibility of polymer or oligomer mixtures. The ability of the theory to predict both upper critical solution temperature (UCST) and lower critical solution temperature (LCST) phase diagrams has been demonstrated by several authors (5–7).

The effect of pressure on the miscibility of polymer-solvent mixtures and oligomer mixtures has been experimentally studied (10–12). We have also studied the effect of pressure on the miscibility of polymer-polymer blends showing LCST behavior (13). These studies have shown:

(a) For mixtures showing UCST behavior with positive heats of mixing, the application of pressure causes the temperature range of miscibility to decrease.

(b) For high molecular mass polymer blends showing LCST behavior, the effect of pressure increases the temperature range of miscibility.

In this paper we deal with the effect of pressure on both oligomer mixtures showing UCST behavior and high polymer mixtures showing LCST behavior. Experimental results were obtained using samples of blends held in a pressure bomb and examined by measurement of turbidity during temperature scans. The apparatus technique, and experimental results are described elsewhere (11, 13).

The theoretical procedure involved obtaining values of the hard core pressure, volume and temperature (P^*, V^*, T^*) of the components from known physical data and a value of the contact interaction parameter, X_{12}, from heat of mixing measurements using oligometric mixtures. The noncombinatorial contact parameter, Q_{12}, was then used as the only adjustable parameter to fit the minimum of the phase diagram to that of the experimental cloud point curve at atmospheric pressure. This value was then used to calculate the spinodal and binodal curves over the whole range of composition and pressure. The procedure used to calculate the binodal and spinodal curves has been described elsewhere (6–9, 13) and will only be described briefly here. It should be pointed out that the assumption that both X_{12} and Q_{12} are independent of both temperature and pressure can only be approximate. Both temperature and pressure may affect the values of X_{12}. To minimize the effect of temperature on X_{12}, the heats of mixing are performed at temperatures close to the phase boundaries. Its pressure dependence, however, cannot be eliminated at the present. Pressure may also cause configurational changes in molecules, an effect that has been found to be greatest for shorter chain lengths (14).

THEORY

To obtain the effect of pressure on the phase diagram of mixtures, the hard core properties of the pure components, T^*, P^*, and V^* were computed from the thermal expansion coefficient, α, thermal pressure coefficient, γ, and density, d, of the corresponding material using

* Present address: ICI PLC, Research and Technology Department, Wilton, UK
** Present address: E.I. Du Pont, Central Research & Development, Wilmington, Delaware, USA, 19898

Eqs 1 to 4. The notation is given in the Symbols List.

$$\tilde{v}_i = \left[1 + \frac{\alpha_i T}{3 + 3\,\alpha_i T}\right]^3, \qquad V_i^* = \frac{M_i}{d_i \tilde{v}_i} \tag{1}$$

$$P_i^* = \gamma_i T \tilde{v}_i^2 \tag{2}$$

$$T_i^* = \frac{T \tilde{v}_i^{3/4}}{\tilde{v}_i^{4/3} - 1} \tag{3}$$

The hard core characteristic pressure, P^*, and temperature, T^*, of the mixture are given by:

$$P^* = \phi_1 P_1^* + \phi_2 P_2^* - \phi_1 \theta_2 X_{12} \tag{4}$$

$$T^* = P^* [\phi_1 P_1^*/T_1^* + \phi_2 P_2^*/T_2^*]^{-1} \tag{5}$$

and $\tilde{v}$ for the mixture can be obtained from:

$$\tilde{v}^{1/3} = [1 - \tilde{T}\tilde{v}/(1 + \tilde{P}\tilde{v}^2)]^{-1} \tag{6}$$

In *Eq 4* the value of the contact energy interaction parameter, X_{12}, can be obtained in a number of ways (19). Values for the mixtures used in this paper were obtained from the heat of mixing measurement of low molecular mass analog materials, as described elsewhere (7, 20).

Knowing these quantities for the pure components and their blends at atmospheric pressures, the phase diagrams of mixtures can be simulated as follows.

By definition, at the binodal curve the two coexistent phases A and B are at chemical equilibrium where,

$$(\Delta\mu_i)_A = (\Delta\mu_i)_B : \qquad i = 1, 2 \tag{7}$$

where $\Delta\mu_i = \Delta\mu_i$ (combinatorial) + $\Delta\mu_i$ (residual). In a system with LCST behavior, as the temperature increases the mixture becomes more unstable; whereas in systems with UCST behavior, as temperature decreases the mixture becomes more unstable. The limit of this metastability is called the spinodal and is given by:

$$\frac{\partial^2 \Delta G_M}{\partial \phi_2^2} = \frac{\partial \Delta\mu_i}{\partial \phi_i} = 0 \tag{8}$$

where ΔG_M is Gibbes free energy change on mixing given by

$$\Delta G_M = \Delta H_M - T[\Delta S_M^{\text{Residual}} + \Delta S_M^{\text{Comb}}) \tag{9}$$

Using the combinatorial entropy of mixing given by the classical Flory-Huggins theory and the residual quantities from the equation-of-state theory of Flory and co-workers (1–4), ΔG_M is given by

$$\begin{aligned}\Delta G_M = {} & \tilde{r} n v^* [\phi_1 P_1^*/\tilde{v}_1 + \phi_2 P_2^*/\tilde{v}_2 - P^*/\tilde{v}] \\ & + \tilde{r} n v^* [\phi_1 P_1^* \tilde{T}_1 \ln \frac{\tilde{v}_1^{1/3} - 1}{\tilde{v}^{1/3} - 1} \\ & + \phi_2 P_2^* \tilde{T}_2 \ln \frac{\tilde{v}_2^{1/3} - 1}{\tilde{v}^{1/3} - 1} - \phi_1 \theta_2 T Q_{12}] \\ & + RT[n_1 \ln\phi_1 + n_2 \ln\phi_2]\end{aligned} \tag{10}$$

The chemical potential of component one in the mixture relative to pure component is defined as:

$$\begin{aligned}\mu_1 - \mu_1^0 = {} & \left(\frac{\partial \Delta G_M}{\partial N_1}\right)_{T,V_1,N_2} \\ & + \left(\frac{\partial \Delta G_M}{\partial \tilde{v}}\right)_{T,N_1,N_2} \left(\frac{\partial \tilde{v}}{\partial N_1}\right)_{T,V_1,N_2} \\ = {} & RT[\ln\phi_1 + (1 - r_1/r_2)\phi_2] \\ & + P_1^* V_1^* \left\{3\tilde{T}_1 \ln \frac{\tilde{v}_1^{1/3} - 1}{\tilde{v}^{1/3} - 1} + \tilde{v}_1^{-1}\right. \\ & \left. - \tilde{v}^{-1} + \tilde{P}_1(\tilde{v} - \tilde{v}_1)\right\} \\ & + \frac{V_1^* \theta_2^2}{\tilde{v}} (X_{12} - T\tilde{v} Q_{12})\end{aligned} \tag{11}$$

and similarly, that for component two in the mixture is:

$$\begin{aligned}\mu_2 - \mu_2^0 = {} & RT[\ln \phi_2 + (1 - r_2/r_1)\phi_1] \\ & + P_2^* V_2^* \left\{3\tilde{T}_2 \ln \frac{\tilde{v}_2^{1/3} - 1}{\tilde{v}^{1/3} - 1} + \tilde{v}_2^{-1}\right. \\ & \left. - \tilde{v}^{-1} + \tilde{P}_2(\tilde{v} - \tilde{v}_2)\right\} \\ & + \frac{V_2^* \phi_2^2}{\tilde{v}} \cdot \frac{S_2}{S_1} (X_{12} - T\tilde{v} Q_{12})\end{aligned} \tag{12}$$

Equations 11 and *12* and the binodal condition can be used to compute the position of the binodal curve. To simulate the binodal curve we used a search procedure whereby positions of equal chemical potential of component one were found and then the minimum differences between the chemical potentials of component two over these compositions were found.

The spinodal curve can be simulated directly by differentiating either *Eqs 11* or *12* as we have shown elsewhere (7–9) or can alternatively be found from the maxima and minima of $\Delta\mu_i$ while carrying out the search procedure for the binodal. The two procedures give identical results.

A similar treatment for the simulation of the binodal and spinodal was applied at elevated pressures by using constant values of T^*, P^*, and V^* and neglecting the effect of pressure on X_{12} and Q_{12} as explained earlier.

RESULTS AND DISCUSSION

Mixtures of Oligomeric Polystyrene and Polybutadiene

The molecular mass, molecular mass distributions, and state parameters of the two polybutadiene and three polystyrene oligomers used in this work are given in *Table 1*. The density and thermal expansion coefficients of polybutadiene were obtained from Ref. 11. Those of polystyrene were calculated using equations obtained from the literature (15). The thermal

Table 1. The Specifications of the Oligomeric Materials and their State Parameters.

Notation	Oligomer	$\overline{Mn}$	$\overline{Mw}/\overline{Mn}$	d^* (g·cm^{-3})	$\alpha x10^4$ (deg^{-1})	γ (Jcm^{-3}K^{-1})
PEGM600	Poly(ethylene glycol) methoxylated	600	1.10	1.0718	7.8	1.08
PPGM400	Poly(propylene glycol) methoxylated	400	1.15	0.95694	8.7	0.85
PPGM1000	"	1000	1.07	0.97752	8.5	0.93
PPGM1500	"	1500	1.08	0.98522	8.3	0.93
PPGM2000	"	2000	1.10	0.98814	8.2	0.95
PBD920	Polybutadiene	920	1.20	0.833	7.0	1.0
PBD2350	"	2350	1.10	0.850	7.0	1.0
PS1200	Polystyrene	1200	1.12	1.0277	6.3	1.1
PS1520	"	1520	1.10	1.046	6.2	1.1
PS3900	"	3900	1.12	1.020	5.8	1.1

* Data for PBD and PS are given at 25°C and those for PEGM and PPGM at 30°C.

pressure coefficients were estimated from their solubility parameter values obtained by the group contribution method (16).

From a combination of these materials, five quasi-binary mixtures were studied. The binary state parameters of these are given in *Table 2*. The values of the contact interaction parameter, X_{12}, were obtained by fitting the experimental heat of mixing data to *Eq 4* with:

$$\Delta H_M = \tilde{r}nv^*\left[\phi_1 P_1^*/\tilde{v}_1 + \phi_2 P_2^*/\tilde{v}_2 - P^*/\tilde{v}\right] \quad (13)$$

The values of the contact entropy parameter, Q_{12}, were adjusted to fit the minima of the phase diagrams to those of the corresponding cloud point curves at atmospheric pressure. The surface area per unit volume ratios were calculated using Bondi's group contribution data (17).

The resulting simulated phase diagrams are shown in *Figs. 1* to *5* along with the experimental cloud point measurements described elsewhere (11). Only results at atmospheric pressure and at 1,000 atmospheres are presented but intermediate results show a comparable fit.

No results are available for the highest molecular weight polystyrene with the highest molecular weight polybutadiene as this was not measured due to problems associated with the high viscosities.

The theoretical and experimental values of dT/dP (the change in temperature of the cloud point per unit change in pressure) for the mixtures are presented in *Table 3*. The quoted values correspond to the maximum of the simulated phase diagrams and that of the cloud point curves respectively. Theoretical values of dT/dP are generally lower, being of the order of 70 percent of the experimental values. This could be due in part to experimental errors in measuring the cloud points or to uncertainties in the various state parameters used.

The shapes of the simulated phase diagrams are not identical to those of the measured cloud point curves, but the fit is quite good considering the approximations used. The fit could be improved by the adjustment of the various state parameters as has been described elsewhere (18), but there is little justification for this as the fit is already satisfactory.

A comparison of the data in *Table 2* shows

Table 2. The Binary State Parameters of Oligomeric Mixtures.

No	Mixture	X_{12}* (Jcm^{-3})	Q_{12} (Jcm^{-3}K^{-1})	S_2/S_1
1	PBD920-PS1200	7.0	0.0047	0.9
2	PBD920-PS1520	7.0	0.0063	0.9
3	PBD920-PS3900	7.0	0.0069	0.9
4	PBD2350-PS1200	7.0	0.0062	0.9
5	PBD2350-PS1520	7.0	0.0056	0.9
6	PEGM600-PPGM400	13.17	0	1.05
7	PEGM600-PPGM1000	13.17	0.0119	1.06
8	PEGM600-PPGM1500	11.65	0.0119	1.075
9	PEGM600-PPGM2000	10.64	0.0113	1.082

* The X_{12} values of PBD-PS mixtures are given at 70°C and those of PEGM-PPGM mixtures at 30°C.

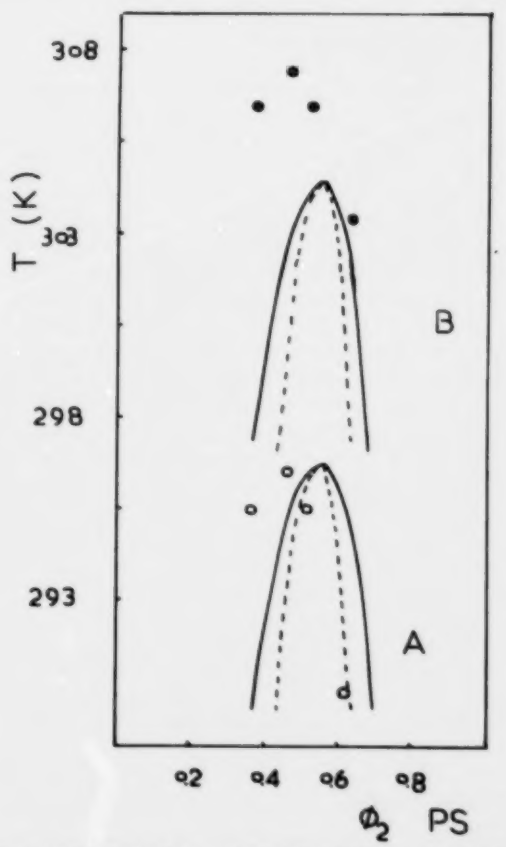

Fig. 1. The simulated (——) binodals and (– – –) spinodals of mixtures of PBD920-PS1200 at A.1 and B.1000 atmospheres. The corresponding experimental cloud point data (11) at (○) 1 and (●) 1000 atmospheres are also shown for comparison.

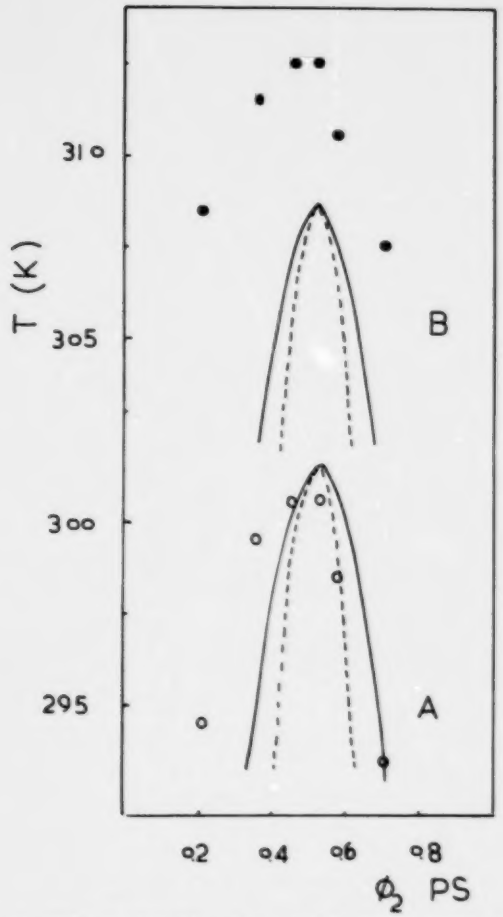

Fig. 2. The simulated (——) binodals and (– – –) spinodals of mixtures of PBD920-PS1500 at A. 1 and B. 1000 atmospheres. The corresponding experimental cloud point data (11) at (○) 1 and (●) 1000 atmospheres are also presented.

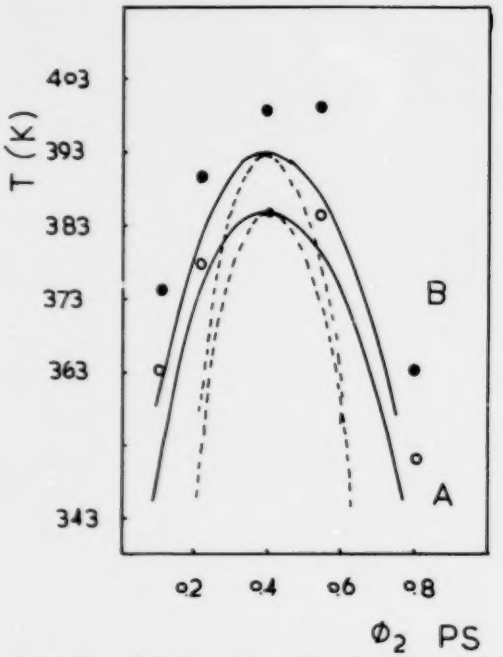

Fig. 3. The simulated (——) binodals and (– – –) spinodals of mixtures of PBD920-PS3900 at A. 1 and B. 1000 atmospheres for the data of Tables 1 and 2. The cloud point data (11) at (○) 1 and (●) 1000 atmospheres are also shown.

that for a constant value of X_{12}, as the molecular mass of the polymers increases the values of Q_{12} required to fit the simulation to the cloud point curve increase. This could be a result of errors in the various parameters such as the molecular masses of the polymers, or to a molecular mass dependence of X_{12}. It could also be a real effect due to differences in ordering of the pure components and the mixtures at various molecular masses as has been found in mixtures of other substances (19).

One can generally conclude that for these mixtures the theory gives a good representation of both the phase behavior at atmospheric pressure and of the effect of pressure.

Mixtures of Oligomeric, Methoxylated Poly(ethylene oxide) and Poly(propylene oxide)

The pure component and binary state parameters of the poly(ethylene oxide), four different molecular mass samples of poly(propylene oxide), and the four mixtures derived from them are given in *Tables 1* and *2*. Due to the large chemical difference of the end groups from the main chain, it was necessary to calculate values of the thermal pressure coefficients, γ, the contact interaction energies, X_{12}, and the surface area per unit volume ratios, S_2/S_1 individually. The resulting simulated phase diagrams at 1 and 1000 atmospheres are shown in *Figs. 6* to *9* along with the experimental cloud point data.

The values of dT/dP are again presented in *Table 3*. It can be seen that the theoretical and experimental values of this quantity agree quite well. The shapes of the phase diagrams are, however, badly mismatched both at low and at high pressure. It should be noted that a measurement of the effect of pressure on the phase diagram is a very selective probe. The effect is predominantly due to the volume change on mixing and the equation-of-state terms in the free energy equation associated with this change. The fact that the theory satisfactorily predicts the value of dT/dP suggests that the theory does estimate the effect of the free volume changes correctly. The fact that the theory does not correctly predict the shape of the curve at any pressure suggests a composition, molecular mass, or system dependence of the interaction terms due to specific effects. The values of Q_{12} used in these simulations are approximately the same except in the case of the blend involving the lowest molecular mass poly(propylene oxide). This could be due to an error in the molecular mass of this oligomer. The

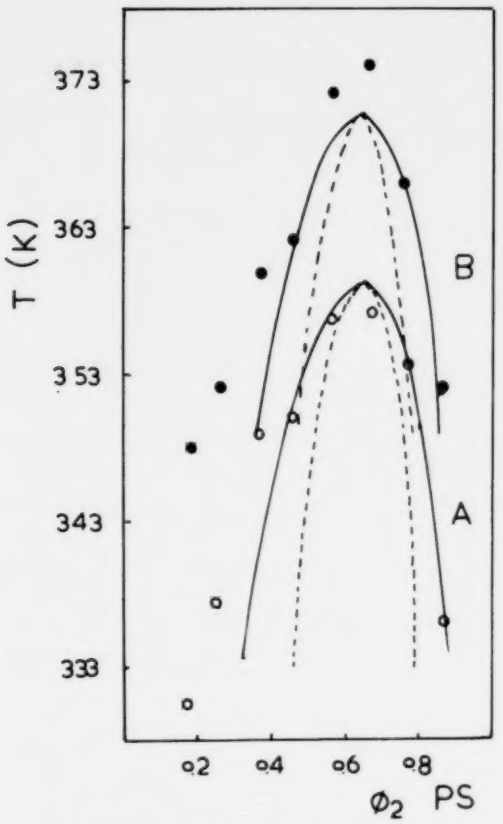

Fig. 4. Theoretically simulated (——) binodals and (– – –) spinodals of mixtures of PBD2350-PS1200 at A.1 and B.1000 atmospheres. The cloud point data (11) of the mixtures at (○) 1 and (●) 1000 atmospheres are also shown.

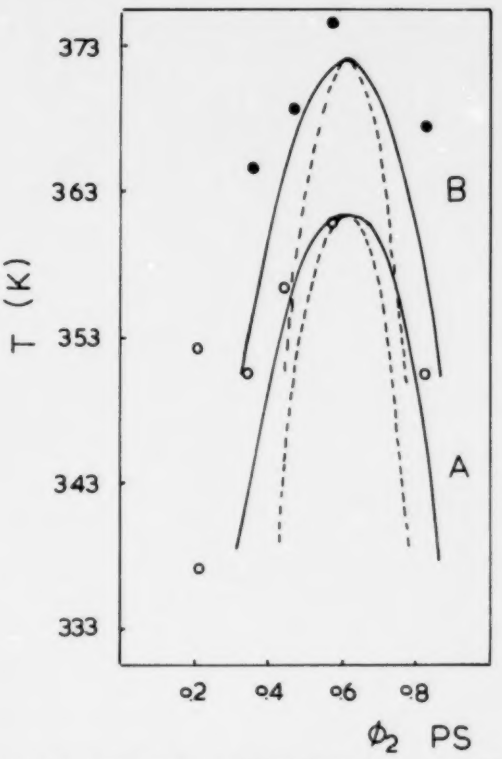

Fig. 5. The simulated (——) binodals and (– – –) spinodals of mixtures of PBD2350-PS1520 at A.1 and B.1000 atmospheres. The cloud point data (11) at (○) 1 and (●) 1000 atmospheres are also shown.

higher molecular masses of poly(propylene oxide) have an improved general agreement between the theoretical predictions and experimental findings. The movement of the theoretical phase diagrams to the left with increased molecular weight can easily be explained in simple Flory-Huggins terms (21).

The phase diagrams of these mixtures at atmospheric pressure have previously been reported by others elsewhere (20). The slightly different values of the parameters used in our simulation were due to the fact that we used the weight average molecular masses instead of the number averages.

Mixtures of High Molecular Mass Polymers

The effect of pressure on the theoretical spinodal curve, of high polymer mixtures, calculated from the spinodal equation, has already been described in a previous publication (13). In this paper we merely add to this a simulation of the binodal curves and use the results for comparison with the oligomer mixtures discussed in the previous sections.

The pure component and binary state parameters of the polymers are given in *Tables* 4 and 5, the justification for and the procedure used in obtaining these values has been described previously (6–9, 13).

Table 3. Theoretical and Experimental Values of $dT/dP \times 10^3$ for Oligomeric Mixtures.

No	Mixture	$dT/dP \times 10^3$ (deg·atm^{-1}) Theory	Experiment
1	PBD920-PS1200	7.7	11.0
2	PBD920-PS1520	7.0	12.0
3	PBD920-PS3900	8.0	15.1
4	PBD2350-PS1200	11.0	15.0
5	PBD2350-PS1520	10.0	13.0
6	PEGM600-PPGM400	10.0	9.0*
7	PEGM600-PPGM1000	10.4	11.0
8	PEGM600-PPGM1500	10.8	9.0
9	PEGM600-PPGM2000	10.0	8.0

* Taken at the same composition as the simulation since it is difficult to decide where the maximum occurs.

The simulated spinodal and the binodal curves for mixtures of ethylene vinyl acetate copolymer (45 weight percent acetate content, EVA45) and chlorinated polyethylene (53 weight percent Cl content, CPE3) at various pressures are shown in *Fig. 10*. Similar results for mixtures of EVA45 and chlorinated polyethylene (43 weight percent Cl content, H48) at the given pressures are shown in *Fig. 11*. The simulated phase diagrams of polyether sulphone

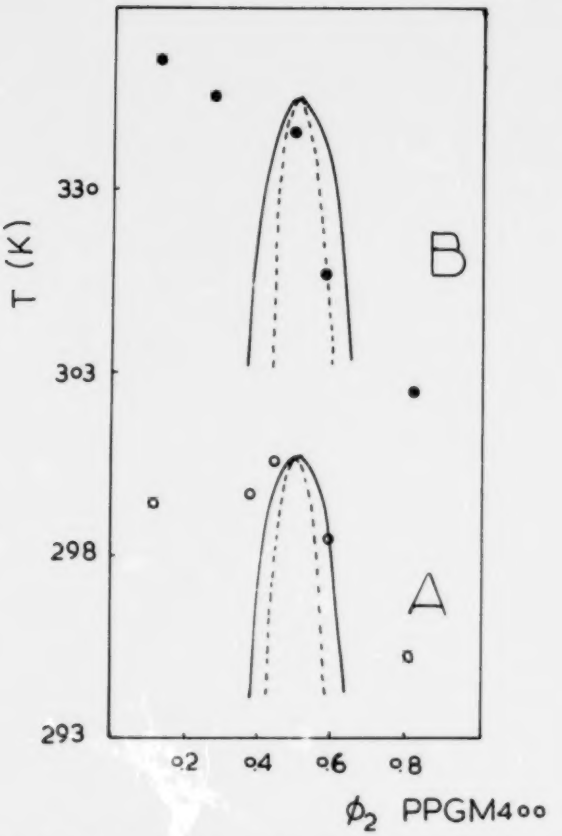

Fig. 6. The simulated (——) binodals and (– – –) spinodals of mixtures of PEGM600-PPGM400 at A.1 and B.1000 atmospheres. The experimental cloud point data (11) at (○) 1 and (●) 1000 atmospheres are also shown.

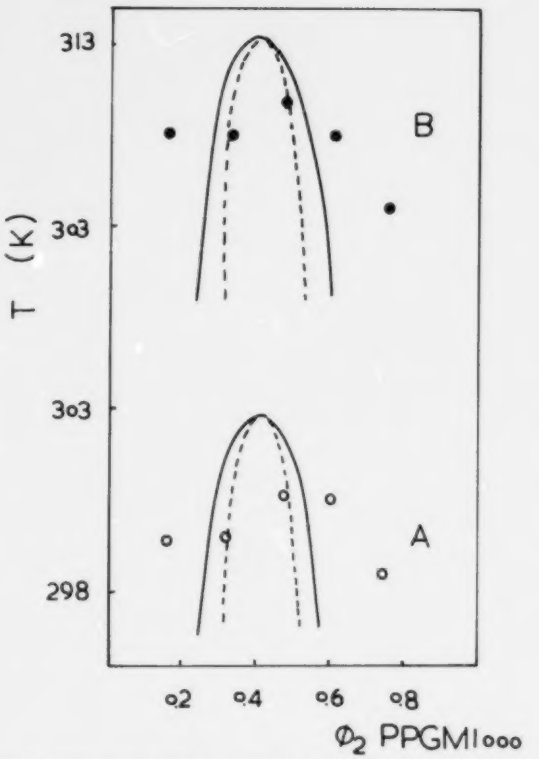

Fig. 7. The simulated (——) binodals and (– – –) spinodals of mixtures of PEGM600-PPGM1000 at A.1 and B.1000 atmospheres. The corresponding experimental cloud point data (11) at (○) 1 and (●) 1000 atmospheres are also shown.

(PES) with poly(ethylene oxide) (PEO) at several pressures are shown in *Fig. 12*. The experimental cloud point data of these mixtures are also presented for comparison. The experimental error on the cloud point measurements is ±1°C.

As shown in these figures, the shape of the phase diagrams do not change with increasing pressure. The flatness of the curves is mainly due to the large values of X_{12}, which were obtained from heats of mixing measurements using analog materials.

Applications of pressure on blends of these mixtures has increased the miscibility, giving positive values of dT/dP as shown in *Table 5*. The calculated values of the volume change on mixing of these mixtures using the values of dT/dP are given elsewhere (13). When comparing these results with those of oligomer mixtures, one should bear in mind that in the latter the cloud point curve probably corresponds fairly closely to the binodal curve, whereas for the high polymer mixtures it may correspond more closely to the spinodal. A large proportion of the phase diagrams in the high polymers mixtures are inaccessible due to instrumental limitations making it difficult to explore the shape of these curves especially at higher pressures. Therefore, only conclusions concerning the movement with pressure close to the minimum of the cloud point curves can be made.

The contact entropy parameter, Q_{12}, is the only adjustable parameter used in all these simulations. It is found to be negative for mixtures of high polymers with negative heats of mixing and positive for oligomer mixtures with positive heats of mixing. It is apparent that the equation-of-state theory is successful in predicting the sign and magnitude of the pressure effect for high polymer as well as oligomer mixtures.

CONCLUSION

The equation-of-state theory of Flory and coworkers has been satisfactorily used to simulate the binodal and spinodal curves of oligomer-oligomer and polymer-polymer mixtures at various pressures. The application of pressure on mixtures with negative heats of mixing is predicted to increase the miscibility, whereas it is predicted to decrease the miscibility of mixtures with positive heats of mixing. This is in accord with experimental findings.

SYMBOLS LIST

d = density (g cm^{-3}).
ΔG_M = free energy of mixing (J cm^{-3}).

ΔH = enthalpy of mixing (J cm^{-3}).
P = pressure (J cm^{-3}); 1 atm = 0.101325 J cm^{-3}.
$\tilde{P}_i$ = reduced pressure of species i (dimensionless).
P_i^* = hard core pressure of species i (J cm^{-3}).
$\tilde{P}$ = reduced pressure of mixture (dimensionless).
P^* = hard core pressure of mixture (J cm^{-3}).
Q_{12} = contact entropy parameter (J cm^{-3} K^{-1}).
rN = average number of segments in the mixture.
R = gas constant (J cm^{-3} K^{-1}).
r_i = chain length of molecule i.
S_i = number of contact sites per segment in species i.
ΔS_M = entropy of mixing (J cm^{-3}).
T = temperature (K).
$\tilde{T}_i$ = reduced temperature of species i (dimensionless).
T_i^* = hard core temperature of species i (K).
$\tilde{T}$ = reduced temperature of mixture (dimensionless).
T^* = hard core temperature of mixture (K).
V_i^* = molar hard core volume of component i (cm^3 mol^{-1}).

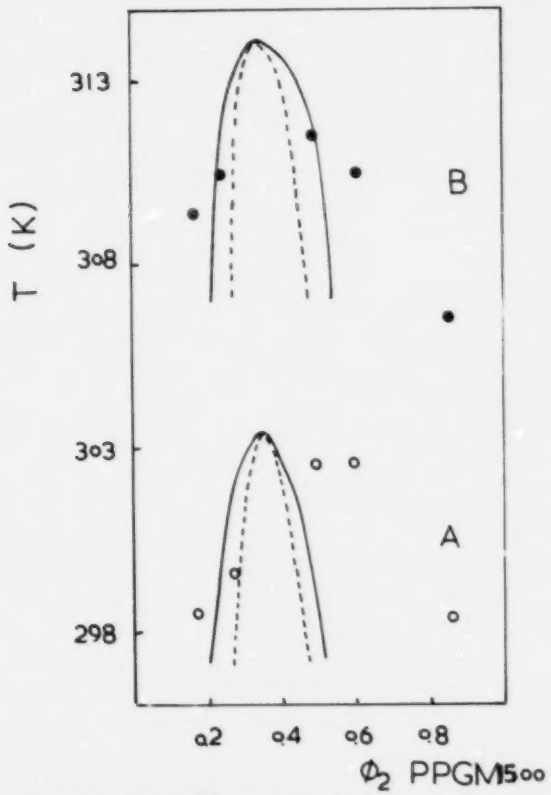

Fig. 8. The simulated (——) binodals and (– – –) spinodals of mixtures of PEGM600-PPGM1500 at A.1 and B.1000 atmospheres. The cloud point data (11) at (○) 1 and (●) 1000 atmospheres are also shown.

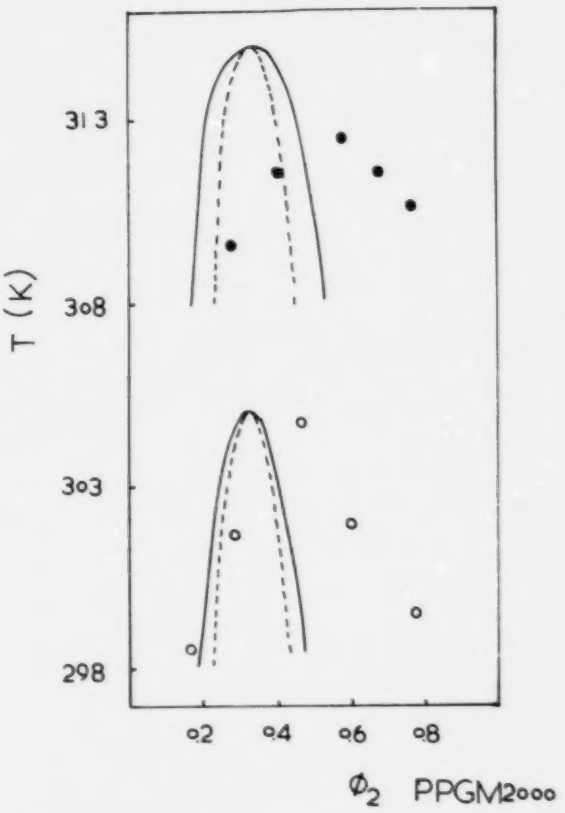

Fig. 9. The simulated (——) binodals and (– – –) spinodals of mixtures of PEGM600-PPGM2000 at A.1 and B.1000 atmospheres. The cloud point data (11) at (○) 1 and (●) 1000 atmospheres are also shown.

Table 4. State Parameters for the Pure Polymeric Materials.

Material	$\alpha \times 10^4$ (K^{-1})	γ(Jcm^{-3}K^{-1})	v_{sp}(cm^{3}g^{-1})	$\bar{M}_w \times 10^{5*}$ (gmol^{-1})
EVA45	4.5103	0.8045	1.0636	2.56
H48	4.4199	0.9544	0.81506	1.82
CPE3	3.6546	0.9592	0.8089	1.2
PES	2.0	1.5	0.7934	0.2
PEO	5.5	1.2	0.9183	0.2

* Relative to polystyrene by GPC.

Table 5. The Binary Parameters of Polymeric Mixtures.

No	Mixture	X_{12}(Jcm^{-3})	Q_{12}(Jcm^{-3}K^{-1})	S_2/S_1	dT/dP(K atm^{-1}) Theoretical	dT/dP(K atm^{-1}) Experimental
1	EVA45-CPE	−3.2	−0.00626	1.03	0.022	0.020
2	EVA45-H48	−2.63	−0.00676	0.98	0.010	0.014
3	PES-PEO	−40.0	−0.0482	1.2	0.044	0.046

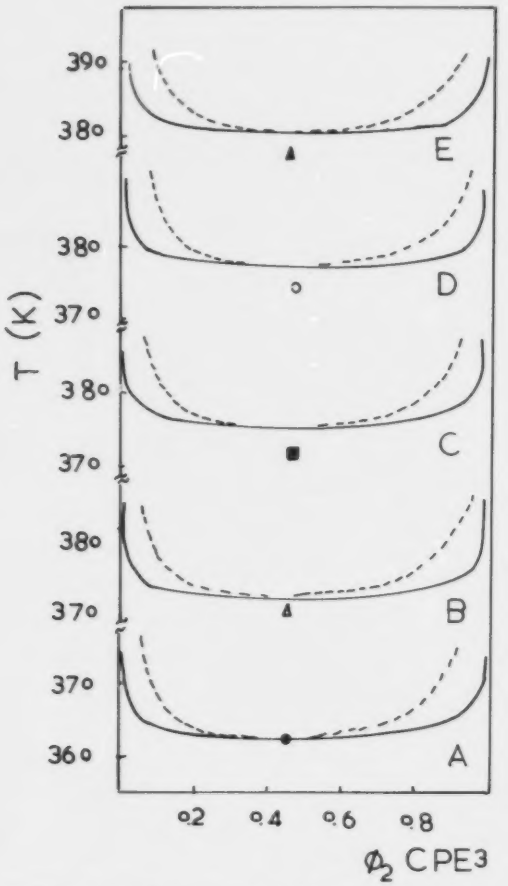

Fig. 10. The simulated (——) binodals and (– – –) spinodals of mixtures of EVA45-CPE3. The experimental cloud point data at the corresponding pressures are:

A 1 atm ; (●)
B 300 atm ; ( )
C 450 atm ; (■)
D 550 atm ; (○)
E 750 atm ; (▲)

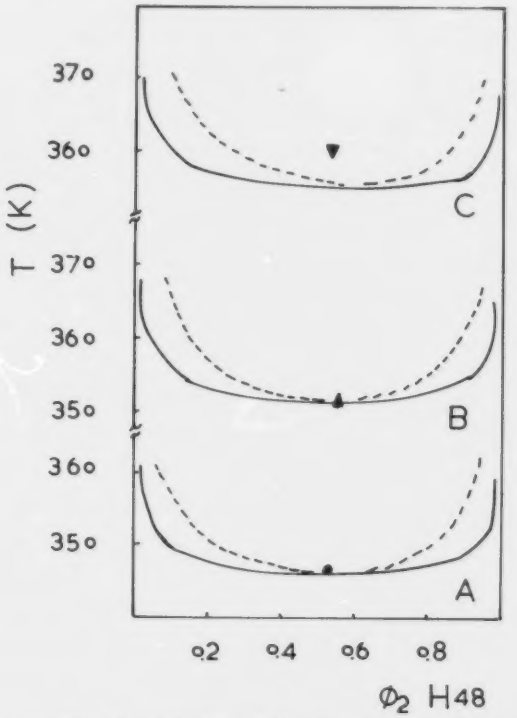

Fig. 11. The simulated (——) binodals and (– – –) spinodals and measured cloud point data of mixtures of EVA45-H48. The experimental cloud point data at the corresponding pressures are:

A 1 atm ; (●)
B 300 atm ; (▲)
C 858 atm ; (▼)

v_{sp} = specific volume of component i ($cm^3\ g^{-1}$).
$\tilde{v}_i$ = reduced volume of component i (dimensionless).
v_i^* = hard core volume of component i (cm^3).
$\tilde{v}$ = reduced volume of mixture (dimensionless).
v^* = hard core volume of mixture (cm^3).
X_{12} = contact interaction parameter ($J\ cm^{-3}$).
α = thermal expansion coefficient (K^{-1}).
γ = thermal pressure coefficient ($J\ cm^{-3}\ K^{-1}$).
ϕ_i = segment fraction of species i (dimensionless).

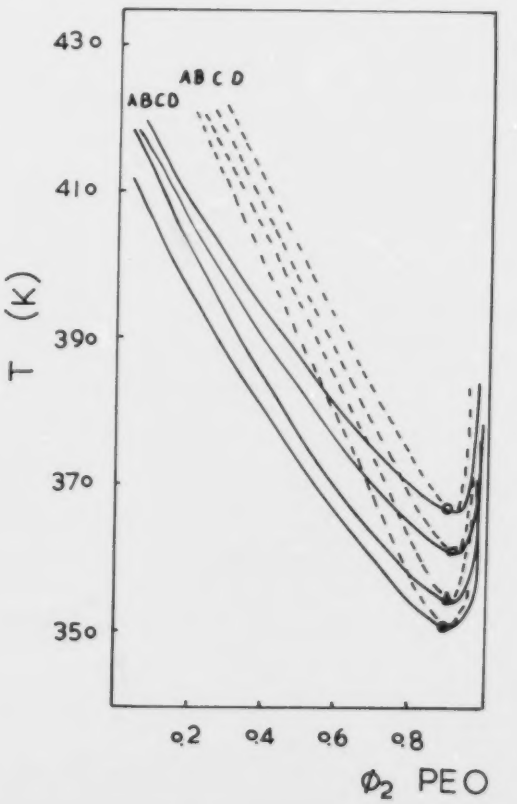

Fig. 12. Measured cloud points and simulated (——) binodals and (– – –) spinodals and measured cloud points for mixtures of PES/PEO at:

A 1 atm ; (●)
B 108 atm ; (▲)
C 221 atm ; (□)
D 348 atm ; (○)

θ_i = site fraction of species i (dimensionless).
$\Delta\mu_i$ = chemical potential of component i (J cm^{-3}).

NOMENCLATURE

PEGM = poly(ethylene glycol methoxylated).
PPGM = poly(propylene glycol methoxylated).
PBD = poly(butadiene).
PS = poly(styrene).
EVA = ethylene vinyl acetate copolymer.
CPE = chlorinated poly(ethylene).
H48 = chlorinated poly(ethylene).
PES = polyethersulphone.
PEO = poly(ethylene oxide).

ACKNOWLEDGMENTS

We would like to thank Sir Geoffrey Allen for useful discussion and to acknowledge the work of the late J. B. P. Tripathi whose unpublished results, obtained while working with Sir Geoffrey Allen, form the basis of this work.

REFERENCES

1. P. J. Flory, *J. Am. Chem. Soc.*, **87**, 1833 (1965).
2. A. Abe and P. J. Flory, *J. Am. Chem. Soc.*, **88**, 2887 (1966).
3. P. J. Flory, R. A. Orwell, and A. Vrij, *J. Am. Chem. Soc.*, **86**, 3567 (1964).
4. B. E. Eichenger and P. J. Flory, *Trans. Faraday Soc.*, **65**, 2035 (1968).
5. L. McMaster, *Macromolecules*, **6**, 760 (1973).
6. Z. Chai, S. Ruona, D. J. Walsh, and J. S. Higgins, *Polymer*, **24**, 263 (1983).
7. S. Rostami and D. J. Walsh, *Macromolecules*, **17**, 315 (1984).
8. D. J. Walsh, S. Rostami, and V. B. Singh, *Makromol. Chem.*, **186**, 158 (1985).
9. D. J. Walsh and S. Rostami, *Polymer*, **26**, 418 (1985).
10. S. Saeki, N. Kuwahara, S. Konno, and M. Kaneko, *Polymer*, **16**, 388 (1983).
11. J. B. P. Tripathi, Ph.D. Thesis, Imperial College (1979).
12. A. B. Wolf and G. Blaum, *J. Polym. Sci. Polym. Symp.*, **61**, 25 (1977).
13. D. J. Walsh and S. Rostami, *Macromolecules*, **18**, 216 (1985).
14. P. E. Schoen, R. G. Priest, J. P. Sheridan, and J. M. Schmur, *J. Chem. Phys.*, **71**, 317 (1979).
15. M. J. Richardson and N. G. Saville, *Polymer*, **18**, 3 (1977).
16. K. L. Hoy, *J. Paint Technol.*, **42**, 76 (1970).
17. A. Bondi, *J. Phys. Chem.*, **68**, 441 (1964).
18. D. J. Walsh and S. Rostami, *Adv. Polym. Sci.*, Vol 70 (1985).
19. P. Trancrede, D. Patterson, and P. Botharel, *J. Chem. Soc. Faraday Trans. II*, **73**, 29 (1977).
20. G. Allen, Z. Chai, C. L. Chong, J. S. Higgins, and J. B. P. Tripathi, *Polymer*, **25**, 239 (1984).
21. P. J. Flory, "Principles of Polymer Chemistry", Cornell University Press (1953).

DISCUSSION

L. A. Utracki: The agreement you showed between the experimental and computed phase transition curves are very impressive; there are rep. ts in the literature of very large effects (over 100°C) due to relatively small changes in the molecular weight or molecular weight disbribution. However, could you clarify for me how the theoretical curves were calculated. In the equation of state you have three parameters: X_{12}, Q_{12}, and S_2/S_1. How were these parameters determined? Was the equation fitted to the experimental data at ambient pressure and then the binodals computed at different pressures, or did you determine these three parameters independently and calculated the phase diagrams at all pressures?

S. Rostami: X_{12} is related to the heat of mixing, and usually measured for low molecular weight materials in a micro-calorimeter. It is, however, difficult to evaluate X_{12} for polymeric materials in this way. Instead, the heat of mixing of oligomeric analogs is measured as before and X_{12} calculated on this basis is assumed to be equivalent of that of high molecular weight materials. This is not a bad approximation. Q_{12} is a correction factor introduced to compensate for the overestimation by Flory's theory of the entropic effects on miscibility. It is used here as an adjustable parameter but can be estimated in number of ways. In my case, I calculated it by fitting the minimum of binodal or spinodal to that of the cloud-point data at ambient pressure. Subsequently, Q_{12} was assumed to be constant for other pressures and all concentrations. As to S_2/S_1, this parameter was calculated from the group theory using the data published by Bondi.

Surface Tension of Polymer Liquids

P. R. COUCHMAN *and* K. E. VAN NESS*

Department of Mechanics and Materials Science
College of Engineering
Rutgers University
Piscataway, New Jersey 08855-0909

A cell theory for the prediction of the surface tension of simple liquids is adapted to polymer liquids. The combinatory, free volume and potential energy zero terms of the partition function are all modified to account for the preservation of connectivity when a surface is created. Theory and experiment are in good agreement without an adjustable surface parameter.

INTRODUCTION

A cell theory relation for the calculation of the surface tension, σ, of simple liquids is adapted to the calculation of σ for polymer liquids. The theory for simple liquids is itself a modified, predictive version (1) of the theory of Prigogine and Saraga (2, 3).

Some general aspects of cell theory for simple liquids are first touched on, then the formal result on which the present theory is based is stated, and the various terms of which it is constituted are described. The nature of the specific changes in the terms of this surface tension relation when it is used for polymers are indicated and their explicit forms are given. Finally, theory and experiment are compared for two polymers.

THEORY

In order to form a relation for the surface tension of simple liquids, we determine the excess configurational partition function for a system with a surface. According to cell theory, each molecule is confined to a cell and the mean potential energy of interaction with the surrounding neighbors is calculated as a function of the distance r of this prisoner from the center of the cell to which it is confined. In this work we evaluate part of the partition function in the convenient square well approximation on the mean field, for which the energy of interaction between a reference molecule at any accessible position r and all other molecules is identically the potential energy when the reference prisoner is at rest at the cell center. The excess configurational partition function can be written as the product of three kinds of contributions: combinatorial terms, potential energy zero terms, and terms of the mean energy of interaction for a prisoner as it moves about the cell with reference to the cell center. This last contribution is in the square well approximation the cell free volume. The potential energy zero term is calculated on the basis of a Lennard-Jones 6-12 potential between molecules at their cell centers.

In the model of the surface as a monolayer with vacancies, the general form of the cell theory relation for the surface tension of a simple liquid of nearly-spherical molecules, the bulk lattice structure of which is fully occupied and is represented as face-centered cubic, can be written as (1, 2)

$$\sigma = -\frac{2}{\sqrt{3}}\frac{kT}{(r^*)^2}\alpha^{1/3}\left\{\ln G + (1-\theta)\ln\frac{\psi_0''}{\psi'} + \theta\sum_{n=0}^{6}\binom{6}{n}\ln\frac{\psi_n''}{\psi'}\theta^{(6-n)}(1-\theta)^n + \frac{E_s^1(0)}{kT} + \frac{E_s^r(0)}{kT}\right\} \quad (1)$$

Here the (1 1 1) plane is taken as parallel to the surface and T denotes the absolute temperature. In *Eq 1*, G is the excess entropy of mixing of holes and surface molecules (a combinatory factor) and θ is the fraction of occupied surface sites. The $\frac{\psi_n''}{\psi'}$ represent the ratios of the surface/bulk cell free volumes, ψ_n'' being the free volume associated with a surface prisoner surrounded by n adjacent vacant cells, and ψ' being the bulk cell free volume. All $\frac{\psi_n''}{\psi'}$ are weighted according to the probability of such events occurring, assuming random mixing of holes and surface molecules. $E_s^1(0)$ and $E_s^r(0)$ are potential energy zero changes due to creation of the surface for, respectively, first nearest neighbor in-

* Present address: Department of Physics and Engineering, Washington and Lee University, Lexington, Va 24450.

teractions and all higher order interactions. To be more specific about the free volume, ψ' is calculable from the bulk equation of state and a Lennard-Jones force constant, D_o, this is a measure of the molecular diameter. The surface term ψ_n'' is taken as the linear weighted sum of contributions from the terms ψ_o'' and ψ_6'' (1, 2). The surface cell free volume is a function then of the same parameters as ψ' and one additional parameter, β, which is a measure of the increased width of the square well when a surface prisoner moves toward a region of vacancies.

The first of two improvements we have made in the use of the form of *Eq 1* is the connection of β to the critical point spacing, making unnecessary the previous use of this as a constant obtained by a one-point fit of a version of this relation to an experimental value of σ (2). The connection comes through the requirement that σ and the excess surface entropy vanish at the critical point. In practice, we take that the energetic and free volume contributions to *Eq 1* become negligible at the critical point. This gives that in terms of the first neighbor separation distances a_c and a at, in turn, the critical point and the temperature of interest,

$$\beta \simeq \frac{a_c - a}{D_o} \tag{2}$$

where a_c can be obtained directly from bulk data. The second principal modification of *Eq 1* is an improved calculation of the sum designated as $E_s'(0)$. Prigogine and Saraga (2) had estimated this as if the fraction of all orders of nearest neighbors removed by creation of the surface were given by that for first nearest neighbors. However, these differ significantly up to at least tenth nearest neighbors (1). Bond counting for the f.c.c. structure gives that (1)

$$E_s'(0) = [p\alpha^2 - (q - s\theta - t\theta^2)\alpha]\,\frac{z\epsilon^*}{2} \tag{3}$$

where p, q, s, and t are fractions which weight both the effect of number and distance on the contribution of each order of nearest neighbors to $E_s'(0)$. In *Eq 3*, $\alpha = (v^*/v)^2$, and z, ϵ^* are in turn the coordination number of the f.c.c. lattice and the maximum depth of the intermolecular potential well. In the predictive form of *Eq 1*, the use of *Eq 3* rather than the original estimate of $E_s'(0)$ eliminates an error in the calculation of σ that can be as large as 50 percent (1).

We use *Eq 1* derived for simple liquids as a basis for the calculation of the surface tension of polymer liquids. To draw a formal parallel between these two kinds of liquids it is necessary to model the latter as if they were in some respects constituted of quasi-free entities (quasimers); these have the chemical formula of mers of the chain. The use of *Eq 1* as it stands would, though, involve the use of effective parameters including contributions from both van der Waals and covalent bonds. However, when the surface is created, only van der Waals bonds are broken, chain connectivity is preserved.

The preservation of chain connectivity is reflected by changes in both the cell free volume terms of *Eq 1* and the first nearest neighbor energetic contribution to σ. Details of these changes are given below.

THE CELL FREE VOLUME

There are two modifications of this when *Eq 1* is used for polymers. Discussed in turn, these are the effect of the preservation of connectivity at the surface on the number of ways a prisoner can arrange adjacent connected bonds at the surface compared to the bulk, and a restriction of the free volume of a surface prisoner (with respect to a bulk prisoner) due to a decrease in the fraction of van der Waals bonds when the surface is created.

For every arrangement of holes and molecules around a surface prisoner, there is a change in the number of ways of arranging covalent and van der Waals bonds with respect to the bulk. For linear polymers this difference we estimate to first order as

$$\frac{\zeta_n''}{\zeta'} = \frac{\dfrac{(z - mz - n)!}{(z - mz - n - z_c)!\ z_c!}}{\dfrac{z!}{(z - z_c)!\ z_c!}} \tag{4}$$

where $m = (1/4)$, the fraction of first neighbors missing above the surface plane for a surface prisoner, and z_c is the average number of covalent bonds per mer (for high molecular weight linear polymers, $z_c = 2$). A leading term of this expression was given previously by Roe (4).

While vacancies surrounding a cell increase the free volume, the preservation of connectivity results in a decreased fraction of van der Waals bonds and a corresponding restriction of the movement of a surface prisoner relative to the bulk. We estimate this fractional change as

$$\frac{\eta_n''}{\eta'} = \left[\frac{\dfrac{(z - mz - n - z_c)}{(z - mz - n)}}{\dfrac{(z - z_c)}{z}}\right]^3 \tag{5}$$

where the fraction is raised to the third power to account for the three effective degrees of freedom of the quasimers.

Summarizing, for chain liquids compared to monomers the ratio $\frac{\psi_n''}{\psi'}$ in *Eq 1* becomes

$$\frac{\psi_n''}{\psi'}\,\frac{\zeta_n''}{\zeta'}\,\frac{\eta_n''}{\eta'}.$$

Setting $z_c = 0$ recovers the monomeric relationship.

THE POTENTIAL ENERGY ZERO TERM

The energy of interaction for first nearest neighbors in *Eq 1* cannot be the quasimer-quasimer bulk interaction as this includes an effect due to connectivity. Rather, the contribution of $E_s^1(0)$ to the surface tension arises from breaking what are literally van der Waals bonds.

To estimate $E_s^1(0)$, consider the quasimer energetically as a linear combination of a monomeric interaction (the model for which is approximated as the chemically stable form of the polymer repeat unit) and of a covalent-type interaction. In this manner, the effective quasimer lattice is modeled as a linear weighted combination of an expandable monomeric array and an essentially rigid covalent-type lattice.

These assumptions allow an estimate of the potential energy change due to missing first nearest neighbors as (1)

$$E_s^1(0) = [m + 1\theta(1 - \theta)] \frac{z\epsilon^*_{mon.}}{2} (\alpha^2_{mon.} - 2\alpha_{mon.}) \quad (6)$$

where m and 1 are fractions derived from first neighbor ruptured bonds (2), $\epsilon^*_{mon.}$ is the L-J force constant for the chemically stable monomer and $\alpha_{mon.}$ is taken as approximately equal to that for the quasimer (1). *Equation 6* is the first nearest neighbor term that would arise if the liquid were, literally, monomeric. Higher order neighbor interactions are assumed to be indifferent to the connectivity requirement. Their contributions to the excess potential energy are then given by the form of *Eq 3* with α, ϵ^* now parameters of the bulk quasimer liquid. The Lennard-Jones constants ϵ^*_{eff}, D_o^{eff} necessary for the use of this form of *Eq 3* can be found by fitting the square well equation of state for the simple liquid to bulk polymer data (1). This equation of state gives the effective separation between quasimers, a_{eff}, to be used in *Eq 3*.

SURFACE POTENTIAL WELL WIDTH

The last parameter to be calculated, β, is as mentioned a measure of the increased well width for a prisoner moving toward an unoccupied region. This cannot be found directly as for simple liquids because experimental data on the critical point is not available for high polymers. However, the quasimer critical point lattice spacing necessary to determine β can be estimated (1) from group additivity (5, 6).

RESULTS

The number of surface vacancies is determined by minimizing the surface free energy with respect to θ at the temperatures of interest. These values of θ were used to calculate the surface tensions that are given in *Table 1*. Calculated average values of $-\frac{\Delta\sigma}{\Delta T}$ are also given there.

Figure 1 illustrates the agreement of our predicted values of σ with experimental data for a particularly simple polymer, polyethylene, and for one with a bulky side group, polystyrene. For the latter there is a modification to the cell partition function over and above those already discussed. This is an asymmetry effect and can be incorporated in *Eq 5* (1) as a modification to z_c, which for the surface prisoner becomes $[z_c + (1/2)]$ and for the bulk prisoner $[z_c + 1]$. The effective bulk force constants for the calculations of *Table 1* and *Fig. 1* were determined from the data of Olabisi and Simha (7) (for polyethylene) and Richardson and Savill (8) (for polystyrene). As a calculational convenience a temperature-independent approximation for β was used (1).

Table 1. Calculated and Observed Values of σ and $\frac{-\Delta\sigma}{\Delta T}$ for Polyethylene and Polystyrene.

		σ, mN/M		$\frac{-\Delta\sigma}{\Delta T}$, mJ/M²/degree	
Substance	T, °K	Calculated	Observed (9)	Calculated	Observed (9)
Polyethylene	413	28.8	28.8	.067	.057
	453	26.1	26.5		
Polystyrene	393	33.2	33.5	.062	.072
	453	29.5	29.2		

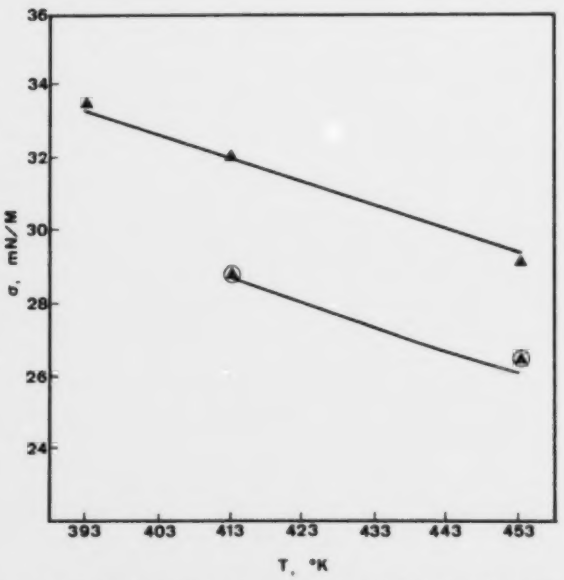

Fig. 1. Calculated and observed values of surface tension as a function of temperature for polyethylene and polystyrene. The lower curve is the predicted relation between σ and T for polyethylene, and the circled triangles are experimental values of the surface tension (9). The upper curve is the prediction for polystyrene and the triangles are experimental values of σ (9).

Generally, calculated surface tensions for polymers differ from experimental data by less than 10 percent and calculated values of $-\frac{\Delta\sigma}{\Delta T}$ are within 20 percent of reported values.

LIST OF SYMBOLS

a = mean distance of separation between first nearest neighbors.

a_{cr} = mean distance of separation between first nearest neighbors at the critical point.

D_o^{eff} = effective hard sphere diameter of the molecule.

$E_s^{1}(0)$ = surface excess potential energy zero due to missing first nearest neighbors.

$E_s^{r}(0)$ = surface excess potential energy zero due to missing neighbors of orders greater than one.

G = combinatory term.

k = Boltzmann's constant.

l = fraction of first nearest neighbor sites for a molecule in the same lattice plane.

m = fraction of first nearest neighbor sites for a molecule in an adjacent plane.

p, q, s, and t = fractions related to potential energy zero changes due to missing nearest neighbors of orders greater than one.

n = number of vacancies adjacent to a surface molecule.

r^* = distance of separation characteristic of minimum energy of interaction, ϵ^*, between a pair of molecules.

T = absolute temperature.

v = volume per molecule.

v^* = volume per molecule characteristic of minimum energy of interaction, ϵ^*.

z = number of first nearest neighbor sites of a molecule.

z_c = average number of covalent bonds per mer.

α = $(v^*/v)^2 = 2(D_o/a)^6$.

α_{eff} = $(v^*_{eff}/v_{eff})^2$.

α_{mon} = $(v^*_{mon}/v_{mon})^2$.

β = measure of increase in surface well width for a surface prisoner moving toward the vapor.

ϵ^*_{eff} = maximum effective potential well depth between a pair of quasimers.

ϵ^*_{mon} = maximum potential well depth between a pair of monomers with the chemical formula of the quasimer.

ζ' = number of arrangements of van der Waals/connected bonds for a bulk molecule.

ζ_n'' = number of arrangements of van der Waals/connected bonds for a surface prisoner with n adjacent vacancies.

η' = fraction of van der Waals bonds for a bulk mer.

η_n'' = fraction of van der Waals bonds for a surface mer with n adjacent vacancies.

θ = fraction of occupied surface lattice sites.

σ = surface tension.

ψ' = free volume of a bulk quasimer.

ψ_n'' = free volume of a surface quasimer with n adjacent vacancies.

ACKNOWLEDGMENT

K. Van Ness gratefully acknowledges the State of New Jersey for their support of this work through a Garden State Fellowship.

REFERENCES

1. K. E. Van Ness, Ph.D. Thesis, Rutgers University, 1986, and K. E. Van Ness and P. R. Couchman to be published.
2. I. Prigogine and L. Saraga, *J. Chim. Phys.*, **49**, 399 (1952).
3. I. Prigogine and V. Mathot, *J. Chem. Phys.*, **20**, 49 (1952).
4. R.-J. Roe, *Proc. Natl. Acad. Sci. USA*, **56**, 819 (1966).
5. R. F. Fedors, *J. Polym. Sci.* (B), **11**, 767 (1973).
6. R. F. Fedors, *Polymer*, **20**, 1255 (1979).
7. O. Olabisi and R. Simha, *Macromolecules*, **8**, 206 (1975).
8. M. J. Richardson and N. G. Savill, *Polymer*, **18**, 3 (1977).
9. S. Wu, *J. Macromol. Sci.*, **C10**, 1 (1974).

DISCUSSION

S. ROSTAMI: These derivations of surface tension are above the glass transition, i.e., in the molten state. Can you extrapolate to below T_g, and if you can, what do you need to do?

P. R. COUCHMAN: Actually, we are thinking of doing that and at the moment I am not certain how. We have got a rough estimate of the surface tension near the glass transition but did not go beyond that.

S. ROSTAMI: How good was that estimate?

P. R. COUCHMAN: Pretty close. I was quite surprised.

Characterization and Control of Interfaces in Emulsified Incompatible Polymer Blends

R. FAYT, R. JEROME, *and* Ph. TEYSSIÉ

Laboratory of Macromolecular Chemistry and Organic Catalysis
University of Liège-SART TILMAN
4000 LIEGE-Belgium

Information on the interfacial region in incompatible polymer mixtures can be gathered using various techniques including electron microscopy, thermal transition analysis, and more sophisticated methods such as nonradiative energy transfer (NRET). Selected examples are reported here to illustrate the exciting potentialities offered by diblock copolymer emulsifiers in controlling interfacial adhesion and devising high performance polymer blends.

INTRODUCTION

The coming of age of polymer melt-blending has certainly provided the easiest and often the most efficient way to generate new higher performance organic materials, starting from largely available monomers and polymers. In spite of the great interest of homogeneous blends (e.g., Noryl), more desirable (1) would be a nonmiscible system, i.e., a heterophase mixture wherein each of the partners retains its own properties, which then sum up in a final product that in addition may also display some new features triggered by the particular phase morphology.

In such systems, however, a satisfactory overall physico-mechanical behavior will critically depend on two demanding structural parameters: a proper interfacial tension leading to a phase size small enough to allow the material be considered as macroscopically "homogeneous," and an interphase "adhesion" strong enough to assimilate stresses and strains without disruption of the established morphology. Unfortunately, that is not the case for most immiscible polymer blends.

That situation has been traditionally alleviated by creating a practically irreversible morphology in the polymerization process itself, as illustrated by the classical examples of high-impact polystyrene and acrylonitrile-butadiene-styrene (ABS) resins. Blending the same rigid and elastomeric polymers would, however, represent a more versatile approach, since it would allow the production of a continuum of different compositions by simply processing various proportions of the base polymers. In order to promote the lacking proper interfacial adhesion, diblock copolymers of tailored structure and molecular weight have been used (2–8), leading to excellent properties of the corresponding final materials even when used in rather low proportions (ca., 1 to 2 weight percent).

This paper presents a few illustrative examples that explore that interface situation: its development, behavior, and influence on the final properties, along with some preliminary approaches for a finer characterization of the molecular arrangements in the interface itself, since such basic knowledge would, of course, provide a very useful tool for devising ever more performant materials.

MICROSCOPIC OBSERVATION OF THE "EMULSIFIER" DIBLOCK COPOLYMER

Considering the determinant effect of block copolymers on immiscible blends properties, it was an obvious step to ascribe that beneficial influence to their presence at the interface and to attempt their direct visualization, as already proposed for solution blending (9). That was done in two rather different cases, worth discussing comparatively.

It has been previously demonstrated that blends of polystyrene (PS) and low density polyethylene (LDPE) could be optimized into very interesting materials (2–6) by using emulsifiers prepared from styrene and butadiene block copolymerization followed by diene block hydrogenation (P(S-b-HBD)). Since that hydrogenation process previously described by Falk (10) can be run under conditions where polyisoprene is not reactive, a triblock copolymer poly (styrene-b-isoprene-b-butadiene) was synthesized in which the relatively short (15,000) isoprene sequence (PI) remained unsaturated upon further hydrogenation and could be stained with OsO_4 for direct observation by transmission electron microscopy (TEM). The micrographs of PS/LDPE/P(S-b-I-b-HBD) blends clearly show (*Fig. 1*) that most of the copolymer is nicely

located at the interface in 80 PE/20 PS as well as in 80 PS/20 PE blends. In this latter material, in fact a high-impact good aging PS, a "salami-type" secondary inclusion structure can even be observed as in classical HIPS, although it is difficult to assess whether these inclusions consist of pure diblock copolymer particles or also contain homopolystyrene. Such an overall situation obviously explains the excellent properties of these materials, which keep their finely dispersed (and sometimes co-continuous) morphology (ca., 0.5 μm) even under drastic processing conditions such as injection molding.

A rough estimation of the interface coverage (continuous and ca. 10 nm thick close to the calculated unperturbed end-to-end chain length of such a PI leads to a surface occupation per molecule of more than 26 nm (11).

For comparison purposes, a blend of 85 PVC/15 SEBS Kraton G was emulsified by a P(HBD-b-MMA) copolymer, since the molecular miscibility of syndiotactic PMMA (s-PMMA) in PVC has been definitively demonstrated in that range of molecular weight (ca., 40,000) by NRET experiments (12). Although that procedure results in the usual phase size decrease down to ca. 1 μm and a definite improvement of the mechanical properties (leading to a very high impact strength material), transmission micrographs (where the PMMA block has been labelled by consecutive hydrazine and OsO_4 treatments) clearly show that a major part of the copolymer is dispersed in the PVC phase instead of concentrated preferentially at the interface (*Fig. 2a*); therefore a definitely higher concentration (ca., 5 percent) of block copolymer is needed in order to reach interesting sets of properties. Similar situations are observed in the case of 80 PS/20 PVC blends with 5 percent of a P(S-b-MMA) copolymer (*Fig. 2b*). That very different behavior dramatically illustrates the prime importance of the interaction parameters balance, to favor selective migration of the emulsifier at the interface. No doubt a properly tailored decrease in interaction of the methacrylate block with PVC (i.e., by controlling microstructure, molecular weight, and composition) would restore a more favorable situation but again at the cost of a long optimization process.

COPOLYMER BEHAVIOR AT INTERFACE FROM NONRADIATIVE ENERGY TRANSFER (NRET) MEASUREMENTS

The application of NRET measurements to synthetic polymers, as pioneered by Morawetz

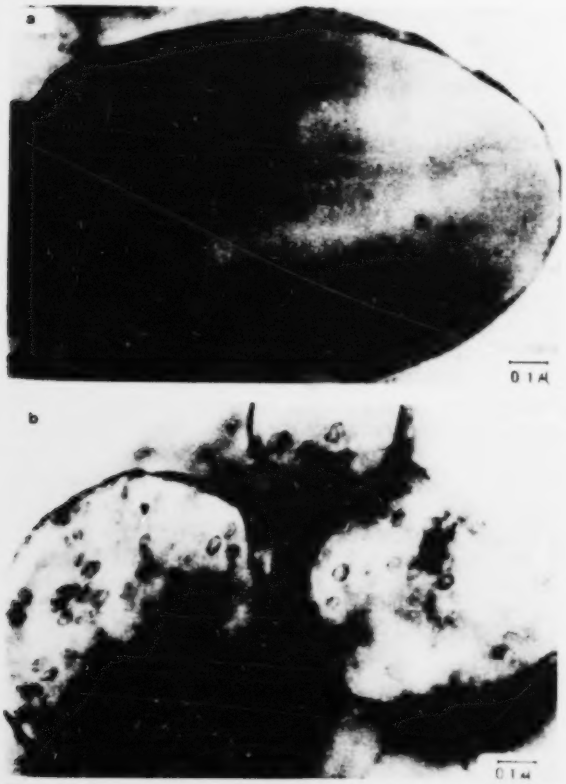

Fig. 1. Transmission electron micrographs of LDPE/PS blends (roll-milled and compression molded) with 10 weight percent P (S-b-I-b-HBD) copolymer added: (a) 80 weight percent LDPE/20 weight percent PS; (b) 20 weight percent LDPE/80 weight percent PS (Reproduced with permission (11) of J. Polym. Sci.).

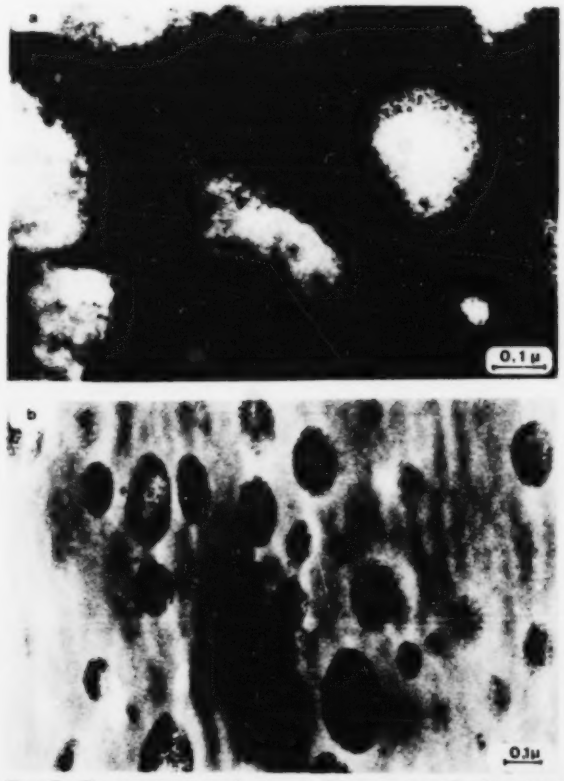

Fig. 2. Transmission electron micrographs of roll milled and compression molded blends: (a) 80 weight percent PVC/15 weight percent Kraton G/5 weight percent P(HBD-b-MMA) copolymer; (b) 20 weight percent PVC/80 weight percent PS with 10 weight percent P(S-b-MMA) copolymer added. PMMA was selectively stained by consecutive hydrazine and OsO_4 treatment.

(13), has provided scientists with a method for the evaluation of different macromolecule interpenetration at the molecular level, giving rise to many applications with respect to polymer chain dynamics and interactions. Thus, it was of great interest to apply that method to an immiscible blend situation, thanks to the post-labeling methods recently developed in our laboratories (12).

In particular, they allowed us to compare a blend of PVC and s-PMMA to an exactly corresponding situation (in terms of composition and molecular weights where the homopolymer was replaced by a P(S-b-MMA) diblock. The PMMA was labelled with 1.5 mol percent anthracene (acceptor), whereas the PVC was grafted with 1 mol percent naphthalene (donor). The NRET from donor to acceptor chromophores depends on the extent to which the chains of the different polymers are able to interpenetrate. The efficiency of the energy transfer is measured by the ratio of the emission intensity of the naphthyl and anthryl labels (I_D/I_A), which is, therefore, a sensitive indicator of polymer miscibility on a scale of a few nm. The fluorescence behavior of these systems is illustrated in *Fig. 3* where it appears that compared to a blank giving an I_D/I_A value of 0.18 (value for a homogeneous system), lower molecular weight (4×10^4) PMMA is practically miscible with PVC on a molecular scale (ca., 2 nm) up to a molar fraction of 0.8; while an increasing molecular weight (15×10^4) results in a somewhat lower solubility (note however, that total phase separation should theoretically give a I_D/I_A value of 13.2). More unexpectedly (12), the labelled PMMA sequence in the block copolymer behaves exactly as free PMMA homopolymer with maximum intermixing, although the PS block is obviously insoluble in PVC and forms its own segregated domains. In other words, a reduction of the interface at the expense of interactions between the s-PMMA block and PVC is an unfavorable process, at least in that range (4×10^4) of molecular weights.

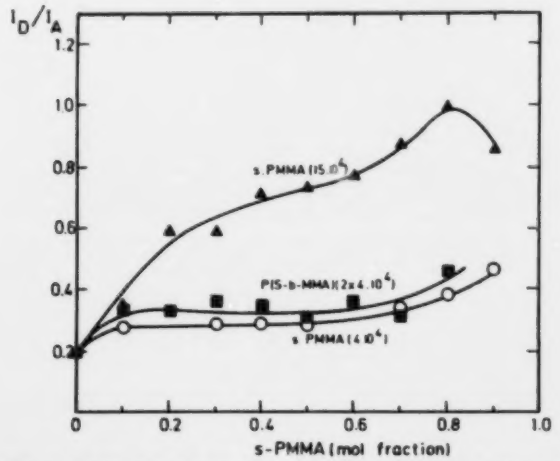

Fig. 3. Emission intensity ratio (I_D/I_A) as a function of molar fraction of syndiotactic PMMA in PVC/s-PMMA and PVC/P(S-b-MMA) blends.

These results certainly support the validity of our approach using tailored polymer emulsifiers P(A-b-C) to bridge the incompatibility gap between polymers, A and B, provided C is miscible with B. They also represent a first exploratory demonstration of a general method to investigate indepth the situation of block copolymers at interfaces, by labelling in turn the different partners in the blend and systematically modifying their structural parameters. Although qualitative, the results can be put on a relative scale indicating existing trends, and thus represent an additional and sensitive key for tailoring these situations.

THERMAL TRANSITIONS AS A PROBE FOR INTERFACES

Certainly of less general application, thermal transitions may however represent, in spite of their indirect indications, an interesting probe for the existence and nature of interfacial regions, particularly for unstable ones. For example, differential scanning calorimetry (DSC) and thermally stimulated depolarization currents (TSDC) have been used to seek thermal transitions indicative of special interphase situations, even transient ones. In particular, three different T_g's have been repeatedly reported in reorganizing two-component heterophase systems, being either block copolymers (14–16) or ion-containing polymers (17). Another example using a dynamic method will henceforth be used to these potentialities.

When measuring the isochronous torsion modulus of 80 PVC/20 PS blends combined with different amounts of a block copolymer P (caprolactone-b-styrene), P (CL-b-S) acting as an emulsifier since polycaprolactone is miscible with PVC (18, 19), one observes the usual features characteristic of such materials: heterophase situation (practically unchanged homopolymers T_g's), decreased phase size, and improvement (see *Fig. 4*) in physico-mechanical properties (i.e., strong increase, by one order of magnitude, of the modulus between the PVC (80°C) and PS (100°C) T_g's). However, one also clearly observes a third transition around 50°C, which counter experiments have shown not to be due to PCL crystallinity; in all probability, it expresses the presence of a crown of PVC "plasticized" by PCL blocks around the PS domains. Moreover, its position is slightly dependent on the amount of copolymer added (10 and 20 percent), and allows one to calculate the possible composition of that mixed interface (in this case 11 to 15 weight percent of PCL respectively), using the Fox-Flory relation (19).

INTERFACIAL ADHESION AS SEEN BY SCANNING ELECTRON MICROSCOPY (SEM)

Although the methods discussed above can certainly lead to a better view of the molecular

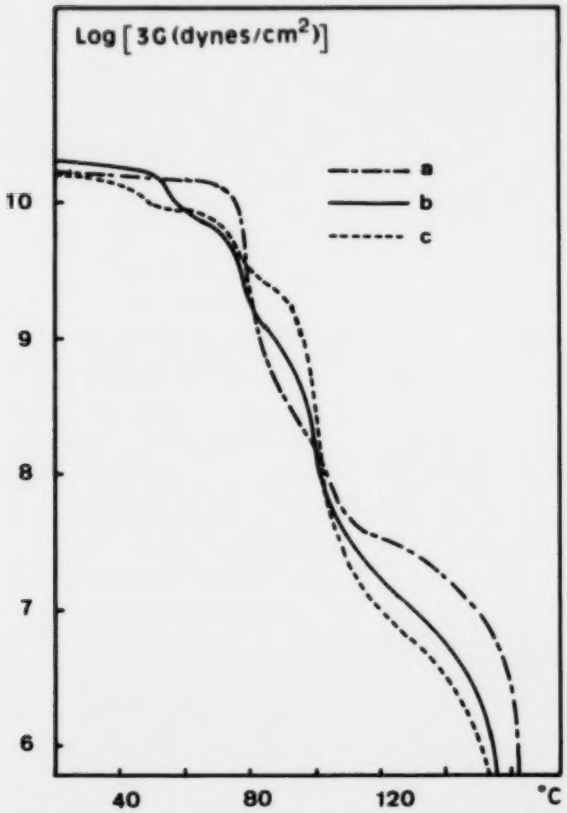

Fig. 4. Torsion modulus versus temperature for PVC/PS blends (roll-milled and compression molded): (a) 80 weight percent PVC/20 weight percent PS; (b) 72 weight percent PVC/18 weight percent PS/10 weight percent P(CL-b-S) copolymer; (c) 64 weight percent PVC/16 weight percent PS/20 weight percent P(CL-b-S) copolymer.

situation at interfaces, they do not provide a clear handle on the essential feature, that is, interphase adhesion under constraint. While physico-mechanical properties do convey that characteristic, it is in a very partial and indirect manner. In spite of the fact that SEM can scarcely locate the emulsifier in interfacial regions (except for a few still questionable cases as illustrated in *Fig. 5a*), it probably represents one of the more direct and illustrative methods for evaluation of that adhesion, when fracture surfaces of different blends are systematically compared. A number of illustrative cases are presented below.

PS-PE blends may represent interesting materials, especially as substitutes for HIPS, displaying excellent weathering characteristics. In the presence of optimized P(S-b-HBD) emulsifiers mentioned earlier, fracture micrographs show indeed an excellent adhesion between finely dispersed phases, interconnected by fibrils of a few dozen nms in diameter, (*Fig. 5b*). In some cases, they also give indication of co-continuous situations from which homo-PS, even if dominant, can be extracted without disrupting the general shape of the sample (2, 5) (*Fig. 5c*).

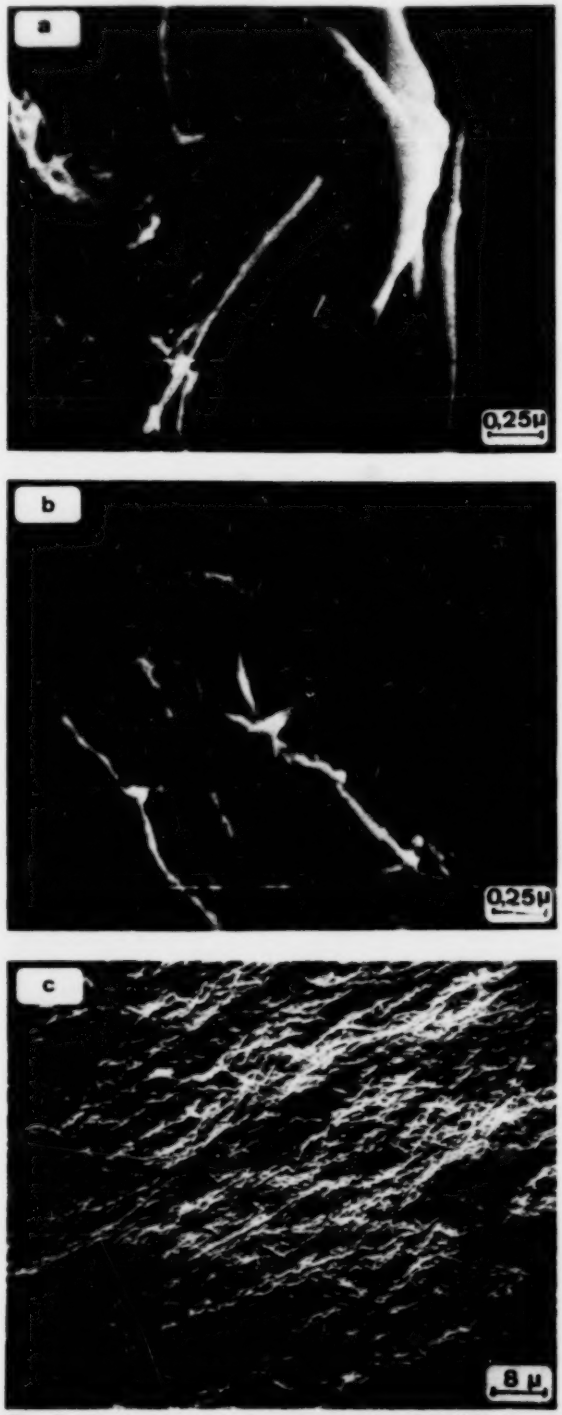

Fig. 5. Scanning electron micrographs of PE/PS blends (roll milled and compression molded): (a) and (b) room temperature fracture surface of 20 weight percent HDPE/80 weight percent PS with 10 weight percent P (S-b-HBD) copolymer added; (c) remaining LDPE phase after THF-extraction of PS in 20 weight percent LDPE/80 weight percent PS with 10 weight percent P (S-b-HBD) copolymer added.

SAN-diene rubber blends are interesting materials similar to ABS, although different from them to some extent. Again, scanning micro-

graphs give an interesting clue to the adhesion situation in such blends: compared to weak heterogeneous materials when no copolymer is used, superbly intermixed products are obtained when a P(BD-b-MMA) copolymer is added, wherein the syndiotactic PMMA sequence strongly interacts with SAN. The excellent adhesion, even better than that of a typical industrial ABS, is evidenced in room-temperature fracture micrographs (*Fig. 6*) leading to higher impact resistance values and better fractograms (load-time) profiles than ABS itself (7). It is worth stressing that in this case, microscopy even provides for a possible relative evaluation of the resulting material performances.

PS-Nylon-6 blends are another attractive combination of two materials offering very different properties. Despite their extremely different solubility parameters, very fine dispersions of these two polymers can be achieved, wherein one can clearly see the "gluing" of the dispersed phase to the matrix (*Fig. 7*) thanks to a suitable copolymer; this latter can be any block copolymer of polystyrene and of another polymer ensuring strong interactions with the polyamide including Nylon-6 itself (20).

A final example pertains to an engineering plastic, namely polyvinylidene fluoride, PVF_2, the very attractive properties of which are unfortunately limited by its high price and some adverse characteristics. Thus it would be of prime interest to fill it with cheaper polymers (or inorganics), thus yielding more economical materials while still retaining the essential PVF_2 properties (i.e., as the matrix continuous phase) plus potential slight improvements promoted by the filler. Again, s-PMMA block copolymers were chosen, based on the miscibility of that polymer with PVF_2. One variation on that theme is illustrated in the micrographs of *Figure 8*, demonstrating how a very coarse and weak blend of 80 PVF_2/20 Noryl (itself a blend of HIPS and polyphenylene oxide) is progressively converted, upon addition of increasing amounts of P(S-b-MMA), into an extremely fine dispersion of perfectly adhering phases, up to a point where they become practically indistinguishable. Needless to say, a parallel improvement of the physico-mechanical properties of the corresponding materials is recorded (8).

CONCLUSIONS

The selected but certainly nonexhaustive examples discussed here clearly illustrate the exciting potentialities offered by diblock copolymer emulsifiers, in devising high performance polymer blends. It has to be stressed, however, that *optimization* of their structural and size characteristics is an extremely critical key process, often implying painstaking feedback cycles between synthesis and evaluation, an imperative requirement due to narrow structural "windows" within which the high performance properties develop.

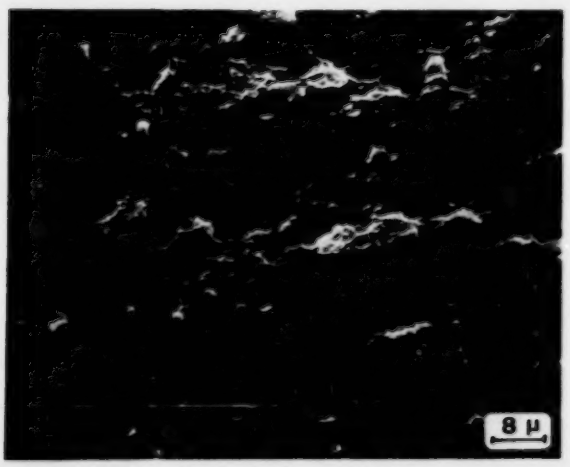

Fig. 6. Scanning electron micrograph of fracture surface (from a Charpy impact test) of 66.5 weight percent SAN/ 23.5 weight percent Solprene 411, SB thermoplastic elastomer/10 weight percent P(BD-b-MMA) copolymer (roll-milled and compression molded blends).

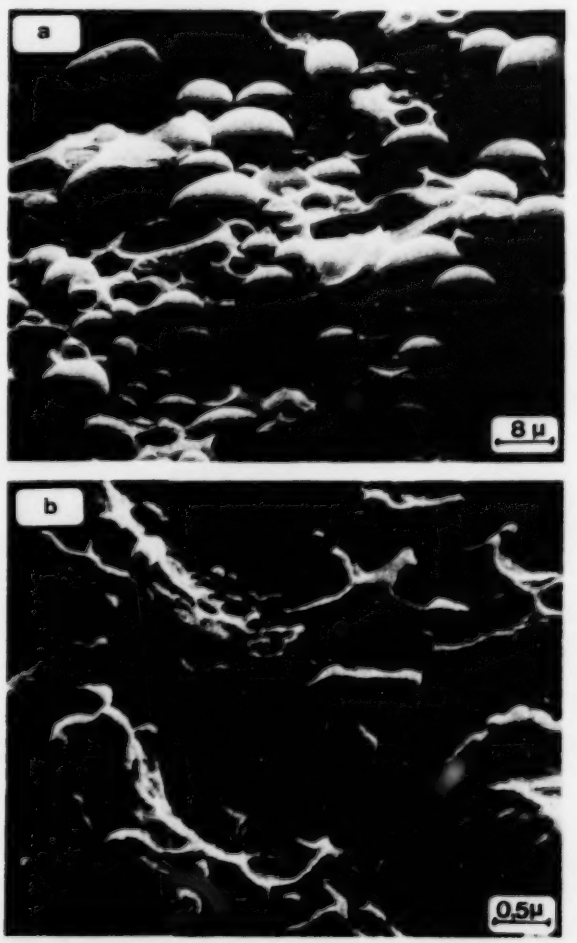

Fig. 7. Scanning electron micrographs of room temperature fracture surface of 50 weight percent PS/50 weight percent Nylon-6 blends (roll-milled and compression molded): (a) without copolymer; (b) with 5 weight percent copolymer added.

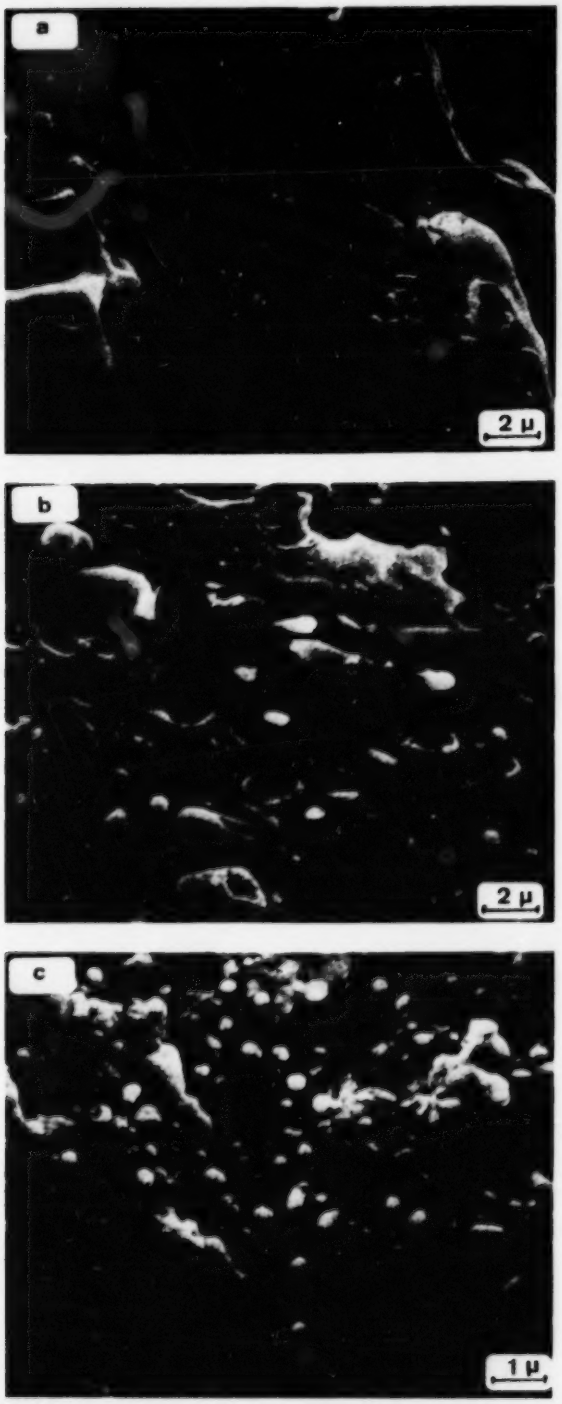

Fig. 8. Scanning electron micrographs of room temperature fracture surfaces of 80 weight percent PVF_2/20 weight percent Noryl blends (roll-milled and compression molded): (a) without copolymer; (b) with 2 weight percent P(S-b-MMA) copolymer; (c) with 12 weight percent P(S-b-MMA) copolymer. Reprinted with permission (8) of J. Polym. Sci.

With that respect, deeper understanding of the necessary structural and processing features for further improving that general approach is obviously desirable. Beside valuable theoretical approaches (such as those of Meier (21) and Noolandi *et al.* (22)), a detailed experimental characterization of the interface situation will be a necessary foundation in this field. Thus it is fortunate that a number of powerful, if delicate, physical techniques are now available for that purpose: electron microscopy (SEM, TEM), solid-state NMR spectroscopy (possibly using D or ^{13}C labelled copolymers), scattering techniques using synchroton radiation (23), and last but not least, the nonradiative energy transfer method will certainly help us to unravel the fascinating behavior of these interfaces and to meet the challenge of using them to fabricate better materials.

ACKNOWLEDGMENTS

The authors are indebted to Services de la Programmation de la Politique Scientifique (Brussels) for general basic support to IRSIA for an interindustry (CRIF, Labofina, Solvay)-University grant, and to their coworkers, B. Albert, J. Heuschen, and T. Ouhadi. They want to thank M. Palumbo, J. Linet, and Y. Lambert for skillful technical assistance.

REFERENCES

1. O. Olabisi, L. M. Robeson, and M. T. Shaw, "Polymer-Polymer Miscibility," Academic Press (1979).
2. R. Fayt, R. Jérôme, and Ph. Teyssié, *J. Polym. Sci., Polym. Lett. Ed.*, **19**, 79 (1981).
3. R. Fayt, R. Jérôme, and Ph. Teyssié, *J. Polym. Sci., Polym. Phys. Ed.*, **19**, 1269 (1981).
4. R. Fayt, R. Jérôme, and Ph. Teyssié, *J. Polym. Sci., Polym. Phys. Ed.*, **20**, 2209 (1982).
5. R. Fayt, R. Jérôme, and Ph. Teyssié, *Makromol. Chem.*, **187**, 837 (1986).
6. R. Fayt, R. Jérôme, and Ph. Teyssié, to be published in *J. Polym. Sci., Polym. Phys. Ed.*
7. R. Fayt and Ph. Teyssié, *Macromolecules*, in press.
8. T. Ouhadi, R. Fayt, R. Jérôme, and Ph. Teyssié, *J. Polym. Sci., Polym. Phys. Ed.*, in press.
9. M. Schlienger, Ph. D. Thesis, Mulhouse (France) (1976).
10. J. C. Falk, *J. Polym. Sci., A1*, **9**, 2617 (1971).
11. R. Fayt, R. Jérôme, and Ph. Teyssié, *J. Polym. Sci., Polym. Lett. Ed.*, **24**, 25 (1986).
12. B. Albert, R. Jérôme, Ph. Teyssié, and D. Baeyens, *J. Polym. Sci., Chem. Ed.*, in press; R. Fayt and Ph. Teyssié, to be published.
13. H. Morawetz and F. Amrani, *Macromolecules*, **11**, 281 (1978); F. Mikes, H. Morawetz, and K. S. Dennis, ibid., **17**, 60 (1984).
14. J. F. Beecker, L. Marker, R. D. Bradford, and S. L. Aggarwal, *J. Polym. Sci.*, Part C, **26**, 117 (1969).
15. B. Morese-Sequela, M. St. Jacques, J. M. Renaud, and J. Prud'homme, *Macromolecules*, **13**, 100 (1980).
16. G. C. Meyer and J. M. Widmaier, *J. Polym. Sci., Polym. Phys. Ed.*, **20**, 389 (1982).
17. J. Horrion, R. Jérôme, and Ph. Teyssié, *J. Polym. Sci., Polym. Lett. Ed.*, **24**, 69 (1986).
18. E. M. Woo, J. W. Barlow, and D. R. Paul, *Polymer*, **26**, 763 (1985).
19. J. Heuschen, Ph. D. Thesis, University of Liège (Belgium) (1977).
20. D. Petit, R. Jérôme, and Ph. Teyssié, *J. Polym. Sci., Polym. Chem. Ed.*, **17**, 2903 (1979).
21. D. J. Meier, *J. Polym. Sci., Part C*, **26**, 81 (1969); *Polym. Prepr., Am. Chem. Soc. Div. Polym. Chem.*, **15**, 171 (1974); in "Block and graft copolymers," J. J. Burke and V. Weiss, eds, Syracuse Univ. Press, Syracuse, New York (1973).

22. J. Noolandi and K. M. Hong, *Macromolecules*, **17**, 1531 (1984).
23. T. P. Russel, *Polym. News*, **11**, 70 (1985).

NOMENCLATURE

LDPE	=	low density polyethylene.
HDPE	=	high density polyethylene.
PS	=	polystyrene.
PMMA	=	polymethylmethacrylate.
s-PMMA	=	syndiotactic PMMA.
PVC	=	polyvinyl chloride.
PCL	=	poly-ϵ-caprolactone.
SAN	=	styrene-co-acrylonitrilepolymer.
PVF_2	=	polyvinylidene fluoride.
HIPS	=	high impact polystyrene.
ABS	=	acrylonitrile-butadiene-styrene copolymer.
SEBS	=	styrene-ethylene butene-styrene triblock copolymer.
P(S-b-I-b-HBD)	=	styrene-isoprene-hydrogenated butadiene triblock copolymer.
P(S-b-HBD)	=	styrene-hydrogenated butadiene diblock copolymer.
P(BD-b-MMA)	=	butadiene-methylmethacrylate diblock copolymer.
P(S-b-MMA)	=	styrene-methylmethacrylate diblock copolymer.
P(CL-b-S)	=	caprolactone-styrene diblock copolymer.

DISCUSSION

A. P. Plochocki: How did you prepare your blends? Did you mix in a molten state?

Ph. Teyssié: We used different methods and different mixers, but most often a two-roll mill to follow the kinetics of dispersion by microscopy. However, these di-blocks were also used in other classical operations, e.g., extrusion, and they work very well.

C. L. Beatty: Did you see any difference in morphology changing the blending method?

Ph. Teyssié: Not really. Of course you have to mill for a few minutes, until equilibrium. If you have the proper blocks, mixing for 30 seconds may be sufficient.

L. W. Kleiner: Have you determined the equilibrium concentration of compatibilizers in these blends?

Ph. Teyssié: Yes. This will be published very soon. The optimum concentration depends a lot on the optimum structure that you want to develop. If you optimized the copolymer, and that is not an easy process, then one percent is enough; you will reach a plateau in the properties and morphology. If you use too much of it, then you loose. In general, for well tailored block copolymers 1 to 2 percent is enough.

L. A. Utracki: In principle, you are achieving the enhancement of polymer blend properties by treating the two-phase polymeric liquid mixture as an emulsion, stabilizing the system with an emulsifier, called here two-block compatibilizer. You are controlling the dispersion and in general achieving greater reproducibility of properties by modifying the interfacial properties in the molten state. This immediately suggests three questions: (i) did you develop adequate means of characterization of the interfacial properties, e.g., to measure the interfacial tension; (ii) how the solidification in the presence of a difference in the thermal expansion coefficient affects the interfacial behavior; and (iii) is the method suitable only to generate droplet-type morphology or can it be also used efficiently to enhance properties in blends with co-continuous structures?

Ph. Teyssié: Yes, we are trying to optimize the performance of immiscible polymer blends by addition of small amounts of specially designed interfacial agents. As far as the measurement of the interfacial properties are concerned, we are using several approaches which I mentioned during the presentation. Microscopy with or without staining, nonradiative energy transfer (NRET), scattering techniques, or NMR. However, there is a need to develop a simple experimental method to characterize the interface. The most universal at the moment seems to be the NRET, but it requires chemical modification of the system.

Formation of Dispersed Phase in Incompatible Polymer Blends: Interfacial and Rheological Effects

SOUHENG WU

E. I. du Pont de Nemours & Company
Central Research and Development Department
Experimental Station
Wilmington, Delaware 19898

The formation of dispersed phase in blends of incompatible polymers during melt extrusion with a co-rotating twin screw extruder was studied, using nylon and polyester as the matrix and ethylene-propylene rubbers as the dispersed phase. A master curve is obtained, i.e., $G\eta_m a/\gamma = 4p^{\pm 0.84}$, where G is the shear rate, a the particle diameter, γ the interfacial tension, η_m the matrix viscosity, η_d the dispersed-drop viscosity, and $p = \eta_d/\eta_m$. The plus (+) sign applies for $p > 1$, and the minus (−) sign for $p < 1$. Thus, the dispersed-drop size is directly proportional to the interfacial tension and the ±0.84 power of viscosity ratio. The dispersed drops are the smaller, when the interfacial tension is the lower and the viscosity ratio is the closer to unity. The interfacial tension is largely controlled by the polarities of the two phases, and can be varied over several orders of magnitude by using appropriate dispersants.

INTRODUCTION

The size and shape of the dispersed phase are important factors that determine the mechanical properties of incompatible polymer blends. In rubber-toughened plastics, two types of behavior have been observed. In blends that dissipate fracture energy mainly by matrix crazing, the toughness is the greatest at an optimum rubber particle size (1). Examples are blends with matrices of polystyrene and poly(methyl methacrylate). On the other hand, in blends that dissipate fracture energy mainly by matrix yielding, a sharp brittle-tough transition occurs at a critical rubber particle size, or when the interparticle distance is at the critical value (1). Examples are blends with matrices of nylon and thermoplastic polyesters.

Melt extrusion is an important process for making polymer blends. During extrusion, the components are melt-blended, and the minor phase is broken up to form the dispersed phase. The size and shape of the dispersed phase are much controlled by the interfacial tension, rheological properties, and the complex strain field of the extruder. In this work, we study the interfacial and rheological effects on the dispersion process during melt extrusion of polymer/rubber blends in a co-rotating twin screw extruder.

EXPERIMENTAL

Materials

Two nylon 66 resins (coded as nylon Z-1 and Z-2) and one poly(ethylene terephthalate) (coded as PET) were used as the matrix phase. Fourteen ethylene-propylene rubbers of essentially the same chemical composition (63 percent ethylene and 37 percent propylene by weight), but of different molecular weights were used as the dispersed rubber phase in the binary polymer/rubber blends. Eight of the 14 rubbers are nonreactive (coded as EP rubbers), i.e., they do not contain any reactive groups that could react with the matrix. On the other hand, the other six rubbers are reactive (coded as EPX rubbers), i.e., they contain less than 1 percent by weight of carboxyl groups. The reactive rubbers can react with the matrix to form graft copolymers, which act as *in situ* formed dispersant. The molecular weights and the code names for all the materials used are listed in *Table 1*.

All the polymers (nylons and PET) were vacuum-dried at 120°C overnight, and all rubbers at 80°C overnight before use.

Melt Extrusion

Binary polymer/rubber blends were prepared by melt extrusion, using a co-rotating twin

Table 1. Molecular Weights and Polarity of Materials.

Polymer	M_n, kg/mole	M_w, kg/mole	Polarity, x
Nylon 66 resins			
Nylon Z-1	17	35	0.344
Nylon Z-2	24	131	0.344
Poly(ethylene terephthalate)			
PET	16	37	0.221
Nonreactive ethylene-propylene rubbers (EP)			
EP-1	14	92	0
EP-2	21	88	0
EP-3	23	99	0
EP-4	21	79	0
EP-5	18	90	0
EP-6	25	89	0
EP-7	19	75	0
EP-8	19	70	0
Reactive ethylene-propylene rubbers (EPX)			
EPX-9	14	92	—
EPX-10	21	88	—
EPX-11	18	73	—
EPX-12	16	87	—
EPX-13	17	69	—
EPX-14	16	66	—

screw extruder (Werner and Pfleiderer, ZSK-28D, 28 mmϕ with No. 4 screw configuration) at 200 rpm. All blends contained 15 percent by weight of a rubber (dispersed phase) and 85 percent by weight of a polymer (matrix phase). Four series of blends were prepared: PET/EP rubber, nylon Z-1/EP rubber, nylon Z-1/EPX and nylon Z-2/EP rubber, as indicated in *Table 2*.

The extruder barrel has five zones. Typical temperature settings along the barrel were 280°C for zones 1 and 2, 250°C for zone 3, 230°C for zones 4 and 5, and 280°C for the die. The melt temperature was measured at the die and controlled at 280°C or 325°C, depending on the materials used as indicated in *Table 2*. The extrudate was quenched in an ice-water trough.

Pellets (about 0.3 cm in size) of the polymer and the rubber were fed into the extruder through a hopper blanketed with dry nitrogen to prevent moisture absorption. The port on zone 2 of the barrel was maintained below 1 mm Hg pressure.

Dispersed Rubber Particle Size

During melt extrusion, the rubber was dispersed as spheroidal particles in the polymer matrix. No composite particles were formed, i.e., the matrix phase did not contain small embedded droplets of the rubber.

The rubber particle size and distribution were determined by electron microscopy, as discussed before (1, 2). About 100 to 500 particles were scanned with an image analyzer to obtain the size distribution and average diameters.

Rheological Measurements

The apparent viscosity of the polymers and the rubbers were measured at the extrusion temperatures as a function of apparent shear rate, using a capillary extrusion rheometer. The capillary die used was 0.0378 cm in radius and 2.54 cm in length with an L/D ratio of 33.6 and an entrance angle of 90°. The Bagley and Rabinowitsch corrections were not made.

Table 2. Extrusion Melt Temperature and Interfacial Tension.

Polymer/Rubber Pair	Extrusion Melt Temp., °C	Interfacial Tension, mN/m	
		280°C	325°C
PET/EP rubber	325	6.2	5.7
Nylon Z-2/EP rubber	325	9.7	8.8
Nylon Z-1/EP rubber	280	9.7	8.8
Nylon Z-1/EPX rubber	280	0.25	0.25

Interfacial Properties

Because of high melt viscosities, the interfacial tensions between the polymer and the rubber were not measured directly for the present systems, but rather were calculated from the surface tensions and the polarities of the two phases (in the case of polymer matrix and the nonreactive EP rubber), or from the interfacial thickness (in the case of polymer matrix and the reactive EPX rubbers). The surface tensions of the melts were measured directly by the pendent drop method. The polarities were measured by the contact angle method. These methods have been discussed and reviewed in detail elsewhere (3). On the other hand, the interfacial thickness between the polymer matrix and the dispersed rubber was measured by electron microscopy.

The various methods used for the calculation of interfacial tension were established previously (3), and briefly discussed later.

RESULTS AND DISCUSSION

Rheological Properties

The melt viscosities of the polymers and the rubbers are plotted as a function of shear rate at 280, 300, and 325°C in *Figures 1* to *5*. In these bilogarithmic plots, the three matrix polymers give approximately straight lines, whereas the rubbers give obvious but small curvatures with the exception of EF-8 rubber, which shows a considerable change in slope near 100 s^{-1}.

The curves for the matrix polymers may be roughly expressed by the power law

$$\eta = \eta_0 G^{\beta} \qquad (1)$$

where η is the melt viscosity, G the shear rate, and η_0 and β are constants. On the other hand, for the rubbers, *Eq 1* cannot be used over the entire shear rate ranges tested, but can adequately represent the data over a narrower range. The β values for the matrix polymers (taken over the entire shear rate ranges) and for the rubbers (taken over 100 to 1000 s^{-1} ranges) are listed in *Table 3*. Newtonian behavior corresponds to $\beta = 0$, and shear-thinning behavior corresponds to $0 < \beta < 1$. Using the β values as a guide, we see that the three matrix polymers

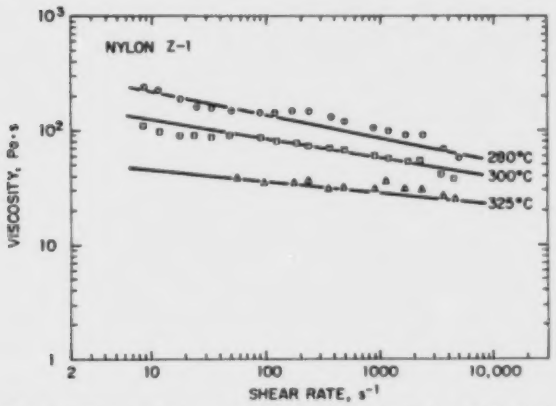

Fig. 1. Viscosity vs. shear rate for nylon Z-1 at 280, 300, and 325°C.

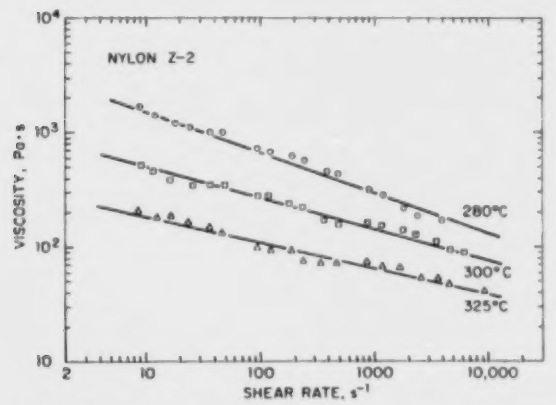

Fig. 2. Viscosity vs. shear rate for nylon Z-2 at 280, 300, and 325°C.

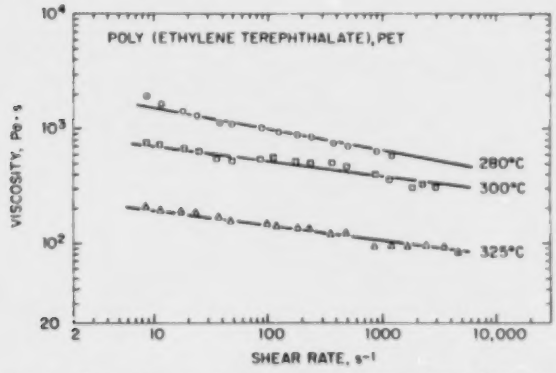

Fig. 3. Viscosity vs. shear rate for PET at 280, 300, and 325°C.

are more Newtonian-like and less viscoelastic than the rubbers which are more viscoelastic and less Newtonian-like.

Interfacial Tension and Polarity

The surface tensions and their nonpolar (dispersion) and polar components for the nylons, the PET and the EP (nonreactive) rubbers are listed in *Table 4*. The surface tension is related to its components by

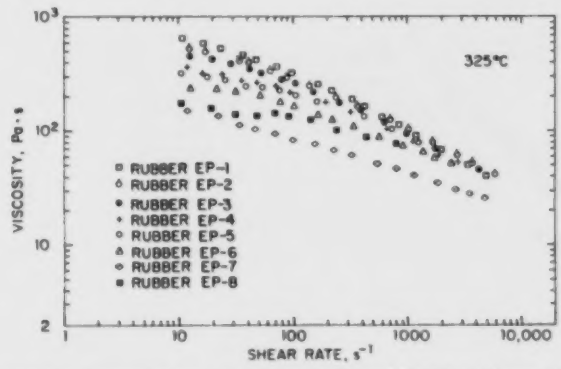

Fig. 4. Viscosity vs. shear rate for various EP rubbers at 325°C.

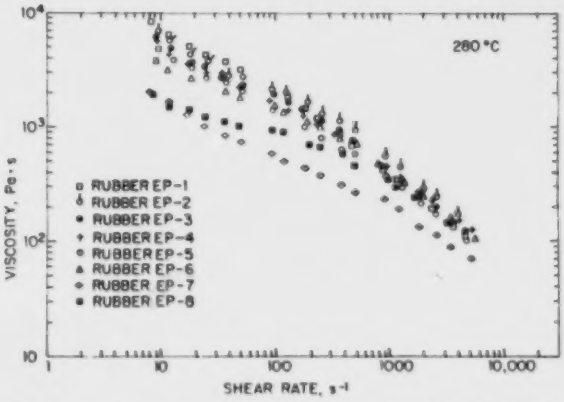

Fig. 5. Viscosity vs. shear rate for various EP rubbers at 280°C.

Table 3. Values of Viscosity Power-Law Coefficient β.

Material	Value of β		
	280°C	300°C	325°C
PET	0.18	0.13	0.12
Nylon Z-1	0.21	0.17	0.10
Nylon Z-2	0.35	0.29	0.23
EP-1 rubber	0.66	—	0.47
EP-2 rubber	0.64	—	0.45
EP-3 rubber	0.64	—	0.44
EP-4 rubber	0.61	—	0.41
EP-5 rubber	0.62	—	0.44
EP-6 rubber	0.64	—	0.35
EP-7 rubber	0.49	—	0.31
EP-8 rubber	0.44	—	0.25
EPX-9 rubber	0.66	—	0.47
EPX-10 rubber	0.64	—	0.45
EPX-11 rubber	0.61	—	0.41
EPX-12 rubber	0.62	—	0.44
EPX-13 rubber	0.49	—	0.31
EPX-14 rubber	0.44	—	0.25

$$\gamma = \gamma^d + \gamma^p \quad (2)$$

where γ is the surface tension, γ^d its nonpolar component and γ^p its polar component.

The polarity x is the ratio of the polar component to the total surface tension, i.e.,

$$x = \gamma^p/\gamma \quad (3)$$

and is independent of temperature (3), i.e.,

$$dx/dT = 0 \quad (4)$$

The polarity values, determined by contact angle method at room temperature, for the matrix polymers and the EP rubbers are listed in *Table 1*. The components of surface tension are obtained by

$$\gamma^d = (1 - x)\gamma \quad (5)$$

and

$$\gamma^p = x\gamma \quad (6)$$

The surface tension and its components thus obtained are listed in *Table 4*.

The interfacial tensions γ_{12} between the nylons and the EP rubbers and between the PET and the EP rubbers were calculated from the surface tensions and their components by (3)

$$\gamma_{12} = \gamma_1 + \gamma_2 - \frac{4\gamma_1^d\gamma_2^d}{\gamma_1^d + \gamma_2^d} - \frac{4\gamma_1^p\gamma_2^p}{\gamma_1^p + \gamma_2^p} \quad (7)$$

which has been shown to be applicable to polymer melts (3). The interfacial tensions thus obtained are listed in *Table 2*, with a probable error of ±0.5 mN/m.

Note that the surface tensions and their components for the two nylons are the same, and those for all the EP (nonreactive) rubbers are also the same, as listed in *Table 4*. This is because the two nylons have the same chemical compositions, and all the EP (nonreactive) rubbers have essentially the same chemical compositions; the only main difference is in the molecular weights. It is known that in the high molecular weight ranges, the surface tensions are practically independent of molecular weight (3). Therefore, the interfacial tensions between PET and the various EP rubbers are practically the same, and so are the interfacial tensions between the nylons and the various EP rubbers, as listed in *Table 2*.

Table 4. Surface Tension and Its Components for Nylon, PET and Nonreactive EP Rubbers.

	Surface Tension and Components, mN/m					
	280°C			325°C		
Material	γ	γ^d	γ^p	γ	γ^d	γ^p
Nylons	29.6	19.7	9.9	26.7	17.8	8.9
PET	27.7	21.6	6.1	24.8	19.3	5.5
EP rubbers	17.9	17.9	0	14.9	14.9	0

On the other hand, the interfacial tension between nylon and EPX (reactive) rubbers cannot be calculated by *Eq 7*, since the EPX rubbers react with the nylon matrix during the melt extrusion to form graft copolymers which act as *in-situ* formed dispersant as discussed before (2). Therefore, the exact chemical composition of such an interface is unknown and is not simply a physical mixture of the two contiguous phases. However, their interfacial tensions can be calculated from the measured interfacial thickness between the nylon matrix and the rubber phase, discussed below.

Statistical mechanical theories of polymer interfaces give the scaling relations (4, 5)

$$\gamma_{12} \propto \chi^{1/2} \quad (8)$$

and

$$L \propto \chi^{-1/2} \quad (9)$$

where L is the interfacial thickness and χ the Flory-Huggins χ parameter (3–5). Therefore, we have (3)

$$\gamma_{12} \propto L^{-1} \quad (10)$$

Thus, γ_{12} should be inversely proportional to L. However, least-squares regression of experimental data gave (3)

$$\gamma_{12} = 7.6L^{-0.86} \quad (11)$$

where γ_{12} is in mN/m and L is in nm.

Table 5 shows that *Eq 11* adequately predicts the interfacial thickness between some polymers, measured by small-angle X-ray scattering (SAXS) (6, 7), small-angle neutron scattering (SANS) (8) and transmission electron microscopy (TEM) (9).

The interfacial thickness between nylon and EPX rubbers was measured to be ~50 nm by TEM. Using this value in *Eq 11*, the interfacial tension between nylon and EPX rubbers is calculated to be 0.25 mN/m at 280°C with a probable error of ±0.05 mN/m, as listed in *Table 2*.

As can be seen in *Table 2*, the interfacial tension (at 280°C) between nylon and EP rubbers is the highest (9.7 mN/m), that between PET and EP is somewhat lower (6.2 mN/m), and that between nylon and EPX rubbers is the lowest (0.25 mN/m). This is mainly due to the differences in the polarities of the two phases. That is, the greater the polarity difference, the higher the interfacial tension (3).

Table 5. Comparison of Experimental and Calculated Interfacial Thickness for Some Polymer Pairs.

	Interfacial Thickness, nm			
	Experimental			Calculated from γ_{12} by *Eq. 11*
Polymer Pair	Value	Method	Reference	
Polystyrene vs. polybutadiene	1.3	SAXS	(6)	1.3
	1.4	SANS	(8)	1.3
Polystyrene vs. polyisoprene	1.5	SAXS	(7)	1.3
Polystyrene vs. poly(methyl methacrylate)	5.0	TEM	(9)	6.1

Equation 7 can be rewritten in the form of Good and Girifalco equation (10), i.e.,

$$\gamma_{12} = \gamma_1 + \gamma_2 - 2\Lambda(\gamma_1\gamma_2)^{1/2} \qquad (12)$$

where Λ is the interaction parameter given by (3)

$$\Lambda = \frac{2(1-x_1)(1-x_2)}{g_1(1-x_1)+g_2(1-x_2)} + \frac{2x_1x_2}{g_1x_1+g_2x_2} \qquad (13)$$

where $g_1 = (\gamma_1/\gamma_2)^{1/2}$, $g_2 = (\gamma_2/\gamma_1)^{1/2}$, and x_1 and x_2 are the polarities of the two phases, respectively. It has been shown that Λ has the maximum value of unity, or more exactly, $\Lambda_{max} = 2/(g_1 + g_2)$, and its value decreases with increasing difference in the polarities of the two phases. Thus, the interfacial tension decreases as the polarities of the two phases are more matched (3).

Effective Strain Rate in Extruder

In the extruder, the materials are subjected to complex shear and elongational deformations, and complex temperature profiles along the various sections of the extruder barrel. The materials are fed through the hopper at room temperature, and are transported through the solid-conveying, melting, melt-conveying and mixing zones of the extruder. The temperature increases and reaches the final melt temperature in the mixing zone. The viscosity and the viscosity ratio of the two phases vary with the temperature as they travel through the extruder. Dispersion of the rubber can occur at any stage during the extrusion. Therefore, it is difficult to characterize the type and magnitude of the strain rate in an extruder by a single number. However, an "effective shear rate" may be determined and used as a crude but convenient parameter.

The shear rate in a co-rotating twin screw extruder has been analyzed by Burkhardt and coworkers (11) given by

$$G = (v_o/h)\,|(h^2/2\pi Dn\eta)(dP/dz)|(2y/h) - 1| + \cos\theta| + (2v_o/h)|2 - (3y/h)|\sin\theta \qquad (14)$$

where the first term on the right is due to down-channel flow, and the second term is due to cross flow, $v_o = \pi Dn$ is the linear circumferential screw velocity, D the screw diameter, n the screw revolution per unit time, h the channel depth, θ the helix pitch angle, dP/dz the pressure gradient in the z direction (along the screw helix), y the channel-depth coordinate with $y = 0$ on the barrel surface, and η the melt viscosity. For the present screw and extruder, it can be shown that $(h^2/2\pi Dn\eta)(dP/dz)|(2y/h) - 1| \ll \cos\theta$, and *Eq 14* can be simplified to (12)

$$G \simeq n \qquad (15)$$

where G is the effective shear rate in s^{-1} and n is the screw speed in rpm. We used a screw speed of 200 rpm throughout this work. Thus, the effective shear rate of the extruder was of the order of 200 s^{-1}.

Alternatively, the effective shear rate may be determined by using the theoretical and experimental finding that the dispersed particles have the smallest average size when the viscosities of the two phases are the same. In this method, a series of eight EP rubbers (EP-1 through EP-8) was dispersed in PET matrix by extrusion at 325°C. Note that in this series, the interfacial tensions are the same, but the melt viscosities vary. The number-average particle diameter a_n was the smallest with EP-6, listed in *Table 6*. Thus, PET and EP-6 rubber should have the same viscosity at the effective shear rate of the extruder.

Figure 6 shows the viscosity versus shear rate for PET and some EP rubbers at 325°C. The shear rate at which PET and EP-6 have the same viscosity is found to be about 150 s^{-1}, which should be the effective shear rate of the extruder. This value is quite similar to the value of 200 s^{-1} based on *Eq 15*. Considering the crude nature of these estimates, we therefore somewhat arbitrarily chose the value of 100 s^{-1} as the effective shear rate for this work. Since a constant screw speed was used throughout this work, any error in our particular choice of shear rate would only cause a systematic error, but should not change the qualitative outcome of our studies.

Table 6. Number-Average Particle Diameter of EP Rubbers Dispersed in PET Matrix by Melt Extrusion.

EP Rubber	Viscosity Ratio, p at 100 s^{-1} and 325°C	Number-Average Particle Diameter, a_n, μm
EP-1	2.24	4.3
EP-2	2.04	3.2
EP-3	1.84	2.3
EP-4	1.63	2.5
EP-5	1.53	2.1
EP-6	1.22	1.6
EP-7	0.58	2.8
EP-8	0.94	2.1

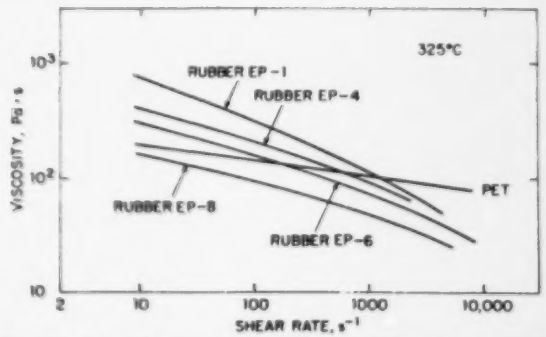

Fig. 6. Viscosity vs. shear rate for PET and some EP rubbers at 325°C, used to determine the effective shear rate of the co-rotating twin screw extruder.

Particle Size and Distribution

The particle size distribution in all the blends was found to obey the log-normal distribution. The differential size distribution data for a nylon/EPX blend are shown in a histogram in *Fig. 7*. The cumulative distribution plot gives a straight line as shown in *Fig. 8*.

The ratios of the weight-average to the number-average particle sizes for all the blends are in the range of 1.8 to 2.4. In the log-normal distribution, the various averages are related to one another by definite relationships (13). We used the number-average particle diameter a_n throughout in this work. Other averages may alternatively be used without changing the qualitative features of our analysis.

Analysis of Dispersion Process

The deformation and breakup of a single Newtonian liquid drop in a Newtonian liquid matrix in uniform and steady shear field was first studied theoretically and experimentally by Taylor (14) in his classic work. Our present system is quite different from Taylor's in many respects, i.e., our drop and the matrix are both viscoelastic, and the strain field is a complex combination of nonuniform, transient shear and elongational fields. Furthermore, the viscoelastic properties of the materials change with the temperature profile along the extruder barrel. Nevertheless, Taylor's analysis provides a basis for analyzing our experimental results.

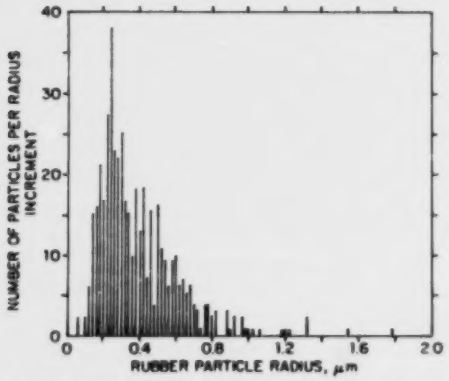

Fig. 7. Histogram for the differential particle size distribution of a nylon Z-1/EPX-11 blend.

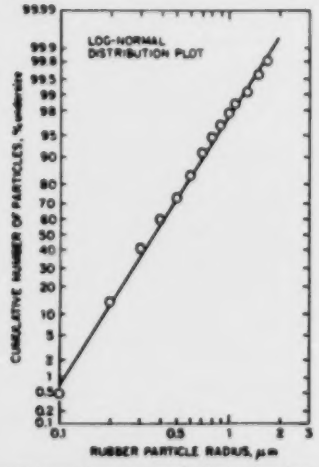

Fig. 8. Cumulative log-normal distribution plot for the particle size of the nylon/rubber blend shown in Fig. 7.

Taylor (14) considered an initially spherical Newtonian drop suspended in a Newtonian matrix in uniform and steady shear field. Upon shearing, the drop is deformed into an ellipsoid with its major axis oriented at an angle ϕ with respect to the direction perpendicular to the flow direction, shown in *Fig. 9*. Several assumptions were made: (a) The drop and the shear rate are sufficiently small so that the inertial effects are negligible; (b) There is no slippage at the drop surface; (c) The tangential stress is continuous at the drop/matrix interface; (d) The normal stress is discontinuous at the interface, and is balanced by the interfacial tension.

The normal stress difference across the drop/matrix interface is given by

$$\delta P_n = -4(G\eta_m/F_o)\sin(2\phi) \qquad (16)$$

where F_o is a function of the viscosity ratio, p, i.e.,

$$F_o = \frac{16p + 16}{19p + 16} \qquad (17)$$

and

$$p = \eta_d/\eta_m \qquad (18)$$

The interfacial capillary stress is given by the Laplace relation,

$$\delta P_i = \gamma(1/C_1 + 1/C_2) \qquad (19)$$

where C_1 and C_2 are the two principal radii of curvature.

The drop will continue to elongate and eventually break up, when the viscous normal stress tending to elongate and disrupt the drop is greater than the interfacial capillary pressure tending to resist the deformation and breakup. Therefore, the condition for drop breakup is $-\delta P_n > \delta P_i$, i.e.,

$$4(G\eta_m/F_o)\sin(2\phi) > \gamma(1/C_1 + 1/C_2) \qquad (20)$$

where the orientation angle $\phi \simeq \pi/4$ at equilibrium (14–18). For small deformations, the drop is roughly spherical, $C_1 \simeq C_2 \simeq a/2$ and $\phi =$

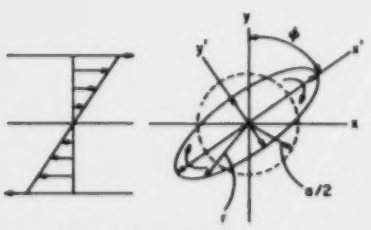

Fig. 9. Drop deformation and orientation in uniform shear.

$\pi/4$. Therefore, the critical condition for drop breakup is given by

$$G\eta_m a/\gamma \geq F_o \quad (21)$$

We propose to extend the Taylor's criterion to the case of viscoelastic drop in a viscoelastic matrix by writing

$$G\eta_m a/\gamma \geq F(p)/\sin(2\phi) \quad (22)$$

where $F(p)/\sin(2\phi)$ is an empirical function of the viscosity ratio p, orientation angle ϕ, and perhaps some still-unknown elastic parameters of the system. The orientation angle ϕ may show either positive or negative deviations from the Newtonian value of $\pi/4$, depending on the viscoelastic properties of the system (18, 19). The left side of *Eq 22* is the Weber number, i.e., the ratio of viscous force to interfacial force.

Of course, such an extension is crude, since the elastic effects are not explicitly treated. However, the elastic effects are implicitly accounted for. A family of $F(p)/\sin(2\phi)$ curves may be obtained; each corresponds to a different elasticity of the system. In the present systems, all the drop phases have a similar elasticity, and all the matrix phases also have a similar elasticity. Furthermore, the drop phase is much more elastic than the matrix phase. Therefore, the various blends have similar viscoelastic characteristics, and have, in a way, the characteristics of the limiting case of a viscoelastic drop in a Newtonian matrix. It is thus perhaps not unreasonable to expect that *Eq 22* could be used to correlate the experimental results for the present systems.

Interfacial and Rheological Effects

Figure 10 plots the number-average particle diameter a_n versus the viscosity ratio p at the effective shear rate of the extruder ($100\ s^{-1}$) and the extruder melt temperature (see also *Table 2*). Curve 1 is for the PET/EP-rubber series; curve 2 is for the nylon Z-2/EP-rubber series; curve 3 is for the nylon Z-1/EP-rubber series; and curve 4 is for the nylon Z-1/EPX-rubber series. The matrix viscosity and the interfacial tension are the same, but the rubber viscosities are different within each series. Note also that the matrix viscosities are the same for curves 3 and 4, but different among the other curves; the interfacial tensions are the same for curves 2 and 3, but are different among other curves.

Figure 11 plots the critical Weber number ($G\eta_m a_n/\gamma$) versus the viscosity ratio p. It can be seen that all the data points for various blends fall into a single master curve. The value ($G\eta_m a_n/\gamma$) appears to have the lowest value at $p \simeq 1$. This means that smallest particles are obtained when the viscosity ratio is about unity. As the viscosity ratio increases above unity or decreases below unity, the dispersed particles become larger.

The portion of the curve for $p > 1$ can be expressed as a straight line, given by

$$G\eta_m a_n/\gamma = 4(\eta_d/\eta_m)^{0.84} \quad \text{for} \quad p > 1 \quad (23)$$

On the other hand, there are only a few data points available for $p < 1$, and so the shape of the curve in this region is uncertain. However, we tentatively draw a V-shaped curve based on some previous observations discussed later. If this is true, then for $p < 1$, we have

$$G\eta_m a_n/\gamma = 4(\eta_d/\eta_m)^{-0.84} \quad \text{for} \quad p < 1 \quad (24)$$

It should be noted that in many polymer/rubber blends, the rubber usually has higher viscosity than the polymer, i.e., $p > 1$.

The master curve (*Fig. 11*) and *Eqs 23* and *24* quantitatively delineate the interfacial and the rheological effects on the size of dispersed phase. *Table 7* illustrates some examples. The effective shear rate is $100\ s^{-1}$. Blends A and B have about the same viscosity ratio $p \simeq 1$, but very different interfacial tensions at a ratio of about 40. Therefore, the particle sizes are very different, having about the same ratio of 52, confirming that particle size is directly proportional to interfacial tension. On the other hand,

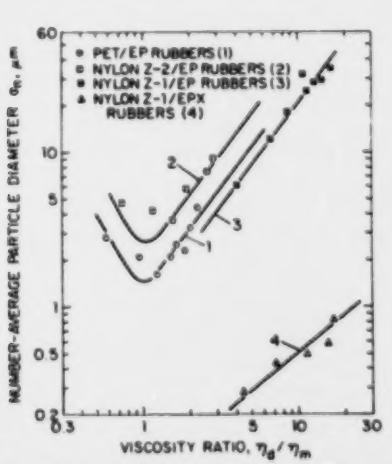

Fig. 10. Equilibrium number-average particle diameter a_n vs. the viscosity ratio $p = \eta_d/\eta_m$. Curve 1 = PET/EP blends; curve 2 = nylon Z-2/EP blends; curve 3 = nylon Z-1/EP blends; curve 4 = nylon Z-1/EPX blends.

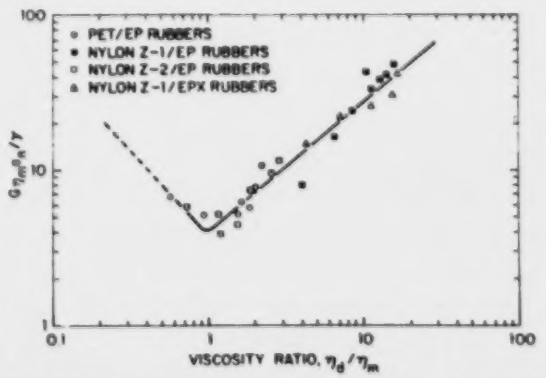

Fig. 11. Dimensionless master curve of $G\eta_m a_n/\gamma$ vs. η_d/η_m for the melt extrusion using a co-rotating twin screw extruder.

blends B and C have the same interfacial tension 0.25 mN/m, but very different viscosities at a ratio of 4.4. Therefore, the particle size are very different, having a ratio of $(4.4)^{0.84} \simeq 3.5$, confirming that the particle size is proportional to $p^{0.84}$. It should be noted that the interfacial tension can be readily varied over wide ranges by using an internal or external dispersant with little effects on bulk properties and viscosity. Therefore, interfacial tension is a much more effective means for controlling the particle size.

Comparison with Previous Work

Previous work (17–20) on the breakup of a single Newtonian drop in a Newtonian matrix in steady uniform shear has shown that drop breakup cannot occur when $p > 4$ or $p < 0.003$. The plot of critical Weber number versus p gives a U-shaped master curve, shown in *Fig. 12*. Drop breakup is the easiest in $0.1 < p < 1$. On the other hand, for a viscoelastic drop in a Newtonian matrix, or a Newtonian drop in a viscoelastic matrix, the master curve becomes more V-shaped, as the elasticity of the system increases (18, 19). Viscoelastic drops can break up even for $p > 4$.

Figure 12 compares the present master curve for viscoelastic systems in co-rotating twin screw extruder with those for Newtonian systems in uniform steady shear (17, 18) and in elongational (hyperbolic) flow (21). Drop breakup occurs much more easily in elongational field than in shear field. In elongational field, drops break up easily even for $p \gg 4$.

In the present system, drop breakup occurs even when $p > 4$. This appears to arise from a combination of several factors: the viscoelastic effects, complex transient shear, complex viscosity/temperature profile along the extruder barrel, and perhaps more importantly the presence of elongational field in the extruder. Previous work on the mixing of polymer melts in Brabender mixer with or without a Koch static mixer has also shown similar effects (22, 23).

Applications to Other Blends

Our results indicate that drop breakup is the easiest when $p \simeq 1$, other factors being equal. Let us consider the case for $p = 1$. *Eq 23* becomes

$$(a_n)_{min} \simeq 4\gamma/G\eta_m \quad \text{for} \quad p \simeq 1 \qquad (25)$$

which may be used to estimate the minimum particle diameter $(a_n)_{min}$ obtainable for a given polymer pair. Let us consider the case where $G = 100\ s^{-1}$ and $\eta_m = 100$ Pa·s. The measured interfacial tensions at 180°C for a number of polymer pairs are listed in *Table 8*. Using *Eq 25*, $(a_n)_{min}$ is calculated and listed in *Table 8*. The particle sizes obtainable (ranging from 0.16 to 4.1 μm) are directly proportional to the interfacial tension (ranging from 0.4 to 10.2 mN/m). These estimates are qualitatively consistent with previous observations (22, 23).

In the present work, only one mode of dispersion was observed, i.e., the minor phase was dispersed into spheroidal particles. This is particularly desirable for this study, as it simplifies our analysis. However, other modes of dispersion may be obtained under different conditions (volume ratio, strain field, and elastic effects), such as lamellar sheets, fibrils, or spheroids with connecting fibrils (24, 25). However, the

Table 7. Effects of Interfacial Tension and Viscosity Ratio on the Dispersed Particle Size.

Code	Blend	η_m, Pa·s	γ_{12}, mN/m	p	a_n, μm: Calc. by *Eq 23*	a_n, μm: Expti.
A	Z-2/EP	110	8.8	~1	3.2	4.2
B	Z-2/EPX	110	0.25	~1	0.09	0.08
C	Z-1/EPX	130	0.25	4.4	0.27	0.28

(Note) $G = 100 s^{-1}$.

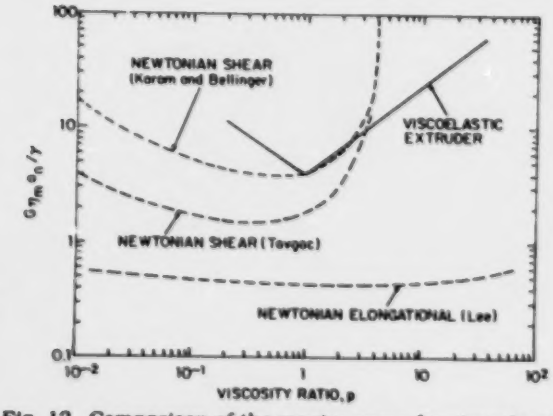

Fig. 12. Comparison of the master curve for viscoelastic blends in co-rotating twin screw extruder with those for Newtonian liquids in steady uniform shear and in elongational (hyperbolic) flow.

Table 8. Predicted Minimum Number-Average Particle Diameter for Various Polymer Pairs for $p = 1$.

Polymer Pair	γ_{12}, at 180°C mN/m	Predicted $(a_n)_{min}$, μm
Polystyrene and polychloroprene	0.4	0.16
Polyethylene and polypropylene	0.8	0.32
Polystyrene and poly(methyl methacrylate)	1.1	0.44
Polyethylene and poly(ethylene-*stat*-vinyl acetate), 25 wt% VAc	1.2	0.48
Poly(methyl methacrylate) and poly(n-butyl methacrylate)	1.5	0.60
Polyoxyethylene and polyoxytetramethylene	3.7	1.5
Polyethylene and polystyrene	5.1	2.1
Polyisobutylene and poly(vinyl acetate)	6.7	2.7
Polyethylene and poly(methyl methacrylate)	9.0	3.6
Polyethylene and poly(vinyl acetate)	10.2	4.1

(Notes) $G = 100\ s^{-1}$; $\eta_m = 100$ Pa·s.
Interfacial tensions are taken from Ref. 3.

concept developed here should be generally (if qualitatively) applicable.

CONCLUSION

The formation of dispersed phase during melt blending with a co-rotating twin screw extruder can be described by a master curve relating the Weber number $G\eta_m a_n/\gamma$ to the viscosity ratio $p = \eta_d/\eta_m$. The particle size is directly proportional to the interfacial tension and $p^{0.84}$ for $p > 1$ or $p^{-0.84}$ for $p < 1$. Thus, the particle size is smaller when the interfacial tension is lower, and the viscosity ratio is closer to unity. Smallest particles are obtained when $p \simeq 1$, other factors being equal. However, the interfacial tension can be more readily varied over a wide range than the viscosity with little effects on bulk properties by controlling the polarities or using dispersants.

Viscoelastic drops can break up during extrusion even for $p > 4$, because of elastic effects, the presence of an elongational field, and the complex viscosity-temperature profile along the extruder barrel. This is different from the case of a Newtonian drop in a Newtonian matrix in uniform steady shear.

NOMENCLATURE

- a = particle diameter.
- a_n = number-average particle diameter.
- C_j = principal radius of curvature in the j direction.
- D = screw diameter.
- dP/dz = pressure gradient along screw helix.
- EP = ethylene-propylene rubber (non-reactive), *Table 1*.
- EPX = ethylene-propylene rubber (reactive), Table 1.
- $F_d(p)$ = Newtonian correction function for reduced shear.
- $F(p)$ = non-Newtonian correction function for reduced shear.
- G = shear rate, or effective shear rate.
- g_j = $(\gamma_j/\gamma_i)^{1/2}$.
- h = screw channel depth.
- L = interfacial thickness.
- L/D = length to diameter ratio of capillary tube.
- n = screw speed in revolution per unit time.
- PET = poly(ethylene terephthalate), *Table 1*.
- p = viscosity ratio, η_d/η_m.
- rpm = revolution per minute.
- SANS = small-angle neutron scattering.
- SAXS = small-angle X-ray scattering.
- T = temperature.
- TEM = transmission electron microscopy.
- v_o = screw circumferential velocity.
- x = polarity.
- y = coordinate along screw channel depth.
- Z-1 = nylon 66 resin, *Table 1*.
- Z-2 = nylon 66 resin, *Table 1*.
- β = viscosity power law coefficient.
- δP_i = capillary pressure across drop/matrix interface.
- δP_n = viscous normal stress across drop/matrix interface.
- γ = surface or interfacial tension.
- γ^d = nonpolar (dispersion) component of γ.
- γ^p = polar component of γ.
- γ_{12} = interfacial tension.
- η = viscosity.
- η_d = viscosity of the drop.
- η_m = viscosity of the matrix.
- η_o = viscosity power law coefficient.
- θ = screw helix pitch angle.
- Λ = interaction parameter of Good and Girifalco.
- ϕ = drop orientation angle.
- χ = Flory-Huggins interaction parameter.

REFERENCES

1. S. Wu, *Polymer*, **26**, 1855 (1985).
2. S. Wu, *J. Polym. Sci. Polym. Phys. Ed.*, **21**, 699 (1983).
3. S. Wu, "Polymer Interface and Adhesion," Marcel Dekker, New York (1982).
4. E. Helfand and A. M. Sapse, *J. Chem. Phys.*, **62**, 1327 (1975).
5. J. Noolandi, *Polym. Eng. Sci.*, **24**, 70 (1984).
6. R. J. Roe, M. Fishkis and J. C. Chang, *Macromolecules*, **14**, 1091 (1981).
7. T. Hashimoto, A. Todo, H. Itoi and H. Kawai, *Macromolecules*, **10**, 377 (1977).
8. F. S. Bates, C. V. Berney and R. E. Cohen, *Macromolecules*, **16**, 1101 (1983).
9. H. Van Oene and H. K. Plummer, *Preprints, Org. Coat. Plast. Chem.*, American Chemical Society, **37**(2), 498 (1977).
10. L. A. Girifalco and R. J. Good, *J. Phys. Chem.*, **61**, 904 (1957).
11. K. Burkhardt, H. Herrmann, and S. Jakopin, *SPE ANTEC Tech. Papers*, **36**, 498 (1978).
12. Courtesy of Werner & Pfleiderer Corporation, 663-T, East Crescent Avenue, Ramsey, NJ 07446.
13. L. Silverman, C. E. Billings, and M. W. First, "Particle Size Analysis in Industrial Hygiene," Academic Press, New York (1971).
14. G. I. Taylor, *Proc. R. Soc. London*, **226A**, 34 (1954); *ibid.*, **138A**, 41 (1932).
15. R. Cerf, *J. Chem. Phys.*, **48**, 59 (1951).
16. R. Roscoe, *J. Fluid Mech.*, **28**, 273 (1967).
17. H. J. Karam and J. C. Bellinger, *Ind. Eng. Chem., Fundam.*, **7**, 576 (1968).
18. T. Tavgac, Ph.D. Dissertation, Chemical Engineering Department, University of Houston, Houston, Texas (1972).
19. R. W. Flumerfelt, *Ind. Eng. Chem., Fundam.*, **11**, 312 (1972).
20. S. Torza, R. G. Cox, and S. G. Mason, *J. Colloid Interf. Sci.*, **38**, 395 (1972).
21. W. K. Lee, Ph.D. Dissertation, Chemical Engineering Department, University of Houston, Houston, Texas (1972).
22. K. Min, J. L. White, and J. F. Fellers, *Polym. Eng. Sci.*, **24**, 1327 (1984).
23. H. P. Schreiber and A. Olguin, *Polym. Eng. Sci.*, **23**, 129 (1983).
24. R. Fayt, R. Jerome, and Ph. Teyssie, *Polym. Eng. Sci.*, this issue.
25. H. Van Oene, *J. Colloid Interf. Sci.*, **40**, 448 (1972).

Phase Transitions During Shear Flow of Two-Phase Polymer Blends

I. Theory. Transition to "Homogeneous" Melt State

J. LYNGAAE-JØRGENSON *and* K. SØNDERGAARD

Instituttet for Kemiindustri
The Technical University of Denmark
2800 Lyngby, Denmark

A hypothesis for critical conditions for a transition from a two-phase system to a homogeneous state during simple shear flow is advanced. It is predicted that at sufficiently high shear stress a homogeneous state is the stable steady state structure.

INTRODUCTION

Since Silberberg and Kuhn (1) in 1952 reported that a homogeneous one-phase solution results if a velocity gradient is maintained in a stable two-phase system, a number of studies have been performed on such systems and a number of theories have been developed.

Rangel-Nafaile, Metzner and Wissbrun (2) reviewed studies on solubility phenomena in deforming solutions and developed an expression for stress-induced phase separation in polymer solutions. Other recent studies in this field were published by Wolf *et al.* (3–7), by Mazich and Carr (8), and by Vrahopoulou-Gilbert and McHugh (9). There is no general consensus as to the influence of stress during flow on phase equilibria at present, and in fact observations from different sources are conflicting.

Most observations of dilute solutions with upper critical solution temperatures indicate that phase separation may be provoked by mechanical deformation (2), or stated differently, that the critical solubility temperature is increased by flow. Wolf *et al.* (3–7), however, developed a theory which predicts that the solubility temperature is decreased by flow, and this is in accordance with Silberberg's (1) observations. Wolf calculated the equilibrium size of droplets formed in a phase-separated system. From a force balance, he derived an expression saying that the equilibrium droplet size r is a decreasing function of shearing rate and that when r approaches the radius of gyration of the polymer molecules, redissolution will have occurred.

In this paper, we develop an expression for a critical stress for a phase transition to a homogeneous one-phase system during simple shear flow of an incompatible blend. The main purpose of this research is to investigate the possibility of producing systems with co-continuous interpenetrating phases with very large interfaces. Such a structure is predicted for a homogeneous blend which, without shearing, would be within the spinodal part of a phase diagram if the shearing is stopped. Phase separation would follow the spinodal decomposition mechanism and within volume fractions of 0.15 to 0.85 give rise to an interconnected co-continuous phase structure (10, 11).

THEORETICAL

The free energy of a closed system of two components without flow is a function of state and is in principle given where, say, three intensive state parameters are given (temperature, pressure, and composition). A truly comprehensive number of theories have been formulated that may be used to calculate the chemical potential of a mixture. Many of these expressions may be written as (12):

$$(\mu_A - \mu_A^0)_{mix} = RT\left[\frac{1}{\bar{X}_A}\ln\Phi_A + \left(\frac{1}{\bar{X}_A} - \frac{1}{\bar{X}_B}\right)\Phi_B + \chi^*\Phi_B^2 + F\right] \quad (1)$$

where μ_A is the chemical potential per repeat unit of polymer A; μ_A^0 is the chemical potential of pure A in the reference state; $\bar{X}_A$ is the number of A repeat units per molecule of polymer A; $\bar{X}_B$ is the equivalent number of A repeat units in polymer B; Φ_A and Φ_B are volume fraction of polymer A and polymer B, respectively; R is the gas constant; T is absolute temperature; χ^* is a function related to the (classical) Flory-Huggins interaction parameter, χ; and F is a complex function, dominated by free volume effects.

At low temperatures or high pressures

$$\chi^* \to \chi \quad \text{and} \quad F0.$$

If the system is placed in a simple shear flow field we assume that the free energy is determined by temperature, pressure, composition, degree of orientation, α_x, and number of "effective interfacial sites," N^*:

$$\Delta F_T = F_1(P, T, \Phi_A, \alpha_x, N^*) \tag{2}$$

The free energy is an increasing function of interfacial area, A:

$$\Delta F_T = F_2(P, T, \Phi_A, \alpha_x, A) \tag{3}$$

but it is argued that the area may be substituted by an apparent quantity called effective interfacial sites, N^*, defined so that ΔF is the same with A and N^*, all other factors being equal. N^* is measured in entanglement equivalents. By this substitution we replace a necessary and sufficient criterion with a necessary but not sufficient criterion. N^* is a fictitious quantity that cancels out during the derivation.

Furthermore, we assume that the total free energy consists of two contributions:

$$\Delta F_T = \Delta F_{mix} + \Delta F_{el}$$

The first term on the right side corresponds to the change in free energy on mixing. The second part is a contribution due to the flow field—namely by virtue of the entanglement concept (13) and $\Delta F_{el} = F_1(P, T, \alpha_x, N^*)$. The chemical potential corresponding to the elastic part is found by differentiation of ΔF_{el}.

We consider a dispersed system and look for the differential changes corresponding to transfer of A-units from the two-phase state to a homogeneous melt state.

Before "homogenization", we have two phases (one of which is assumed to be nearly pure polymer A), we have interfaces (corresponding to an unknown number of effective interfacial sites N^*) both phases and interfaces in an oriented state. After homogenization, we have one phase in an oriented state.

The change in chemical potential corresponding to transfer of units from the two-phase to the one-phase state is

μ_A, homogeneous phase $-$ μ_A, two-phase and

μ_B, homogeneous phase $-$ μ_B, two-phase

We have two contributions in connection with the transfer: 1) a mixing contribution and 2) an elastic contribution due to interphase destruction. The mixing contribution for a nonoriented system is: $(\mu_A - \mu_A^0)_{mix}$ and is given by *Eq 1*. In the following, component A is the component where:

$$(\mu_A - \mu_{ref.A})_{mix.}^{max.} \geq (\mu_B - \mu_{ref.B})_{mix.}^{max.}$$

Since the change will be evaluated at constant stress and we assume that the stress is the same in phase A and phase B, we get $\Delta F_{el,A} = \Delta F_{el,B}$ and, consequently, that the contribution of orientation is independent of state. Therefore,

$$(\mu_{A,oriented} - \mu_{A,oriented}^0)_{mix} = (\mu_A - \mu_A^0)_{mix}$$

A critical condition for a transition from a two-phase system to one single homogeneous phase is that we can transfer differential amounts of the components from the two-phase system to a homogeneous phase in such a way that the contribution to the free energy is always negative or zero, or that:

$$(\mu_A - \mu_{ref})_{el} + (\mu_A - \mu_{ref})_{mix.}^{max.} \leq 0$$

for component A,

where the reference state might be taken as the A rich phase of the two-phase system. For convenience, we use the standard reference state μ_A^0 (pure amorphous A). If the composition of the A rich phase (discrete phase) is not nearly pure A, a contribution—$(\mu_{A,discrete\ phase} - \mu_A^0)$—must be added to *Eq 4*. However, this contribution is usually small.

$$(\mu_A - \mu_A^0)_{el} + (\mu_A - \mu_A^0)_{mix.}^{max.} \leq 0. \tag{4}$$

The approach is based on the fact that (14):

a) The equations of state are valid in the steady state.
b) The reversible processes are separable over definable steady state paths.
c) The necessary thermodynamic functions are definable for the steady state.

At isothermal conditions, we assume that the melt behaves as a lightly crosslinked network with nonpermanent network points. The elastic part is evaluated as the destruction of in the surface localized extra entanglements in a continuous phase with nonpermanent crosslinks (entanglements).

In this evaluation, the final state is a state without these extra entanglements, and the starting state is the state with these localized surface sites.

The change is defined as:

$$(\Delta\mu_A)_{el} = (\mu_{A,final} - \mu_{A,start})_{el} = -\frac{1}{A}\left(\frac{\partial \Delta F_{el}}{\partial N^*}\right)_{T,P,\alpha_x}$$

where both states are oriented states. A is the number of repeat units per chain between entanglements.

Equation 4 can be written:

$$(\Delta\mu_A)_{el} + (\mu_A - \mu_A^0)_{mix.}^{max.} \leq 0 \tag{5}$$

The elastic free energy function at steady state is assumed to be given by an equation of state of the form:

$$\Delta F_{el} = F_3(P, T, \alpha_x, N)$$

$$d\Delta F_{el} = \left(\frac{\partial \Delta F_{el}}{\partial P}\right)_{T,\alpha_x,N} dP + \left(\frac{\partial \Delta F_{el}}{\partial T}\right)_{P,\alpha_x,N} dT + \left(\frac{\partial \Delta F_{el}}{\partial \alpha_x}\right)_{P,T,N} d\alpha_x + \left(\frac{\partial \Delta F_{el}}{\partial N}\right)_{P,T,\alpha_x} dN$$

for ΔF_{el}, P, and T constant:

$$\left(\frac{\partial \Delta F_{el}}{\partial N}\right)_{P,T,\alpha_x} = -\left(\frac{\partial \Delta F_{el}}{\partial \alpha_x}\right)_{P,T,N}\left(\frac{\partial \alpha_x}{\partial N}\right)_{P,T,\Delta F_{el}} \quad (6)$$

In the following text, the case where $\alpha_x \gg 1$ is considered. P is the pressure, T is absolute temperature, α_x is a conformational tensor component α_{11}, and N is the number of entanglements per unit volume.

$$\Delta F_{el} = NRT\, F_4(\underline{\alpha}) \simeq \tfrac{1}{2}\, NRT\alpha_x^2$$

(a first approximation) (7)

$$\tau_{11} \cong NRT\alpha_x^2$$

or

$$\Delta F_{el} \cong \tfrac{1}{2}\, \tau_{11} \quad (8)$$

and τ_{11} is uniquely related to $\tau_{21} = \tau$

Equation 6 can now be written:

$$\left(\frac{\partial \Delta F_{el}}{\partial N}\right)_{P,T,\alpha_x} = -\left(\frac{\partial \Delta F_{el}}{\partial \alpha_x}\right)_{P,T,N}\left(\frac{\partial \alpha_x}{\partial N}\right)_{P,T,\tau} \quad (9)$$

where x, y, and z are the principal axes of deformation of the chains between entanglements; x represents the largest deformation.

If equivalent surface restricted entanglements and entanglements (crosslinks) are assumed equivalent, we have:

$$\left(\frac{\partial \alpha_x}{\partial N}\right)_{P,T,\tau} = \left(\frac{\partial \alpha_x}{\partial N^*}\right)_{P,T,\tau}$$

Near the transition to homogeneous phase, we assume:

$$(N^* + N)RT\alpha_x^2 \cong NRT\,\alpha_x^2$$

where N is the number of entanglements per unit volume, i.e., entanglement density.

$$\Delta F_{el} = \frac{NRT}{2}\left(\alpha_x^2 + \alpha_y^2 + \frac{1}{\alpha_y^2\alpha_x^2} - 3\right) \quad (10)$$

For $\alpha_x \gg 1$

$$\Delta F_{el} = \frac{NRT}{2}\,\alpha_x^2$$

$$\left(\frac{\partial \Delta F_{el}}{\partial N}\right)_{P,T,\alpha_x} = \tfrac{1}{2}\, RT\alpha_x^2 \quad (11)$$

In order to introduce directly measurable quantities in the final expressions, the following derivation is used. A number of assumptions are made, e.g., randomly coiled linear polymer molecules, isothermal conditions, constant volume, the molecular weights (M) are much larger than the critical molecular weight (M_c) for entanglement formation, constant segment concentration, intertial forces neglected (etc.).

Steady state uniaxial extensional flow is considered. Astarita and Marucci (15) express the energy equation under isothermal conditions as follows:

$$P = D + \dot{U}_{el} \quad (12)$$

where P is the stress power, i.e., the work done by internal stresses per unit time, D is the rate of energy dissipation, and $\dot{U}_{el}$ is the rate of change of elastic energy. At steady state, $\dot{U}_{el} = 0$, consequently $\tau_{11} = \tau_{11,f}$ from *Eq 12*, where $\tau_{11,f}$ is a "frictional stress." At high rates of deformation ($\lambda\dot{\epsilon} > 1$) and $\bar{M}_w \gg M_c$, we assume that the outer force is balanced by the elastic response of the deformed entanglement network, $\tau_{11} = \tau_{11,el}$, where $\tau_{11,el}$ is an elastic stress. In the stationary state, we have:

$$\tau_{11,el} = \tau_{11} = \tau_{11,f} \quad (13)$$

meaning simply that in the stationary state, an equilibrium deformed state of the nonpermanent entanglement network is maintained by frictional forces in the entanglements.

Turning to a single polymer molecule, we define total forces acting on a single polymer molecule by assuming that a total elastic force, f_{el}, and a total frictional force, f_f, per molecule can be related to the stresses in *Eq 13* by multiplication with a scaling factor that is proportional to the number of polymer molecules per unit volume or:

$$f_{el} = f_f \quad (14)$$

The deformation state of a single molecule is defined by an orientation tensor, $\underline{\alpha}$, which for uniaxial extensions is defined as:

$$\underline{\alpha} = \begin{pmatrix} \alpha_x & 0 & 0 \\ 0 & \alpha_y & 0 \\ 0 & 0 & \alpha_z \end{pmatrix} = \begin{pmatrix} \alpha_{11} & & 0 \\ 0 & \alpha_{22} & 0 \\ 0 & 0 & \alpha_{33} \end{pmatrix} \quad (15)$$

where x is the extensional direction and y and z perpendicular directions $\alpha_x = \alpha_y = \alpha_z = 1$ for an undeformed, fully relaxed state. We define the elastic force in analogy with the procedure used in rubber elasticity theory:

$$\Delta F_{el} = \frac{\nu\, RT}{2}(\alpha_x^2 + \alpha_y^2 + \alpha_z^2 - 3),$$

$$\alpha_x \cdot \alpha_y \cdot \alpha_z = 1 \quad (16)$$

$$f_{el} = \frac{\partial \Delta F_{el}}{L_0 \partial \alpha_x}$$

where F_{el} is the free energy per polymer molecule with ν effective entanglements and obtain:

$$f_{el} = \nu\,\frac{RT}{L_0}\left(\alpha_x - \frac{1}{\alpha_x^2}\right); \qquad \nu = \frac{c\,\bar{M}_n}{\rho\, M_c} \quad (17)$$

where L_0 has the dimension of length, c is the polymer concentration, ρ is polymer density, $\bar{M}_n$ is polymer molecular weight, M_c is the molecular weight between entanglements, R is the gas constant, and T is absolute temperature.

$$f_f = \nu\xi(\underline{\alpha})\, L''\dot{\epsilon} \quad (18)$$

where ξ is a frictional factor per entanglement, L'' is a scaling factor, and $\dot{\epsilon}$ is the rate of deformation.

It is assumed that frictional resistance is dominated by entanglement friction.

We write $$\tau_f = \frac{c}{\bar{M}} L' f_f = \frac{c}{\bar{M}} L' \nu L'' \xi \dot{\epsilon} \tag{19}$$

$$\eta_T = \frac{\tau_f}{\dot{\epsilon}} = \frac{c}{\bar{M}} L' L'' \nu \xi \tag{20}$$

where η_T is the Trouton viscosity, $\bar{M}$ is an average molecular weight, and L' is a scaling factor. For $\dot{\epsilon} \to 0 \to \eta_T \to \eta_{T,0} \cdot \eta_{T,0} = \frac{c}{\bar{M}} L' L'' \nu \xi$ (1). Since $\eta_{T,0}$ is a unique function of $\bar{M}_w$, $\bar{M}$ may be equal to $\bar{M}_w$. If ξ is a function of α_x only, we may write

$$\frac{\eta_T}{\eta_{T,0}} = F(\alpha_x) \tag{21}$$

By analogy with *Eq 19*, we write

$$\tau_{el} = \frac{c}{\bar{M}_w} L' f_{el} = \frac{c^2 RT}{\rho M_c} \frac{\bar{M}_n}{\bar{M}_w} \frac{L'}{L_0} \left(\alpha_x - \frac{1}{\alpha_x^2} \right) \tag{22}$$

or since $\tau_{11,el} = NRT(\alpha_x^2 - \alpha_z^2)$, we must assume that $\frac{L'}{L_0} = \frac{\alpha_x}{a'}$, where a' is a constant and N is the entanglement density (the number of entanglements per unit volume).
Insertion in *Eq 13* gives:

$$F'(\alpha_x) = a' \frac{\eta_{T,0} (\bar{M}_w/\bar{M}_n) M_c \rho}{c^2 RT} \dot{\epsilon} = a' \lambda \dot{\epsilon} \tag{23}$$

where λ is a time constant.

Alternatively,

$$F''(\alpha_x) = \frac{\tau_{11}}{K_1} \tag{24}$$

where $K_1 = \frac{\eta_{T,0}}{\lambda}$

Thus, the viscosity function from *Eq 21* may be expressed in one of the forms:

$$\frac{\eta_T}{\eta_{T,0}} = F_1(\lambda \dot{\epsilon}) \quad \text{or} \quad \frac{\eta_T}{\eta_{T,0}} = F_2\left(\frac{\tau}{K_1}\right) \tag{25}$$

The hypothesis is: if steady state can be reached, a plot of dimensionless viscosity against dimensionless extension rate or dimensionless stress is a master curve for materials with the same "frictional properties".

The maximum relaxation time estimated by stress relaxation measurements indicate that if $\lambda_{max} = a'\lambda \Rightarrow a' \approx 1$ (16).

For simple shearing steady state flow between parallel planes, a hypothesis was established assuming that a single polymer molecule as an average over space and time may be deformed from a state where most or all molecule segments (repetition units) are distributed within a sphere into a state where the segments are contained in a deformed body with elliptical main-cross-sections and main axes deformed according to deformation ratios α_x', α_y', and α_z'. The average orientation in chains between entanglements is tilted some angle relative to the flow direction. Deformation ratios after principle axes are α_x, α_y, α_z. However, if the minimum entropy production principle governs the steady state and if the friction in neighboring entanglements increases with the velocity difference between two neighboring entanglements, the body containing the segments of a polymer molecule may have its largest deformation ratio nearly in the flow direction. In general we may write the elastic free energy of an entangled system (at least as a good approximation) as (17):

$$\Delta F_{el} = \frac{NRT}{2} (\alpha_x^2 + \alpha_y^2 + \alpha_z^2 - 3)$$

where α_x, α_y, and α_z are deformation ratios of the chains between entanglements (crosslinks) after principal axes. These axes may be tilted with respect to the direction of sliding.

The elastic shear stress is then (18): $\tau_{21,el} = NRT\left(\alpha_x - \frac{1}{\alpha_x}\right)$. We write these expressions per polymer molecule as

$$\Delta F_{el} = \frac{\nu RT}{2} (\alpha_x^2 + \alpha_y^2 + \alpha_z^2 - 3)$$

$$\text{and} \quad f_{el} = \nu RT \left(\alpha_x - \frac{1}{\alpha_x}\right) = f_f \tag{26}$$

It is again assumed that the stresses are proportional to the number of polymer molecules per unit volume or:

$$\tau_{21,el} \propto \frac{c}{\bar{M}_w} L' f_{el} \quad \text{and} \quad \tau_{21,f} \propto \frac{c}{\bar{M}_w} L' f_f$$

which in general may be written:

$$\tau_{21,el} = b\, \tau_{21,f} \tag{27}$$

where b is a constant.

If the polymer molecules at high shear stresses are deformed nearly in the flow direction (direction 1), that is, if the principal axes of the chains nearly coincide with direction 1 and if the polymer molecule as a hole is deformed to a compressed body with the largest dimension in direction 1, it may be predicted that:

$$\tau_{11,el} \cong b \frac{c}{\bar{M}_w} \alpha_1 f_{el}, \qquad b \text{ is a constant where}$$

$$\alpha_x \cong \alpha_1, \ \alpha_y \cong \alpha_2, \ \alpha_z, = \alpha_3$$

In general, $\alpha_1 = \alpha_x \cos \Phi$, where Φ is the angle between the average direction of the principal axis of the largest deformation of chains between entanglements and the flow direction. In the non-Newtonian range it may be assumed that Φ is small.

In general, one should then expect that $\tau_{11} = G(\varrho) \frac{c}{\bar{M}_w} L' f_{el}$ and $\tau_{21} \overset{\alpha}{=} \frac{c}{\bar{M}_w} L' f_f$ and from *Eq 14*

$$\tau_{11} = G(\varrho) \frac{c}{\bar{M}_w} L' f_{el} = G(\varrho)\, b\, \tau_{21},$$

where $G(\varrho)$ is a function of $(\alpha_x, \alpha_y, \alpha_z)$, which as a first approximation may be written

$$|\tau_{11}| = b' \cdot \alpha_x^q \cdot |\tau_{21}| \tag{28}$$

The relation between total frictional force, f_f, on a single polymer molecule and shear stress is written as $\tau_{21} = \frac{c}{M_W} L' f_f$ and $f_f = \nu \xi \Delta u = \nu \xi F(\alpha_2) \cdot \dot{\gamma}$, where Δu is the average velocity difference between neighboring entanglements, ν is the number of entanglements per polymer molecule, $\xi(\varrho)$ is an average frictional coefficient per entanglement, and $\dot{\gamma}$ is the shear rate. Direction 1 is the flow direction, direction 2 is that of the velocity gradient, and direction 3 is the "neutral" direction.

Postulating that the volume of a body containing segments of a single polymer molecule is constant gives:

$$\alpha_x \cdot \alpha_y \cdot \alpha_z = 1 \tag{29}$$

and using the empirical relation:

$\frac{\tau_{33} - \tau_{22}}{\tau_{11} - \tau_{22}} \cong 0.1$ and the relations

$\tau_{11} - \tau_{22} = G'(\varrho)\, K_1(\alpha_x^2 - \alpha_y^2)$,

$\tau_{11} - \tau_{33} = G'(\varrho)\, K_1(\alpha_x^2 - \alpha_z^2)$ and

$\tau_{22} - \tau_{33} = G'(\varrho)\, K_1(\alpha_y^2 - \alpha_z^2)$ one can express

α_x, α_y, and α_z as functions of $\lambda\dot{\gamma}$ or $\frac{\tau_{21}}{K_1}$.

Since the functions $\frac{\eta}{\eta_0}$, $\frac{1}{K_1}(\tau_{11} - \tau_{22})$ and $\frac{1}{K_1}(\tau_{22} - \tau_{33})$ are functions of ϱ, one obtains:

$$\frac{\eta}{\eta_0} = F_3(\lambda\dot{\gamma}) \quad \text{or} \quad \frac{\eta}{\eta_0} = F_3'\left(\frac{\tau_{21}}{K_1}\right) \tag{30}$$

$$\frac{1}{K_1}(\tau_{11} - \tau_{22}) = F_4(\lambda\dot{\gamma})$$

$$\text{or} \quad \frac{1}{K_1}(\tau_{11} - \tau_{22}) = F_4'\left(\frac{\tau_{21}}{K_1}\right) \tag{31}$$

$$\frac{1}{K_1}(\tau_{22} - \tau_{33}) = F_5(\lambda\dot{\gamma})$$

$$\text{or} \quad \frac{1}{K_1}(\tau_{22} - \tau_{33}) = F_5'\left(\frac{\tau_{21}}{K_1}\right) \tag{32}$$

The relations represented by *Eqs 30* and *31* are found to represent groups of materials well (16, 19).

Application of *Eq 27*

$$\tau_{21,el} = b\, \tau_{21,f} \tag{27}$$

with $\tau_{21,el} = \frac{c}{\bar{M}_W} L' \nu RT \left(\alpha_x - \frac{1}{\alpha_x}\right)$

where $\nu = \frac{c\,\bar{M}_n}{\rho\, M_c}$ (*Eq 17*) gives

$$L' \frac{c^2 RT}{\rho \frac{\bar{M}_W}{\bar{M}_n} M_c} \alpha_x = b\, \tau_{21}; \quad \frac{\bar{M}_W}{\bar{M}_n} = H, \quad \frac{b}{L'} = a \tag{33}$$

$$\alpha_x = a \frac{\rho\, HM_c}{c^2\, RT} \tau_{21}$$

Insertion of *Eq 33* in *Eq 11* gives:

$$\left(\frac{\partial \Delta F_{el}}{\partial N}\right)_{P,T,\alpha_x} = \tfrac{1}{2}\, RT\alpha_x^2$$

$$= \frac{a^2\rho^2 H^2 M_c^2}{2c^4\, RT} \tau_{21}^2; \qquad \left(\frac{\partial \Delta F_{el}}{\partial N}\right)_{P,T,\alpha_x}$$

is expressed in terms of energy per chain between entanglements. Consequently, $A = \frac{M_c}{M_A}$

$$\Delta\mu_{el} = -\frac{1}{A}\left(\frac{\partial \Delta F_{el}}{\partial N}\right)_{P,T,\alpha_x} \tag{34}$$

$$= -\frac{a^2\rho^2 M_A H^2 M_c}{2c^4\, RT} \tau_{21}^2$$

where M_A is the molecular weight of a repetition unit of the A phase (the discrete phase). The rest of the symbols are defined for the B phase.

The derivation presented above rests on a number of assumptions. It is not a "theory" with "a priori" validity since it is not derived from first principles alone. However, the assumptions leads to a number of hypotheses such as *Eqs 30*, *31*, and *32*, which are in good agreement with experimental data (16, 19). Furthermore, *Eq 34* for $\Delta\mu_{el}$ together with an expression for the chemical potential change on melting (20) leads to an expression for the melting point of samples with low degree of crystallinity in simple shear flow, which is in reasonable accordance with experimental data (16).

The average value of the constant a in *Eq 34* is found from the melting point model to be: $a = 7.7$. This value of a is (of convenience) found using for the critical molecular weight, the molecular weight where the exponent in the equation $\eta_0 = K \cdot \bar{M}_w^n$ changes from ~1 to ~3.5. (This means that we use an estimate that is approximately two times the molecular weight between entanglements.)

Insertion of *Eq 1* and *Eq 34* in *Eq 5* leads to:

$$\tau_c^2 = Q\, RT^2 \cdot \left\{\frac{1}{\bar{X}_A} \ln \Phi_A + \Phi_B\left(\frac{1}{\bar{X}_A} - \frac{1}{\bar{X}_B}\right) + \chi^* \Phi_B^2 + B\right\} \tag{35}$$

where

$$B = \frac{1}{\tilde{T}_A}\left[(\tilde{\rho}_A - \tilde{\rho}) + \tilde{P}_A(\tilde{v} - \tilde{v}_A) + \tilde{T}_A\left((\tilde{v} - 1)\ln(1 - \tilde{\rho}) - (\tilde{v}_A - 1)\ln(1 - \tilde{\rho}_A) + \frac{1}{\bar{X}_A}\ln\frac{\tilde{\rho}}{\tilde{\rho}_A}\right)\right] \quad (36)$$

(in accordance with the lattice fluid theory (21)).

$$Q = 0.035\,\frac{\rho_B^2 R}{M_A M_{C,B} H_B^2}$$

and $\chi^* = \tilde{\rho}(\chi + (1 - \frac{v_A^*}{v_B^*}\lambda_{AB})) \approx \chi$

For $B \approx 0$ and $\chi^* \simeq \chi$:

$$\tau_c^2 = Q\,RT^2 \cdot \left\{\frac{1}{\bar{X}_A}\ln\Phi_A + \left(\frac{1}{\bar{X}_A} - \frac{1}{\bar{X}_B}\right)\Phi_B + \chi\Phi_B^2\right\} \quad (37)$$

where a tilt ~ symbolizes reduced variables of state, τ_c is the critical stress for phase transition to homogeneous state, Φ_A and Φ_B are the volume fractions of polymer A and polymer B corresponding to the spinodal branch close to $\Phi_A = 0$ (~pure B), and the other variables are defined below.

This expression is interesting in relation to our purpose because it predicts that a transition to a homogeneous melt state is possible for $\tau > \tau_{cr}$. If the shearing is stopped and if the composition of the melt is inside the spinodal range in the phase diagram, an interpenetrating co-continuous phase structure is predicted by Cahn (10, 11). This behavior was observed by McMaster (22) in his comprehensive study of a SAN/PMMA with approximately the same molecular structure as the blends we have selected. McMaster obtained a transition to the spinodal range by rapid heating from below the lower critical temperature to the temperature of observation.

A principal sketch of the kind of structure we seek to prepare is shown in *Fig. 1*.

Fig. 1. Sketch of an interpenetrating co-continuous structure (with air pockets for clarity).

This method is not the only method that permits the production of a interpenetrating co-continuous structure. Similar structures may be prepared by monitoring the polymerization processes of polymer blend (via interpenetrating networks) and by melt processing via the so-called phase inversion mechanism without creation of a homogeneous phase.

However, spinodal decomposition leads to a structure with very finely distributed phases, (e.g., with minor phase thicknesses of fractions of a μm). A condition for the treatment is that the entanglement network passes through the interfaces of the two-phase system. This condition limits the applicability of the hypothesis to material combinations that are "nearly compatible." However, melt fracture prevents the application of shear stresses larger than 10^5–10^6 Pa.

"Melt fracture" seems to represent the most serious restriction to the application of the hypothesis given by *Eqs 35* and *36* in the main text. The hypothesis will be incorrect for two-phase systems with small interfacial thicknesses.

ACKNOWLEDGMENT

The authors wish to express their gratitude to the Danish Council for Scientific and Industrial Research for financial support of the project.

NOMENCLATURE

List of Symbols (for part I and part II)

A	=	the number of repeat units (of polymer A) per chain between entanglements.
A	=	interfacial area.
a	=	a dimensionless constant.
a'	=	a dimensionless constant in *Eq 23*.
b	=	a dimensionless constant in *Eq 27*.
b'	=	a dimensionless constant in *Eq 28*.
c	=	polymer concentration.
D	=	the rate of mechanical energy dissipation.
F	=	a function (dominated by free volume contributions).
ΔF	=	total free energy change.
ΔF_{mix}	=	free energy change on mixing.
ΔF_{el}	=	free energy change due to deformation of chains between entanglements.
f_{el}	=	an elastic force (on a single polymer molecule) per polymer molecule.
f_f	=	a frictional force per polymer molecule.
H	=	$\bar{M}_w/\bar{M}_n$.
K_1	=	constant—a modulus in *Eq 24*.
L_0	=	a parameter with dimension of: length.
L'	=	a parameter with dimension of: length.

L'' = a parameter with dimension of: length.
M = molecular weight.
M_A = molecular weight of a repeat unit of polymer A.
$\bar{M}_n$ = number average molecular weight.
$\bar{M}_w$ = weight average molecular weight.
M_c = critical molecular weight where the exponent in the equation $\eta_0 = K \cdot M_w^a$ changes from ~1 to ~3.5.
N = the number of entanglements per unit volume.
N^* = the number of "effective interfacial sites" (measured in entanglements-equivalents per unit volume).
P = work done by internal stresses per unit mass, stress power.
P = pressure.
$\tilde{P}$ = reduced pressure: P/P^*.
P^* = characteristic pressure, an equation of state parameter.
R = the gas constant.
T = absolute temperature.
$\tilde{T}$ = reduced temperature: T/T^*.
T^* = a characteristic temperature, an equation of state parameter.
T_g = the glass transition temperature.
$\dot{U}_{el}$ = the rate of change of elastic energy.
Δu = the average velocity difference between neighboring entanglements (on the same polymer molecule).
V_B = molar volume of a repeat unit of polymer.
v = specific volume, subscript symbolize polymer, e.g., v_A for polymer A.
$\tilde{v}$ = reduced specific volume: v/v^*.
v^* = closepacked volume, an equation of state parameter.
X = number of repeat units per molecule.

Greek Symbols

α = the coefficient of thermal expansion.
$\underline{a}$ = orientation tensor.
$\alpha_x, \alpha_y, \alpha_z$ = deformation ratios (of chains between entanglements) after principal axes.
α_{nn} = orientation tensor components.
$\dot{\gamma}$ = shear rate.
$\delta_a, \delta_p, \delta_h$ = the solubility parameter contributions due to dispersion forces, polar forces, and hydrogen forces, respectively.
$\dot{\epsilon}$ = elongation rate (rate of deformation).
η = shear rate dependent viscosity.
η_0 = zero shear viscosity.
η_T = trouton viscosity.
λ = characteristic time constant.
μ_i = the chemical potential per repeat unit of polymer i.
μ_i^0 = the chemical potential of a repeat unit in the pure liquid reference state.
μ_{ref} = the chemical potential of a repeat unit in a reference state.
ν = number of entanglements per polymer molecule.
ξ = average frictional coefficient per entanglement: $\xi = \xi(\alpha)$.
ρ = polymer density.
$\tilde{\rho}$ = reduced density: ρ/ρ^*.
ρ^* = $1/v^*$.
τ = shear stress: τ_{21}.
τ_{nn} = stress tensor components.
$\tau_{21.f}$ = a frictional shear stress.
$\tau_{21.ef}$ = an elastic shear stress.
τ_c = the critical shear stress.
Φ_i = volume fraction of polymer i.
Φ_i = in *eq 35*, Φ_A and Φ_B are spinodal volume fractions.
χ = Flory-Huggins interaction parameter.
χ^* = interaction function.

REFERENCES

1. A. Silverberg and W. Kuhn, *Nature*, **170**, 450 (1952).
2. C. Rangel-Nafaile, A. B. Metzner, and K. Wissbrun, *Macromolecules*, **17**, 1187 (1984).
3. B. A. Wolf, *Macromolecules*, **17**, 615 (1984).
4. H. Kraemer, J. R. Schmidt, B. A. Wolf, *Proc. 28th IUPAC, Macromol. Symp.*, p. 778 (1982).
5. B. A. Wolf, *Makromol. Chem., Rapid Commun.*, **1**, 321 (1980).
6. B. A. Wolf, *J. Polym. Sci., Polym. Lett. Ed.*, **18**, 789 (1980).
7. J. R. Schmidt and B. A. Wolf, *Colloid Polym. Sci.*, **257**, 1188 (1979).
8. K. A. Mazich and S. H. Carr, *J. Appl. Phys.*, **54**, 5511 (1983).
9. E. Vrahopoulou-Gilbert and A. J. McHugh, *Macromolecules*, **17**, 2657 (1984).
10. J. W. Cahn, *Acta Mettallurgica*, **9**, 795 (1961).
11. J. W. Cahn, *J. Chem. Phys.*, **42**, 93, (1965) *Trans. Met. Soc., AIME*, **242**, 166 (1968).
12. I. C. Shanchez, Chapter 3 in: D. R. Paul and S. Newman, "Polymer Blends," Vol. I, Academic Press, N.Y. (1978).
13. W. W. Graessley, "The Entanglement Concept in Polymer Rheology," *Adv. Polym. Sci.*, **Vol. 16** (1974).
14. H. H. Hull, "An Approach to Rheology Through Multivariable Thermodynamics," Soc. Plast. Eng. (1981).
15. G. Astarita and G. Marucci, "Principles of a Non-Newtonian Fluid Mechanics," McGraw-Hill, N.Y. (1974).
16. J. Lyngaae-Jørgensen, "Relations Between Structure and Rheological Properties of Concentrated Polymer Melts," Thesis, Instituttet for Kemiindustri, The Technical University of Denmark (1980).
17. L. R. G. Treloar, *Proc. Roy. Soc., London, A.*, **351**, 301 (1976).
18. L. R. G. Treloar, "The Physics of Rubber Elasticity," 3rd ed., Clarendon Press, Oxford (1975).
19. J. Lyngaae-Jørgensen, in: B. Mena, A. Garcia-Rejon and C. Rangel-Nafaile, "Advances in Rheology," **Vol. 3**, Elsevier Sci. Publ., Amsterdam, 503 (1984).
20. P. J. Flory, "Principles of Polymer Chemistry," Cornell University Press, Ithaca (1953).
21. R. H. Lacombe and I. C. Sanchez, *J. Phys. Chem.* **80**, 2568 (1976).
22. L. P. McMaster, *Adv. Chem. Ser.*, **142**, 43 (1975).

Phase Transitions During Shear Flow of Two Phase Polymer Blends
II. Styrene-acrylonitrile/Poly(methylmethacrylate) Transition to "Homogeneous" Melt State

J. LYNGAAE-JØRGENSEN *and* K. SØNDERGAARD

Instituttet for Kemiindustri
The Technical University of Denmark
2800 Lyngby, Denmark

An advanced hypothesis derived in Part I (this issue) is tested with selected model blends. Blends of copolymers of styrene and acrylonitrile (SAN) and poly(methylmethacrylate, (PMMA) were studied because they are both amorphous, thermally stable, have large density differences, are easy to cut (in an ultramicrotome) and because comprehensive studies have been reported in the literature on this system. The melt viscosity of the blends were studied using a Rheometrics Mechanical Spectrometer and an Instron capillary rheometer. Light scattering measurements were performed during flow in order to measure the critical transition stress. The phase structure of quenched samples was studied by transmission electron microscopy on ultramicrotome cuts. It was shown that an interpenetrating co-continuous structure develops when flow is stopped, if a homogeneous phase is formed during flow. Melt fracture limits the applicability of this approach to nearly compatible blends.

INTRODUCTION

In Part I, we developed an expression for a critical stress for a phase transition to a homogeneous one-phase system during simple shear flow of an incompatible blend, and in this paper we test the prediction for styrene-acrylonitrile/poly(methylmethacrylate) (SAN/PMMA) blends.

EXPERIMENTAL

Materials

The materials used in the investigated blends were commercial grades of copolymers of styrene and acrylonitrile (SAN). The sources and molecular weight characteristics of these polymers are summarized in *Table 1*.

Blend Preparation

The SAN and PMMA samples were dried in a vacuum oven at 50°C for a week before use. The blends were prepared by melt mixing at 200°C in a Bradender Plasticorder (with a Walzerkneter Type 30 mixing head having a mixing chamber volume of approximately 33 cm^3) using the following procedure:

The two pelletized SAN and PMMA polymers in the desired composition were manually mixed. This mixture was added gradually to the Brabender mixing bowl, which had been preheated to 200°C. The speed of the mixing blades was set at 20 rpm, and mixing continued until a constant torque was reached, which took about 12 to 15 min. The well-mixed blends from the Brabender were compression molded into 1-mm thick sheets at 200°C in a hydraulic press, followed by air cooling to room temperature. The samples cut from these sheets were used for rheological and morphological characterization.

Pure SAN and PMMA were also subjected to the same mixing condition in order to study their possible degradation during mixing. The molecular characteristics of pure polymers determined by Gel Permeation Chromatography (GPC) technique before and after melt mixing in the Brabender are shown in *Table 2*. *Table 2* confirms that no appreciable degradation took place at 200°C during melt blending of SAN and PMMA.

Table 1. Starting Polymers for SAN-PMMA Blends.

	Copolymer of Acrylonitrile and Styrene (SAN)		Poly(methylmethacrylate) (PMMA)
Commercial Name	DOW SAN 110	BASF Luran 388S	ICI Diakon LO 951
Density (g/cm^3)	1.085	1.08	1.17
Melt Index (g/10 Min)		7	16
$\bar{M}_w$	1.45×10^5	1.96×10^5	8.4×10^4
$\bar{M}_N$	6.35×10^4	8.2×10^4	4.0×10^4
$\bar{M}_w/\bar{M}_N$	2.28	2.39	2.2
W% AN	29%	25%	
$\bar{X}_N$	727		455
V (cm^3/rep. unit)	81		86.5
M_c			1.05×10^4

Table 2. Molecular Weights of SAN and PMMA Before and After Shearing.

	Dow SAN 110		ICI Diakon LO 951	
Polymer Shearing History	None	After Instron Treatment $\dot{\gamma} > 100\ s^{-1}$ for 2 h	None	After Instron Treatment $\dot{\gamma} \sim 10\ s^{-1}$ for 1 h
$\bar{M}_w$	1.45×10^5	1.54×10^5	8.4×10^4	8.5×10^4
$\bar{M}_n$	6.35×10^4	6.1×10^4	4.0×10^4	3.7×10^4
$\bar{M}_w/\bar{M}_n$	2.3	2.5	2.2	2.3

Gel Permeation Chromatography (GPC)

The molecular weight averages ($\bar{M}_W$, $\bar{M}_n$, and $\bar{M}_z$) of SAN and PMMA and SAN-PMMA blends after processing in the Brabender Plasticorder were determined using the GPC technique. All GPC measurements were made with a Waters Associates Model 200 instrument, which was equipped with four polystyrene gel columns of 10^6, $2 \cdot 10^4$, 10^4 and 10^3 Å nominal porosities. The GPC instrument was run under the following conditions:

Flow rate: 1 ml/min
Injection volume: 2 ml
Sample concentration: $2.5 \cdot 10^{-3}$ g/ml

Tetrahydrofuran (THF) was used as a solvent at room temperature in all the measurements.

The GPC columns were calibrated with narrow distribution polystyrene standards from Pressure Chemical Co. and from the National Bureau of Standards under the above mentioned conditions except the injection volume, which was 0.5 ml. All the molecular weight averages were calculated using the calibration found for PS standards and approximate "Q factor correction."

Rheometry

Melt flow behavior of SAN, PMMA, and their blends in the range of 0.3 to 1000 s^{-1} was determined using an Instron Constant Speed Rheometer. The capillary used had a length/diameter (L/D) ratio of 81.79 with a diameter of 1.245 mm and 90° entrance angle. The Rabinowitsch correction was applied in calculating the wall shear rate ($\dot{\gamma}$). However, the end correction used by Bagley has been neglected in calculating the wall shear stress because the capillary with a large L/D ratio was used in this study and the inlet pressure drop correction was found to be small.

The Rheometric Mechanical Spectrometer (Rheometrics, Inc. Model No KMS-71) was used in the cone and plate and the disk and plate mode.

Mixing

A Brabender Plastograph was used for mixing purposes and after calibration as a measuring unit (1).

Morphology

A JEOL transmission electron microscope (Japan Electronics and Optics Laboratories, Co. Ltd. Tokyo, Model JEM-100B-TR) was used to study the morphology of all SAN-PMMA blends having different blend compositions. Samples were sectioned by using an Ultramicrotome (Reicht OM U3, Austria) at room temperature. Staining was unnecessary since the contrast between SAN and PMMA was sufficient to distinguish the two phases with dark and light regions corresponding to the SAN and PMMA, respectively.

Laser Light Scattering Measurements

Laser Light Scattering Measurements were performed using the set-up sketched in *Fig. 1*. The scattering pattern could be estimated by measuring the intensity as a function of scattering-angle parallel with the flow direction and perpendicular to the flow direction. Phase diagrams have been determined with the same set-up without shearing.

RESULTS

A principal sketch of the kind of structure we seek to prepare is shown in *Fig. 2*. A phase

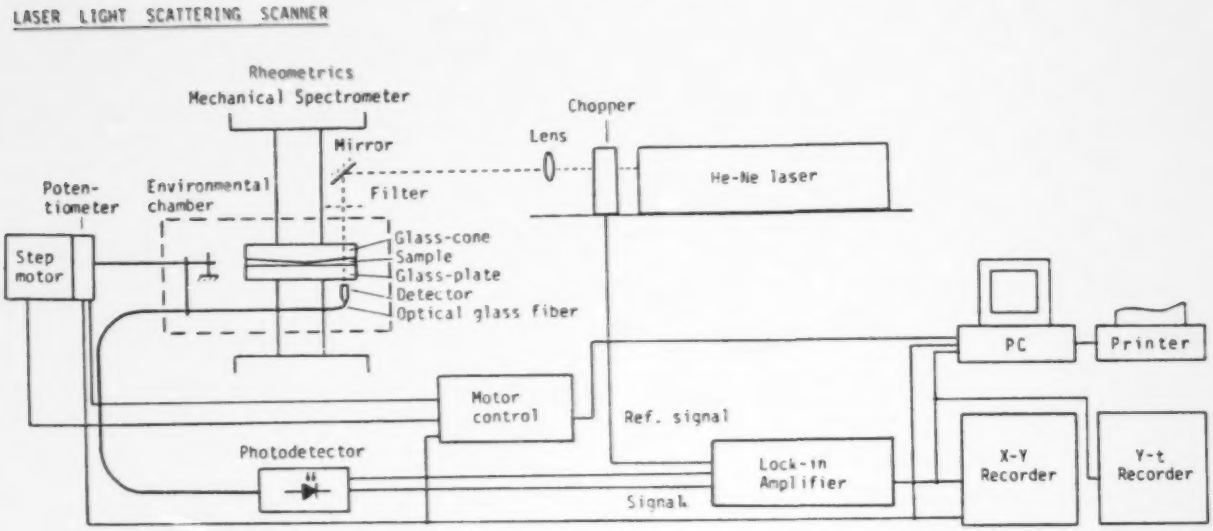

Fig. 1. Principal sketch of the set up used for light-scattering measurements during simple shear flow.

Fig. 2. Sketch of an interpenetrating co-continuous structure (with air pockets for clarity).

diagram for the mixture of PMMA and SAN (29 W% AN) is shown in *Fig. 3*. The points on the phase diagram were obtained from traces of transmittance against temperature. Starting from low temperatures on transparent samples, the temperature is raised with different heating rates. The temperature where the transmittance starts to decrease is measured and extrapolated to zero heating rate. By this technique, we obtain a binodal phase diagram. The exact position of the spinodal curve has not been determined, even though the transmittance-temperature curves and the TEM data give an approximate position.

Rheological Measurements

Figure 4 shows a double logarithmic plot of viscosity against shear stress for pure SAN,

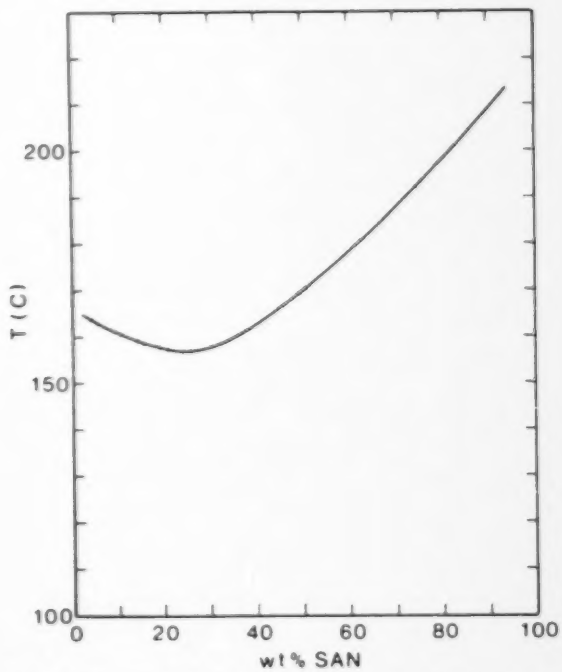

Fig. 3. Phase diagram for the PMMA/SAN system (binodal).

pure PMMA and SAN/PMMA (25/75 by weight) at T = 190°C which, according to *Fig. 3*, is well inside the area of the phase diagram where two-phase behavior is predicted.

Figure 5 shows a similar delineation for a

blend with the same PMMA but with a PS sample (2).

Figure 6 shows a reduced master curve plot for the samples shown in *Fig. 4*, i.e., a plot of $\log \frac{\eta}{\eta_0}$ against $\frac{\eta_0 M_c H \rho}{c^2 RT} \dot{\gamma}$.

Figure 7 shows a similar delineation for the samples shown in *Fig. 5*.

Electron Microscopy

TEM measurements on ultramicrotomic cuts of samples processed at 190°C at different shear rates and with different cooling history are shown in *Figs. 8* to *11* for blends with SAN/PMMA (25/75) and compared with a picture reported by McMaster in *Fig. 12*.

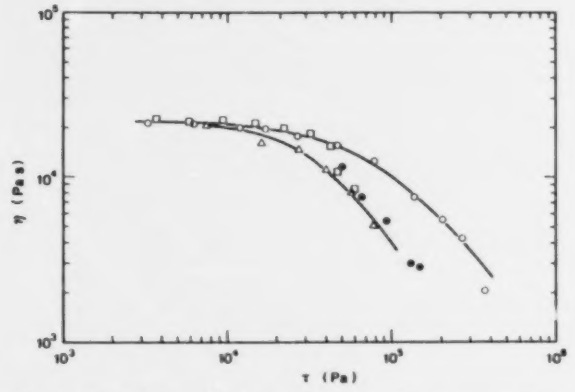

Fig. 4. Double logarithmic plot of viscosity against shear stress at T = 190°C: ○ PMMA, △ SAN, □ SAN/PMMA (25/75) measured with rheometrics mechanical spectrometer, ● measured with Instron (and Brabender) rheometer.

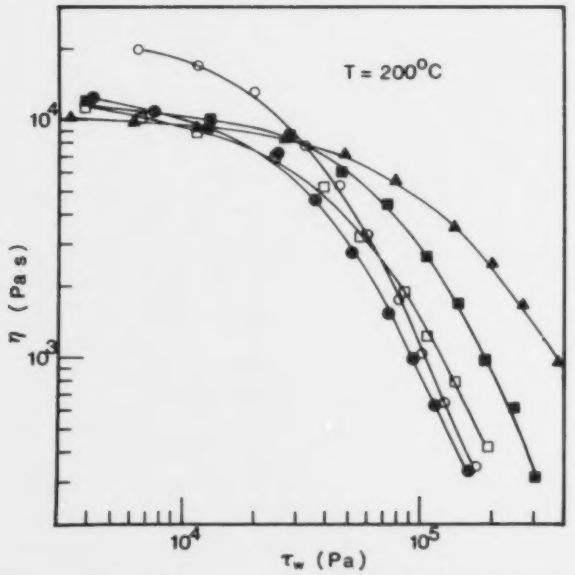

Fig. 5. Viscosity versus shear stress for PS-PMMA blends at 200°C: (○) PS; (●) PS/PMMA = 75/25; (□) PS/PMMA = 50/50; (■) PS/PMMA = 25/75; (▲) PMMA. The PMMA is the same as in Fig. 4.

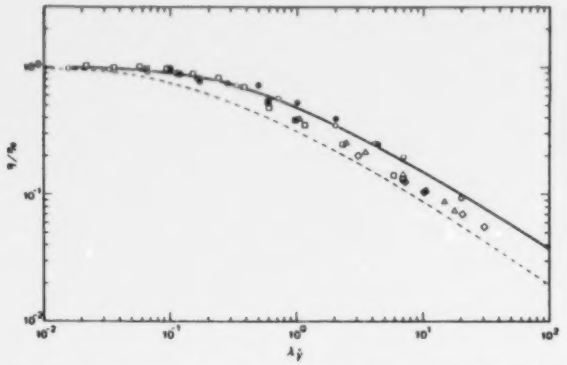

Fig. 6. Delineation of data as "master curves" (20) – log $\frac{\eta}{\eta_0}$ against log $\lambda\dot{\gamma}$ where

$$\lambda = \frac{\eta_0 M_c H}{\rho RT}.$$

● SAN (Dow 110), T = 190°C; ○ PMMA, T = 190°C; ■ and □ SAN/PMMA (25/75): T = 190°C, ▽ and △: T = 180°C, • and ◇: T = 170°C.

Visual Observations

Direct observations of clarity in a Brabender Plasticorder and in the glass-glass plate geometry show that samples are white and milky at low shear rates but gradually change to an optical clear appearance at high shear rates. For measurements performed at 190°C, this transition is estimated to take place at stresses in the range 8×10^4 -10^5 Pa.

Light Scattering Measurements (turbidity)

The light scattering measurements are roughly in accordance with the direct visual observations. The structure breakdown is a relatively slow process as shown in *Fig. 13*. The transition stress, τ_{cr}, is estimated by an iterative process. First, we measured a transmittance time curve in an experiment where the stress is slowly raised as shown in *Fig. 13*. A transition stress is surmised and transmittance-time measurements performed at constant stress. The least constant stress leading to a transmittance such as that found for the homopolymers is taken as τ_{cr}.

DISCUSSION

The rheological measurements indicate that a transition of some kind does take place in the melt. This transition takes place at stresses roughly in accordance with, but slightly higher than, the stresses estimated by visual and turbidity measurements.

In an earlier work, we showed that for blends of PMMA and PS a delineation of $\log \frac{\eta}{\eta_0}$ against $\log \frac{\eta_0 M_c H \rho}{c^2 RT} \dot{\gamma}$ formed a master curve for polymer blends, where η and η_0 are the viscosity and the zero shear viscosity of the blend, and M_c, H, and

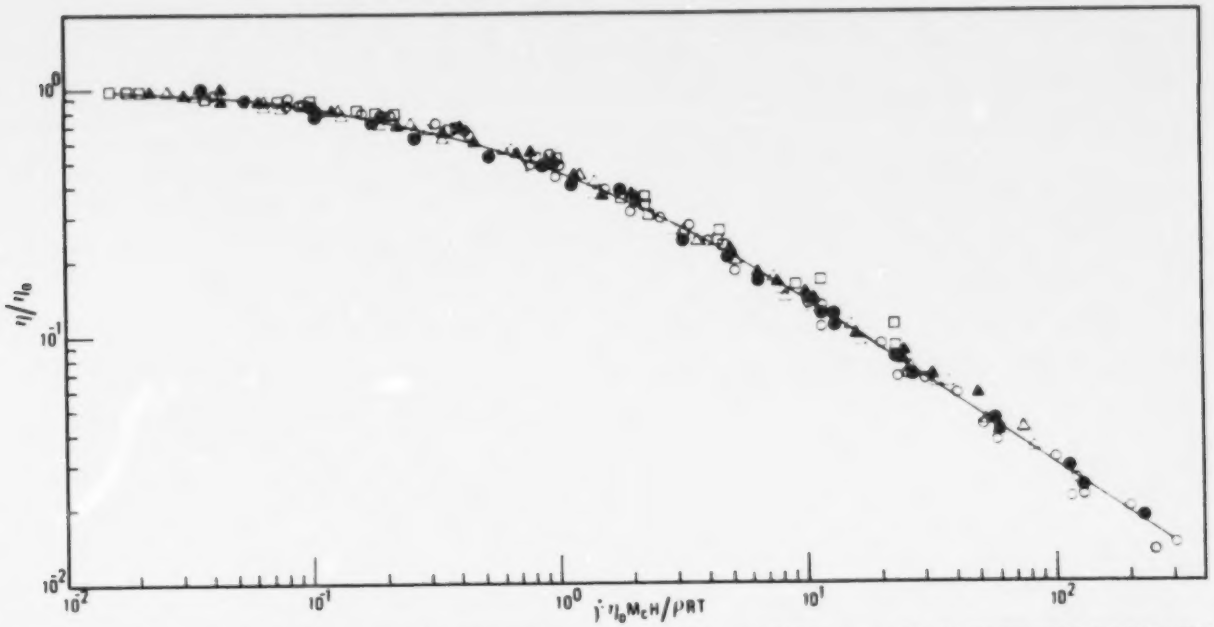

Fig. 7. Master curves for PS-PMMA blends obtained by plotting the reduced viscosity (η/η_0) versus reduced shear rate ($\dot{\gamma}\eta_0 M_c H/\rho RT$) at temperatures of 180°C, 200°C, 220°C, and 240°C, respectively: (○) PS; (●) PS/PMMA = 75/25; (△) PS/PMMA = 50/50; (▲) PS/ PMMA = 25/75; (□) PMMA. PMMA is the same as in Fig. 6.

Fig. 8. Transmission electron microscopy (TEM) picture of a shock cooled sample of SAN/PMMA (25/75) which has been treated at 190°C at $\dot{\gamma} = 9\ s^{-1}$ ($\tau = 6.3 \times 10^4$ Pa) for 20 min. The very thin fibrillar structure is characteristic for samples "processed" at low shear stresses. (Magnification × 8666).

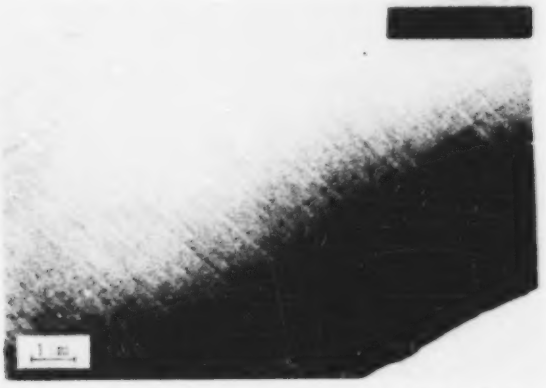

Fig. 9. A picture of SAN/PMMA (25/75) sheared at $\dot{\gamma} = 54\ s^{-1}$ ($\tau = 1.4 \cdot 10^5$ Pa) at T = 190°C for 20 min and shock cooled. No structure (apart from cutting lines) may be detected. (Magnification × 8666).

ρ are defined for the continuous phase. Since PMMA do form the continuous phase in this system, one would expect that this type of delineation would follow the master curve if the structure did not change during flow. The fact that the data fall below the master curve at high shear rates may be taken as an indirect indication of a structure transition.

The direct visual observations and turbidity measurements show that the blends become optically clear at high shear rates indicating that a homogeneous or nearly homogeneous state is formed. In this paper, we define the term homogeneous state operationally as the state where light scattering cannot be detected.

TEM measurements on (SAN/PMMA (25/75))

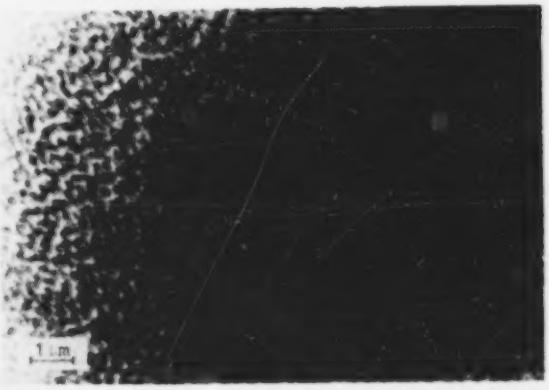

Fig. 10. A picture of the sample shown in Fig. 9 after annealing at 190°C. (Magnification × 8666).

Fig. 11. Sample shown in Fig. 10 at a magnification × 26000. The picture shows the same type of structure as developed by rapid heating from below the lower critical point.

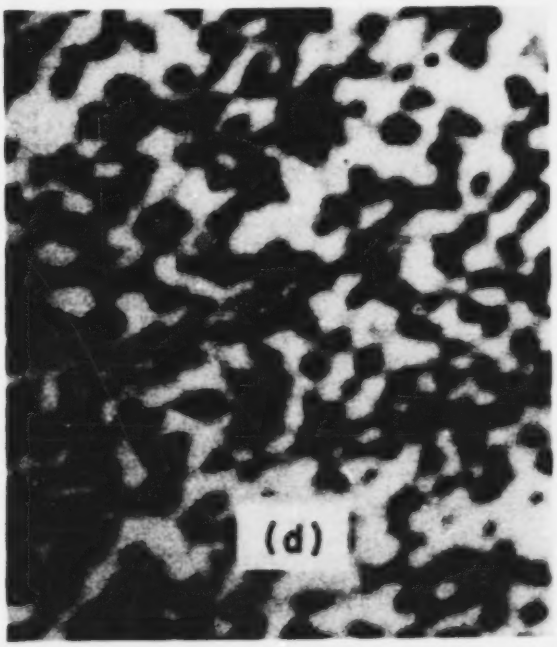

Fig. 12. A picture of a sample of SAN/PMMA (25/75) developed after rapid heating to 180°C from below the lower critical temperature and annealing for 32.4 min determined by McMaster (7).

samples, shock cooled from a sheared system at $T = 190°C$, show highly oriented structures at low shear stresses but no structure at all at stresses above approximately 1×10^5 Pa as shown in *Figs. 8* and *9*, respectively.

If the shearing is stopped, a structure development as described by McMaster (Fig. 12) for rapidly heated homogeneous systems is observed. A system kept at $T = 190°C$ for 10 min. and then cooled shows a typical co-continuous interpenetrating structure as shown in *Figs. 10* and *11*.

An estimation of the critical stress, τ_{cr}, for transition to a homogeneous phase has been calculated in two different ways: 1) by application of the three-dimensional solubility parameter concept (3), and 2) by the assumption that the interaction parameter is independent of concentration and calculation of B from *Eq 36* in Ref. 4.

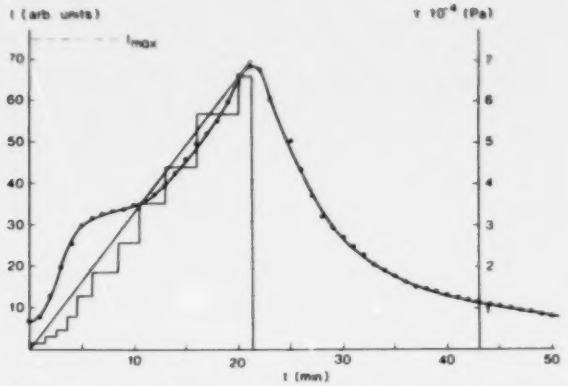

Fig. 13. A plot of transmittance against time with shear stress changing nearly linearly with time.

1: $(\delta_d, \delta_p, \delta_h)_{PMMA} = (18.2, 10.3, 7.7)$ $(J^{1/2}. cm^{-3/2})$ (from Ref. 5) $(\delta_d, \delta_p, \delta_h)_{SAN} = (18.9, 8.8, 5.5)$ estimated from $\delta_{SAN} = \upsilon_{PS}\,\delta_{PS} + \upsilon_{PAN}\,\delta_{PAN}$; $\chi = \dfrac{V_A}{RT}\,\Sigma_1^3\,(\delta_A - \delta_B)_i^2 = 0.1$

δ_d, δ_p, and δ_h are the solubility parameter contributions due to dispersion forces, polar forces, and hydrogen forces respectively; V_A is the molar volume of SAN repetition units; and υ is volume fraction.

The critical concentration corresponding to max. in $(\mu_A - \mu_A^0)_{mix}$ is estimated from the expression:

$$\Phi_A^* = \frac{1}{2} + \left(\frac{1}{X_A} - \frac{1}{X_B}\right)\frac{1}{4\chi} - \frac{\sqrt{\left(2\chi + \left(\frac{1}{X_A} - \frac{1}{X_B}\right)\right)^2 - 8\,\frac{\chi}{X_A}}}{4\chi} \quad (1)$$

The data given in *Table 1* were used for SAN-110 and PMMA Insertion in *Eq 36* in Ref. 4 gives $\tau_{cr} = 1.2 \times 10^5$ Pa.

2: The data given in *Table 3* were used for SAN-110 and PMMA. The data was estimated from Refs. 6 and 7. T^*, p^*, and ρ^* are equation of state parameters for the lattice fluid theory (5). $\tilde{T} = \dfrac{T}{T^*}$, $\tilde{p} = \dfrac{p}{p^*}$ and $\tilde{\rho} = \dfrac{\rho}{\rho^*}$. α is the coefficient of thermal expansion. For the binodal curve, we have that

$$\mu_{A.1} = \mu_{A.2} \quad (2a)$$

and

$$\mu_{B.1} = \mu_{B.2} \quad (2b)$$

is fulfilled for the points on the phase diagram. At 190°C, we have $\Phi_{A.1} \simeq 0$ and $\Phi_{A.2} \simeq 0$,

Table 3. Equation of State Parameters.

	Copolymer of Acrylonitrile and Styrene (SAN)	Poly(methyl-methacrylate) (PMMA)
Commercial Name	DOW SAN 110	ICI Diakon LO 951
α (K^{-1}) for $T \geq T_g$	5.80×10^{-4}	6.15×10^{-4}
α (K^{-1}) – $T < T_g$	2×10^{-4}	2.6×10^{-4}
T^* (K)	756	756
P^* (BAR)	5070	4200
ρ^* (g/cm^3)	1.2	1.36
ρ (g/cm^3) at 20°C	1.085	1.19
ρ (g/cm^3) at 190°C	1.013	1.103

72 for phase 1 and phase 2, respectively. From *Eq. 2b*, we get:

$$\frac{1}{X_B} \ln \Phi_{B.2} + \left(\frac{1}{X_b} - \frac{1}{X_A}\right) \Phi_{A.2} + \chi \Phi^2_{A.2} + B(\Phi_{B.2}) = 0$$

From this equation, we find $\chi = 0.019$, Φ^*_A is now found from *Eq 1* and τ_{cr} from *Eq 35* in Ref. 4.

$$\tau_{cr} = 5.1 \cdot 10^4 \text{ Pa}$$

The critical stress measured in simple shear flow is in the interval $8–10 \times 10^4$ Pa.

The three-dimensional solubility parameter approach should at best give an order of magnitude estimation. The correspondence between calculated and measured values, using *Eq 35* from Ref. 4 with χ = constant, fitted from the phase diagram, seems to be reasonable. Thus, the prediction obtained from *Eq 35* is, at least qualitatively, in accordance with the observed behavior in the sense that a transition is observed at the right shear stresses. If the shearing is stopped, a co-continuous interpenetrating phase structure, equivalent to the one observed by McMaster, is formed.

CONCLUSIONS

A two-phase blend of SAN and PMMA if subjected to high enough shear stresses, forms a homogeneous phase. Here homogeneous is defined as a state where light scattering cannot be detected.

If the shearing is stopped and the sample quenched, a sample with no detectable structure (TEM) is obtained. If the shearing is stopped and the material annealed at 190°C, interpenetrating co-continuous phase structures (TEM) closely resembling those observed by McMaster, which were formed by spinodal decomposition, develop.

A hypothesis is developed which predicts that a transition to a homogeneous state may take place at a critical shear stress. The hypothesis predicts a stress value that is in reasonable agreement with an experimentally observed value.

ACKNOWLEDGMENT

The authors wish to express their gratitude to the Danish Council for Scientific and Industrial Research for financial support of the project.

REFERENCES

1. C. C. N. Lee and J. R. Purdon, *Polym. Eng. Sci.*, **9**, 360 (1969).
2. J. Lyngade-Jørgensen, F. E. Andersen, and N. Alle, In: D. Klempner and K. C. Frisch, eds, "Polymer Alloys III," pp. 105–147, Plenum Press, N.Y. (1983).
3. C. M. Hansen, "The Three-Dimensional Solubility Parameter and Solvent Diffusion Coefficients," Thesis, The Technical University of Denmark (1967).
4. J. Lyngaae-Jørgensen and K. Søndergaard, *Polym. Eng. Sci.*, (Part I).
5. C. M. Hansen and A. Saarnak, Report nr. 667.611:541.8 from Scandinavian Paint and Printing Ink Research Institute (1982).
6. I. C. Shanchez, Ch. 3 in: D. R. Paul and S. Newman, "Polymer Blends," Vol I, Academic Press, N.Y. (1978).
7. L. P. McMaster, *Adv. Chem. Ser.*, **142**, 43 (1975).

DISCUSSION

H. Tolliver: Did you measure the glass transition temperatures of your SAN, PMMA and their blends?

J. Lyngaae-Jorgensen: The polymers have about the same T_g. To measure the glass transition temperature of the blends would not give us any information.

H. Tolliver: Did you determine the strain at break for thin films of PMMA and the blends?

J. Lyngaae-Jorgensen: No. We selected the system for its range of phase transition, not the properties or a need for the properties to be improved. For us, the SAN/PMMA system was a nice model to study. However, we have pressed samples and performed tensile measurements on an Instron testing machine. We did have problems with development of air bubbles in samples annealed for more than approximately 5 min, even with vacuum dried samples, especially at high temperatures. Test results on samples pretreated at 60 rpm and 145°C in a Brabender Plastograph, preheated to and thereafter pressed at 140°C for 2 min is given in the table:

Sample	Tensile strength τ_B (MPA)	Elongation at Break E(%)
PMMA	49	8.8
SAN-110	44	5.7
San-Luran	53	7.5
PMMA/SAN-110(3/1)	46	6.2
PMMA/SAN-Luran(3/1)	46	6.6
Standard deviation	±5	±0.6

The sample dimension was:

Length between jaw's: 31 mm
Width: 9 mm
Thickness: 1.15 mm

Temperature: 23°C
Draw rate: 5 mm/min

S. Rostami: In the SAN/PMMA system the LCST behavior is associated with the negative heat of mixing. Therefore the use of Flory-Huggins theory is not applicable. Furthermore the interaction parameter calculated from the cohesive energy density is totally wrong for systems with the negative heat of mixing.

J. Lyngaae-Jorgensen: That is right. We used throughout the Flory's "equation of state theory" or Sanchez lattice fluid theory not Flory-Huggins theory. The calculation of the interaction parameter was only to get a very rough estimate . . . completely agree.

S. Rostami: What you are doing by applying the homogenous shear field is simply shifting the phase boundary up the temperature scale. The homogenization is a result of effectively moving the stress dependent LCST above the temperature of the measurements. Once the stress field is removed instantaneously, the system becomes unstable and tends to phase separate by a spinodal or binodal mechanism, depending on the degree of overheating.

J. Lyngaae-Jorgensen: Yes.

S. J. Kurtz: It looks interesting that you observed the critical shear stress near 120 kPa. That seems to correspond to critical shear stress for a disentanglement fracture mechanism. Do you see any connection between these two critical phenomena?

J. Lyngaae-Jorgensen: No, I do not think so. We have also worked with systems with significantly lower calculated critical stress than the critical stress for melt fracture, say at least by a factor 10. Here it was a coincidence. Both SAN and PMMA show considerably higher stresses for fracture between the shearing solid surfaces and the melt, than the critical transition stresses we have measured.

A. P. Plochocki: You displayed formation and disappearance of phase structure as a result of shear stress. There is a some ten-year-old theory, which predicts a transition from the particulate type morphology into a stratified one, the theory based on the differential of the normal stresses. Did you consider a possibility that the change of the optical behavior may be related to the change from dispersed to stratified morphology? The transition from particulate to laminar morphology seems to me a more probable explanation of the increase of transparency than the formation of a single phase you claim to have.

J. Lyngaae-Jorgensen: Yes, I know Van Oene's work on the influence of the first stress difference of the two liquids on the interfacial tension coefficient. Here we have something different. When you do light scattering measurements, as we do, the data are sensitive to orientation; we measure scattering of polarized light in two perpendicular directions. With enhanced orientation the intensities become very different. When you stop shearing, the anisotropy persists for a long time. But we do not see anisotropy in our system after homogenization, and when the phase separation occurs, via the spinodal decomposition the scattering is also isotropic. Furthermore, the sample quenched after homogenization seems to have the same uniformity in all directions. No, I do not think that your suspicions are justified.

L. A. Utracki: I agree with Rostami's interpretation of the shear stress effect on position of the phase separation lines, as well as with your statement that a true miscibility can be achieved by shearing. However, if these premises are true, the question to be asked is how far can you effectively move the binodal, or in simple terms: how far away can you be from LCST to be able to truly homogenize the system? I do not know the LCST of PS/PE system, but it must be very low and it is doubtful that it can be rendered miscible by shearing. But, how about PE/PP or LDPE/HDPE blends? Can they be homogenized?

J. Lyngaae-Jorgensen: The hypothesis we have derived is based on a number of simplifying assumptions which we know will not always be correct. However, since "melt fracture" limits the available shear stresses to 10^5–10^6 Pa, this restriction represents the most serious limitation of the approach. The hypothesis will only be applicable to polymer combinations which are "nearly compatible." The PS/PE system cannot be rendered miscible by shearing, but we (tentatively) interpret our data for the PE/PP system as a result of homogenization at high shear stresses. The calculated critical shear stress for this system is $1–2 \times 10^4$ Pa.

Linear Low Density Polyethylenes and Their Blends: Part 1. Molecular Characterization

B. SCHLUND* *and* L. A. UTRACKI

National Research Council Canada
Industrial Materials Research Institute
Boucherville, Quebec, J4B 6Y4

Ten commercial linear low-density polyethylenes (LLDPE) were characterized by solution viscosity, size exclusion chromatography, SEC, and ^{13}C nuclear magnetic resonance. The resins were copolymers of ethylene with butene, hexene, or octene. They were prepared in gas phase (with narrow or very broad molecular weight distribution), or in solution. The macromolecules were found to be linear. For all but the very broad molecular weight distribution resins the average comonomer sequence length was found to be 1; in the other case diad formation was observed. The weight average molecular weights calculated from SEC and intrinsic viscosities agreed quite well. Mechanical degradation of LLDPE was observed during the solution viscosity measurements.

INTRODUCTION

Since its accidental discovery in 1933, polyethylene (PE) has become the largest volume commodity resin satisfying about ⅓ of the total plastics market (1). For this reason, as well as due to their simple chemical nature, PE's have been the most widely studied polymers. By changing the methods of polymerization, feedstock composition and polymerization parameters, literally thousands of grades are being made available to satisfy the growing variety of specific applications. In addition, there is an increasing tendency for post-reaction modification of PE's by blending, orientation, reactive processing, etc.

From the molecular characteristics point of view, all the diversity of PE-grades is due to a combination of four basic parameters: (i) molecular weight, *MW*, varying from about 10^3 (waxes) to over 10^7 (UHMWPE); (ii) molecular weight distribution, $\bar{M}_w/\bar{M}_n = 2$ to 50, where $\bar{M}_w$ and $\bar{M}_n$ represent the weight and number average molecular weight, respectively; (iii) short chain branching (*SCB*) introduced either by a method of polymerization, type of catalyst, and/or co-monomer type and concentration; and (iv) long chain branching (*LCB*) controlled primarily by the polymerization process.

For commercial application the resin grade is specified by the type of polymerization process, density (ρ), "melt index" (*MI*—a crude measure of apparent viscosity at specified temperature and shear stress), and a descriptive indication of the molecular weight distribution, *MWD*: broad, *B*, or narrow, *N*.

The linear low density polyethylene (LLDPE) was invented by DuPont-Canada. Its potential was not adequately explored until 1977 when the aggressively marketed Unipol process was commercialized. Due to severe market pressure, during the last few years there has been a number of changes in the process, responsible for the variety of "new" LLDPE commercial grades. It has been found that changing the type of catalyst can modify the *MWD*, and that changing from one co-monomer to another (e.g., from butene to hexene) has a profound effect on the mechanical properties of the finished product. Currently about 60 percent of LLDPE enters the market as blends. There is a tendency to achieve the blend properties by modifying the polymerization process (2).

It is evident that the future will bring new PE's with improved economy and performance. However, there is the danger that this will be achieved by going into more complex systems, blends and/or copolymers. This seems to be a good time to try to understand how the "simple" LLDPE works. Hopefully, this information will be used as a basis for understanding and predicting the behavior or more complex systems.

In this series of publications, ten LLDPE commercial resins will be discussed. Their molecular structures will be characterized (Part 1) and

* Present Address: CNRS-Laboratoire des Matériaux Organiques Echangeur de Solaise, Autoroute Lyon-Vienne, BP-24 69390 VERNAISON, FRANCE.

the melt flow properties carefully examined under steady state, dynamic (Part 2), and extensional mode of deformation (Part 3). An effort will be made to correlate this information with the processing and properties of the finished product. Next, the selected LLDPE resin will be blended with another LLDPE as well as with high pressure low density polyethylene (LDPE) and the properties of the blends will be examined.

In Part 1 the molecular characterization of the samples will be discussed. The following methods have been used: high temperature size exclusion chromatography (SEC), SEC coupled with low angle laser light scattering (SEC/LALLS), solution viscosity, ^{13}C nuclear magnetic resonance ($^{13}CNMR$) and atomic absorbance.

EXPERIMENTAL

Materials

Ten commercial LLDPE resins, supplied by Esso Chemical Canada, are listed in *Table 1*. All samples were pelletized and overstabilized by addition of 0.2 percent of IRGANOX and IRGAFOS antioxidants.

SEC

A Water Scientific Ltd. GPC/ALC Model 150C with Water Model 130 Data Module as well as a computer "Apple II+" for the data acquisition were used. The instrument was operated at 140°C with 1,2,4-trichlorobenzene (TCB) as a solvent. Four columns (Polymer Lab Inc.) with pore sizes: 10^3, 10^4, 10^5, 10^6 Å were calibrated using 16 narrow *MWD* polystyrenes (PS) samples supplied by Pressure Chemicals and Water Sci. The columns were calibrated (3) at 140°C using 0.1 percent of polymer in TCB.

Due to the closeness of the melting point at T ≤ 145°C, PE's in TCB formed super-macromolecular aggregates, which had to be destroyed by heating at 165°C for 1.5 h (4–7), after which the solution was cooled to 140°C and injected. It was found to be unnecessary to use outside-SEC filtering. The solution was adequately cleaned using an in-line filter (0.5 μm) changed every 20 injections. The measurement conditions are listed in *Table 2*.

SEC/LALLS

The measurements were carried out using a Chromatix KMX-16 laser differential refractometer and KMX-6 LALLS photometer attached to a Waters Sci. Ltd. GPC/ALC, Model 150C instrument. To determine LCB, the previously published (8) procedure was followed with TCB at 145°C.

Solution Viscosity

The measurements were carried out at 140°C in modified Cannon-Ubbelohde capillary viscometers, size D25, with the capillary length and diameter 95 and 0.31 mm respectively, equipped with automatic timer (resolution 10 ms). As a solvent, freshly distilled TCB (without antioxidant) was used. It has been found that the elution time of PE solutions decreases with the number of passes through a capillary, but it is independent of the time the solution remained in the viscometer.

$^{13}CNMR$

The spectra were observed using a Bruker AM-400 spectrometer modified for pulse Fourier Transform spectroscopy. The protons were decoupled from the carbon nuclei using a random noise decoupling field. The pulse with a width of 83.0 μs was located at the high field end at 100.617118 MHz. Solutions containing $c \simeq 10$ g/dl prepared with tetramethylsilane (TMS) as internal reference were scanned at 120°C.

Table 2. SEC Operating Conditions.

Columns, Polymer Lab: 10^3, 10^4, 10^5, 10^6 Å
Temperature: 140°C
Injection volume: 350 ml
Flow rate: 0.5 ml/min
Solvent: 1,2,4-Trichlorobenzene (TCB)
Concentration: less than 0.1 wt% of PE in TCB
Dissolution: 1.5 hrs at 165°C then 2 hrs at 140°C
Antioxidant: Santonox-R, 4,4′-thio-bis-(6-terbutyl m-cresol), 0.1 wt% on polymer

Table 1. Characteristics of LLDPE Resins as Provided by the Manufacturers.

Sample Code	Manufacturer	Density ρ (kg/m³)	Melt Index[a] MI (g/10′)	MWD[b]	Comonomer
LLDPE-1	Exxon Chem.	918	0.5	N	Butene
LLDPE-2	Exxon Chem.	926	0.7	N	Butene
LLDPE-3	Exxon Chem.	920	0.8	B	Butene
LLDPE-4	Exxon Chem.	918	1.0	N	Butene
LLDPE-5	Exxon Chem.	918	1.0	N	Hexene
LLDPE-6	Exxon Chem.	927	0.8	N	Hexene
LLDPE-7	Dow Chem. Co.	920	1.0	N	Octene
LLDPE-8	Exxon Chem.	946	0.04	VB	Hexene
LLDPE-9	Exxon Chem.	946	0.07	VB	Hexene
LLDPE-10	Exxon Chem.	955	0.3	VB	Hexene

[a] 190°C with 2.16 kg.
[b] N, B, and VB stand for: Narrow, Broad, and Very Broad, respectively.
[c] Exxon uses the Unipol, fluidized bed process; Dow uses the solution method.

Atomic Absorbance (AA)

Two samples, LLDPE-3 and LLDPE-8, were analyzed by the AA. The polyethylene samples were pyrolized and the ashes were analyzed for chromium (Cr), titanium (Ti), and vanadium (V).

RESULTS

SEC

As a result of, on the one hand, the multiplicity of grades and the demand for better control of their quality, and on the other hand, development of high temperature, high pressure automatic instrumentation, SEC is becoming a standard method of molecular characterization of PE, overshadowing the traditional ones: intrinsic viscosity, osmotic pressure, light scattering or ultracentrifugation. However, as discussed by numerous authors (3–9) there are still serious problems with reproducibility.

For this reason, before starting characterization of the samples discussed in this paper, a large amount of energy and time were spent examining various procedures used in commercial and academic institutions around the world. Once our own procedure was developed, each step was rigorously followed starting with distillation of TCB, dissolution, control of the instrument, data acquisition, and evaluation. For example, as mentioned before, the in-line filter was changed every 20 injections, the columns were calibrated and their platecount (PC) was measured (using toluene injection) every 40 injections. The columns were changed if PC decreased below 60,000.

With all these efforts a reasonable reproducibility of numerical data was obtained. In *Table 3* the results based on two sets of measurements, eight months apart, are given. The values in parentheses represent another set of measurements done with LALLS as a detector. In this case the values are heavily weighted toward the higher molecular weights. It should also be added that MW measured on pellets and on extruded material were in good agreement.

In *Fig. 1*, schematically the SEC traces for ten LLDPE's are shown. It is evident that the co-monomer does not influence the shape of the distribution curve. The ten LLDPE's can be grouped into three categories: narrow distribution samples No. 1, 2, 4 to 7, very broad distribution samples No. 8 to 10, and the intermediary sample No. 3.

SEC/LALLS

The technique allows detection of the presence of side chains longer than about 12 carbons. Shorter branches do not affect the hydrodynamic volume at the high dilution used in SEC (8). No branching was detected for the ten LLDPE resins by the SEC/LALLS.

Solution Viscosity

Since the data of the viscometer was selected in such a way as to obtain flow times in excess of 3 min, the kinetic energy correction could be neglected (10), i.e.:

$$\eta/\rho = At - B/t^2 \simeq At \qquad (1)$$

where η is the absolute viscosity (Pa·s), t is the efflux time (s), and A and B are viscometer constants. To calculate intrinsic viscosity, $[\eta]$, the Huggins' and Kraemer's Equations, *Eqs 2* and *3*, respectively, were used:

$$\eta_{sp}/c = [\eta](1 + k_H[\eta]c/2)^2 \qquad (2)$$

$$(\ln\eta_r)/c = [\eta](1 - k_K[\eta]c/2)^2 \qquad (3)$$

where k_H and k_K are Huggins and Kraemer interaction constants ($k_H - k_K = 0.5$) respectively, and η_r and η_{sp} are the relative and specific viscosities:

$$\eta_{sp} = \eta_r - 1 = (\eta/\eta_0) - 1 \qquad (4)$$

(η_0 is the solvent viscosity). In *Eqs 1* to *4* the time and rate of shear independent viscosities should be used.

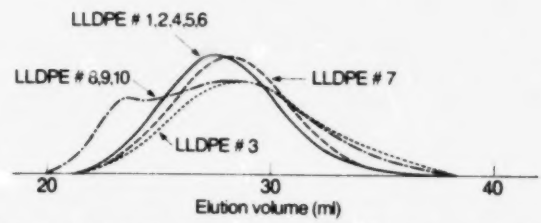

Fig. 1. SEC traces for ten LLDPE samples: solid line represents LLDPE-1, 2, 4, 5,6; dashed line LLDPE-7; dotted line LLDPE-3; and chain line LLDPE-8, 9, 10.

Table 3. SEC Results for LLDPE Samples. (The molecular weight averages are in kg/mole)

No	Sample	$\bar{M}_n$	$\bar{M}_w$	$\bar{M}_z$	$\bar{M}_w$, η[a]
1	LLDPE-1	44 ± 13 (50)	150 ± 4 (237)	342 ± 19 (1230)	113
2	LLDPE-2	47 ± 8 (50)	142 ± 2 (193)	328 ± 12 (777)	119
3	LLDPE-3	16 ± 1 (25)	111 ± 4 (143)	374 ± 57 (692)	94
4	LLDPE-4	40 ± 9 (46)	134 ± 2 (153)	308 ± 41 (519)	113
5	LLDPE-5	34 ± 3 (40)	135 ± 2 (214)	327 ± 25 (1153)	128
6	LLDPE-6	40 ± 6 (59)	144 ± 2 (191)	346 ± 2 (611)	115
7	LLDPE-7	30 ± 3 (41)	127 ± 2 (155)	365 ± 11 (582)	94
8	LLDPE-8	23 ± 1 (32)	256 ± 14 (503)	936 ± 179 (2604)	215
9	LLDPE-9	21 ± 2 (49)	232 ± 6 (459)	889 ± 139 (1926)	193
10	LLDPE-10	17 ± 1 (32)	180 ± 2 (329)	711 ± 11 (1674)	167

[1] The values in parentheses represent the SEC/LALLS results;
[2] $\bar{M}_w$, η are weight averages calculated from viscosity data by means of *Eqs 11* and *12*.

Operationally, it is more convenient to write *Eqs 2* to *4* in terms of t and then correct obtained values of $[t]$ and k_{Ht}, k_{Kt} for the kinetic energy and the concentration dependent density by means of simple algebraic formulas (11). For $B \simeq 0$ the formulas are simplified to read:

$$[\eta] = [t] + D \tag{5}$$

$$k_H = ([t]/[\eta])^2 (k_{Ht} + D/[t]) \tag{6}$$

$$k_K = k_{Kt} ([t]^2 + D^2/2)/[\eta]^2 \tag{7}$$

$$D \equiv 10 (\rho_0^{-1} - \rho_p^{-1}) \tag{8}$$

with ρ_0 and ρ_p being the solvent and polymer density, respectively (ρ in kg/m^3, c in g/dl, and $[\eta]$ in dl/g). For PE/TCB solutions at 140°C: ρ_0 = 1,302.4, ρ_p = 788.5, and D = −0.0050. It is evident from *Eqs 5* and *8* that the density correction D is nearly independent of polymer molecular weight and it becomes important for small $[\eta]$.

It has been found that the efflux time of TCB/LLDPE solutions, t, strongly depends on the number of passes of the solution through the capillary, n, (number of measurements). On the other hand, when testing was interrupted for 2 to 4 hrs (solution left in the viscometer at 140°C) the decrease on t versus n plot continued, indicating absence of thermal degradation. Since, initially, the samples were overstabilized, an additional amount of antioxidant was found to be unnecessary; when used, it resulted in more erratic, but similarly decreasing, t versus n dependence.

In *Fig. 2* an example of data is presented. Here the reduced efflux time, $t_{sp}/c = (t - t_0)/t_0c$, for LLDPE-8 at four concentrations is plotted as a function of the number of measurements. The least square values of the slopes:

$$S = -d(t_{sp}/c)/dn = -(dt/dn)/t_0c \tag{9}$$

are shown in *Fig. 3*. It is evident that within the range of experimental errors, S is independent

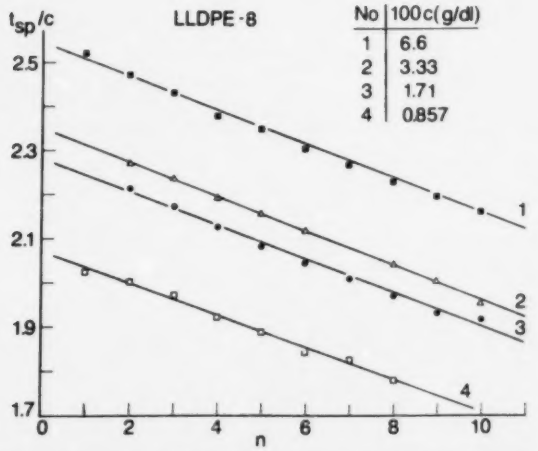

Fig. 2. Specific efflux time versus number of passes through capillary for LLDPE-8 in TCB at 140°C, at the four indicated concentrations.

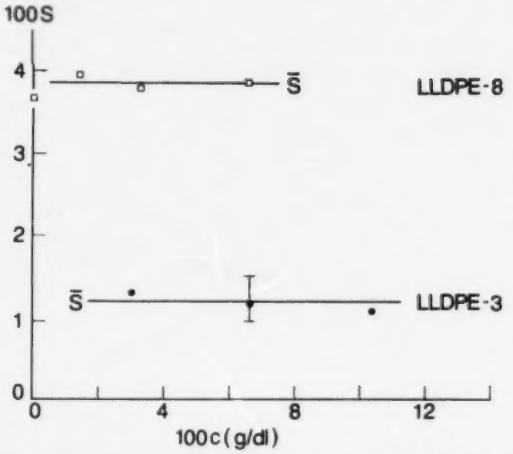

Fig. 3. Correlation between the slope, S, (of the dependence illustrated in Fig. 2) and the concentration, c, for LLDPE-8 (top) and LLDPE-3 (bottom).

of c, i.e., dt/dn is proportional to concentration. The average value of S for a given polymer-solvent pair is indicated as $\bar{S}$.

During these initial measurements a constant volume of solutions, V_1 = 10.0 ml, was placed in the viscometer. Dilutions, if needed, were done outside the instrument. On the other hand, during the standard measurement of $[\eta]$ the dilutions were carried out in the viscometer. To correct the observed efflux time the following relation was used:

$$(t_{sp}/c_k)_{corr} = (t_{sp}/c_k) + V_1\bar{S} \sum_{i}^{k} n_i/V_i \tag{10}$$

where the subscript $i = 1, 2 \cdots k$ is a counter of concentrations, n_i, $i \leq k$, is the number of measurements performed on solution with concentration, c_k, when the total volume of solution in the viscometer is V_i.

An example of the corrected data plotted according to *Eqs 2* and *3* is shown in *Fig. 4*. The values of $[\eta]$, k_H and k_k are corrected for the efflux time variation as well as the polymer solvent density difference, D, are presented in *Table 4*. In the last column, the viscosity-average MW, $\bar{M}_v$ is given. These values were calculated from the Mark-Houwink-Sakurada equation:

$$[\eta] = K\bar{M}_v^a \tag{11}$$

where K and a are parameters listed in *Table 5*. Considering the temperature range of $\bar{M}_w$ and that of $\bar{M}_w/\bar{M}_n$ for the samples listed in *Table 3*, the values of K and a parameters determined by Barlow *et al.* (15) seem to be the most appropriate.

^{13}CNMR

^{13}CNMR has been used (17–19) to determine: co-monomer concentration, average sequence length, triad distribution, run number, tacticity, long chain branching, number average molec-

ular weight, etc. The method is quantitative. Sensitivity of one structural unit per 10^4 carbon atoms or better has been obtained. The procedure of evaluating LLDPE spectra was recently published by Randall and Hsieh (20). In *Fig. 5* the band assignment from their work is reproduced.

The ^{13}CNMR spectra of eight LLDPE samples are presented in *Fig. 6*. It is worth noting that upfield from the methine peak at $\delta = 38.1$ ppm there are no distinguishable features, i.e., within the experimental range of accuracy there are no co-monomer diads, HH, in the investigated LLDPE's. The summary of ^{13}CNMR results is given in *Table 6*. Finally, in *Fig. 7* the

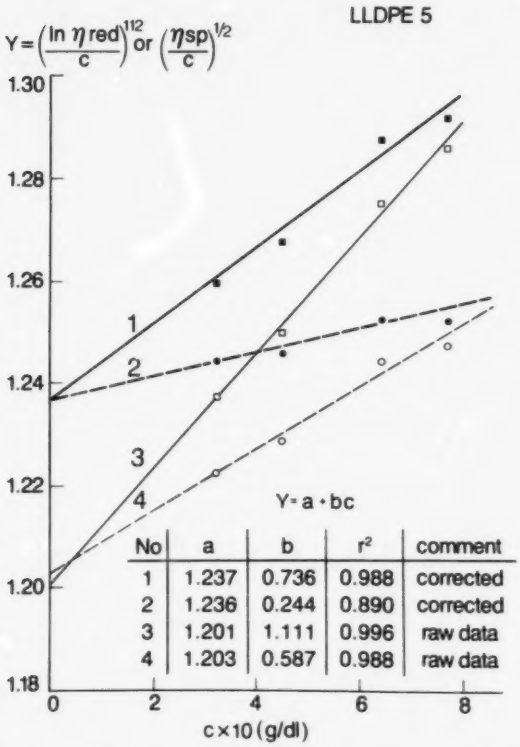

No	a	b	r²	comment
1	1.237	0.736	0.988	corrected
2	1.236	0.244	0.890	corrected
3	1.201	1.111	0.996	raw data
4	1.203	0.587	0.988	raw data

Fig. 4. $(\eta_{sp}/c)^{1/2}$ versus c and $(\ln\eta_r/c)^{1/2}$ versus c for LLDPE-5. Heavier lines, Nos. 1 and 2, represent the corrected data; lighter lines, Nos. 3 and 4, are the experimental results. (r^2 is the correlation coefficient squared of linear regression).

Table 4. Results of the solution viscosity measurements.

No	Sample	[η] (dl/g)	k_H	k_K	$\bar{M}_v$	$\bar{S} \times 10^2$
1	LLDPE-1	1.45	1.56	0.94	81	0.73
2	LLDPE-2	1.54	0.79	0.25	88	1.06
3	LLDPE-3	1.09	2.68	1.99	55	1.17
4	LLDPE-4	1.45	1.59	0.94	81	0.81
5	LLDPE-5	1.53	0.96	0.32	88	1.00
6	LLDPE-6	1.45	1.16	0.58	81	1.14
7	LLDPE-7	1.21	1.51	0.87	63	0.00
8	LLDPE-8	1.82	2.00	1.32	111	3.80
9	LLDPE-9	1.68	2.48	1.77	100	3.72
10	LLDPE-10	1.53	1.01	0.44	88	3.32

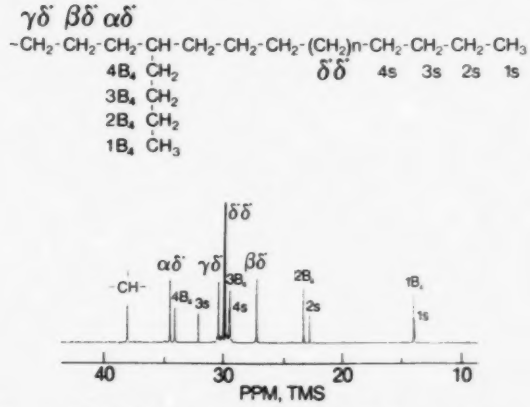

Fig. 5. ^{13}CNMR spectrum of poly(ethylene-co-hexene), LLDPE, after Randall and Hsieh (20).

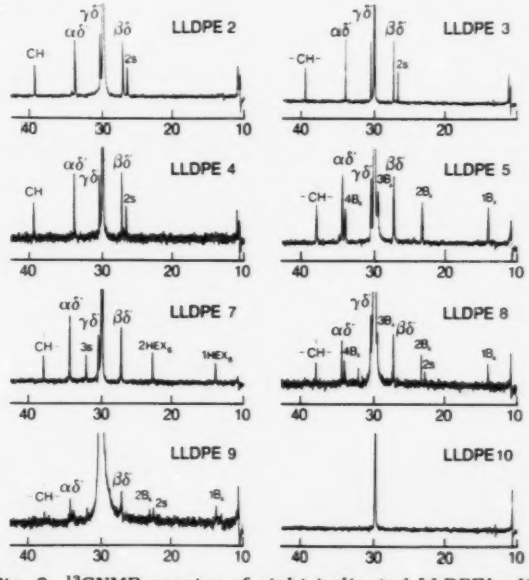

Fig. 6. ^{13}CNMR spectra of eight indicated LLDPE's dissolved in o-dichlorobenzene (10 wt %) at 120°C.

Table 5. *K* and *a* Parameters of the Mark-Houwink-Sakurada Equation for Linear Polyethylene in Trichlorobenzene.

No	Samples Used Type	$\bar{M}_v$	$\bar{M}_w/\bar{M}_n$	T (°C)	Antioxidant	K × 10⁴	a	Ref. No.
1	4 resins	6.3 to 180	3.2 to 6	130	yes	4.95	0.715	12
2	20 fractions	7.6 to 1230	1.2 to 1.4	135	yes	5.1	0.706	13
3	14 fractions	8.8 to 623	1.2 to 1.8	130	no	3.92	0.725	14
4	10 fractions + 1 resin	8.3 to 933	1.6 to 8.1	140	yes	3.95	0.726	15
5	7 resins	91 to 168	7 to 18	139	no	4.37	0.72	16

Table 6. Results of ^{13}CNMR Spectroscopy of LLDPE Samples.

No	Polymer	Co-monomer Type	X	w (wt%)	(Main Triads) × 100 EHE	HEE	EEE	R_n × 100	Average Sequence length H	E
1	LLDPE-1	C4	15.8	6.13	3.354	6.804	89.942	3.378	0.99	28.64
2	LLDPE-2	C4	11.2	4.40	2.318	4.501	93.181	2.284	1.02	42.77
3	LLDPE-3	C4	19.4	7.48	4.088	7.686	87.982	3.966	1.09	24.12
4	LLDPE-4	C4	19.2	7.41	4.525	8.137	86.882	4.297	1.16	22.11
5	LLDPE-5	C6	13.7	7.81	2.932	6.402	90.128	3.708	0.94	26.03
6	LLDPE-6	C6	11.1	6.37	2.362	—	97.638	2.362	1.00	41.34
7	LLDPE-7	C8	14.5	10.7	3.622	7.496	88.882	3.685	0.98	26.15
8	LLDPE-8	C6	4.12	2.43	0.756	2.220	96.316	1.110	1.32	88.77
9	LLDPE-9	C6	2.06	1.23	0.255	1.445	97.364	0.723	1.65	136.67

X is the number of co-monomers per 1000 carbon atoms; *w* is co-monomer content in weight percent; in the triads *E* and *H* represent respectively ethylene and co-monomer unit; R_n is the run number; in the "average sequence length"; *H* represents the average number of co-monomer units and *E* that of ethylene units in the macromolecules.

density is plotted as a function or run number, R_N. As observed before (20) the relation does not depend on the co-monomer type.

Atomic Absorbance (AA)

The results of the atomic absorbance analysis are shown in *Table 7*. A significant difference was found in the ash composition of LLDPE-3 and LLDPE-8; while LLDPE-3 contains 4.39 ppm of Ti, LLDPE-8 primarily V (2.55 ppm). This is in good agreement with the reported observation that LLDPE polymerized with V-catalyst has a larger MWD than that of LLDPE obtained using Ti-based one.

DISCUSSION

On the basis of SEC/LALLS and ^{13}CNMR results it is evident that the LLDPE samples do not have long chain branching. Furthermore, the placement of co-monomer segments in the macromolecules is random for all but the very broad MWD samples, LLDPE-8 to LLDPE-10. In the latter case it seems that there is a preferential diad placement of the hexene monomers. The effect is evident in spite of very low co-monomer concentration. There is information in the literature allowing postulation of different catalysts for these two sample groups (21). On this basis as well as the AA results reported in *Table 7*, it seems that for the first seven resins the catalyst most likely was titanium-based and for the last three, vanadium-based.

It is very satisfying to see that the ^{13}CNMR results confirm very well the published data on LLDPE. In particular, the average sequence length reported in *Table 6* and the correlation between the run number and sample density, shown in *Fig. 7*, are in agreement with the recent Randall and Hsieh report (20).

Now, turning to the measurements of the molecular weights and their averages the SEC, SEC/LALLS and solution viscosity must be jointly considered. In *Table 3* the SEC and SEC/LALLS data are shown. To compare the viscosity results the $\bar{M}_v$ should be converted into $\bar{M}_w$. Using the log-normal distribution (4, 5) the following formula was derived:

$$\bar{M}_w/\bar{M}_v = (\bar{M}_w/\bar{M}_n)_{1-a}$$

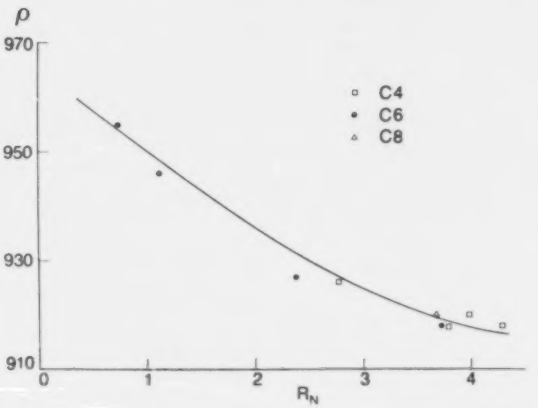

Fig. 7. Ambient temperature density of the investigated LLDPE samples versus the run number as determined by ^{13}CNMR.

Table 7. Results of the Atomic Absorbance Analysis. Samples Analyzed Only for Chromium, Vanadium, and Titanium.
(The data in parts-per-million, ppm)

Element	Results LLDPE-3	LLDPE-8	Instrument Detection Limit
Chromium	0.97 ± 0.02	0.33 ± 0.01	0.05
Vanadium	<0.1	2.55 ± 0.12	0.1
Titanium	4.39 ± 0.22	0.6	0.6

where $a = 0.726$ is the Mark-Houwink-Sakurada exponent. It is evident that $\bar{M}_w$ and $\bar{M}_{w,\eta}$ (from $[\eta]$) are parallel to each other, with $\bar{M}_w$ being larger than $\bar{M}_{w,\eta}$ by 20 ± 9 percent. This difference may be due to the absence of antioxidant during the viscosity measurements. During the $[\eta]$ measurement, it was observed that addition of Santonox-R to the solutions caused only a large scatter of the efflux times. However, in SEC measurements, the absence of the antioxidant was responsible for lower $\bar{M}_w$; the decrease was 15 percent in $\bar{M}_w$'s.

The $\bar{M}_w$'s determined in SEC/LALLS are systematically higher than both $\bar{M}_w$'s and $\bar{M}_{w,\eta}$'s. Furthermore, they increase with MW, e.g.: $M_{w(\text{LALLS})} = 0.0567\ [M_w\ (\text{SEC})]^{1.65}$; $r^2 = 0.951$. This systematic bias toward high molecular

weight may be due to the difference in the SEC detection systems; in SEC only the refractive index detector was used, whereas in SEC/LALLS the data were computed using the low angle light scattering intensity. It is recognized that at low concentrations LALLS "does not see" the small molecular weight fractions (6, 22). This has been quoted as evidence for superiority of the method. It very well may be that the SEC/LALLS results are indeed closer to $\bar{M}_w$ as determined by a direct method. This would mean that the SEC and viscometric data are at least consistent within the framework of the available techniques. It is worth noting that Barlow *et al.*'s constants listed in *Table 5* were determined on the basis of a standard SEC method.

The last property to be discussed is the systematic decrease of the efflux time, t, with the number of passes through a capillary, illustrated in *Figs. 2* and *3*. As the interruption of the test for 2 to 4 hrs did not generate any change in the efflux time, the conclusion was that no thermal degradation occurred. On the other hand, after running the solution through a capillary 50 to 60 times, a much more stable set of t's were obtained, indicating that an end of the flow modification was being reached. The subsequent determination of $[\eta] = 1.23$ for sample LLDPE-8 indicated a severe decrease of $\bar{M}_v$ from 111,000 to 65,000.

As reported in the last column of *Table 4*, the average initial rates of the efflux time decrease, $\bar{S}$, can be grouped into three categories: the high values $\bar{S} \cdot 10^2 = 3.3$ to 3.8 for LLDPE-8, LLDPE-9, and LLDPE-10, the middle ones for LLDPE-1 to 6 and the low value, $\bar{S} = 0$ for LLDPE-7. These three categories seem to be defined by the polymerization conditions.

That passing LLDPE solution through a capillary results in a true mechanical degradation is evidenced by three facts: (i) There is no return to higher efflux times, i.e., once a lower viscosity value is reached it either remains constant or decreases further to an "equilibrium" level upon further passages. (ii) There is a significant drop of the $[\eta]$, from which the ratio of $\bar{M}_v$'s, initial to "equilibrium," equals 111/65 = 1.7. (iii) The solution passed through a capillary 65 times, with an efflux time near its "equilibrium" value, than injected into SEC showed a decrease of the *MW* (in $\bar{M}_w$ and $\bar{M}_z$ by a ratio 1.6 and 1.7, respectively) and narrowing of the *MWD* from $\bar{M}_w/\bar{M}_n = 11.1$ to 7.8.

It has been found that the degradation occurs not during the measuring part of the test, where the solution flows under gravity with $t > 200$ s but rather during the pumping stage, when it is being pushed by air pressure to the upper part of the Cannon-Ubbelohde viscometer in about $t_p \simeq 30$ s. This rather obvious fact has been noted only in the latter part of the study. Lack of control of the "pumping time" was, in part, responsible for the initial experimental error in $\bar{S}$. It has also been observed that when t_p was increased to at least 100 s, $\bar{S} = 0$ was obtained for all samples. In short, for the phenomenon to occur the stress must exceed a critical value.

The mechanical degradation of polymers in dilute solutions has been studied extensively (23–27) and the question concerning possible flow degradation in SEC was recently reviewed (28). There seems to be an agreement that not a shear, but rather an extensional flow at the entrance to the capillary is responsible for the mechanical degradation of macromolecules. For $t_p = 30$ and 100 s, the extensional stress (29, 30) is respectively: $\tau_{11} = 2.10^5$ and 6.10^4 Pa. At concentration 0.1 g/dl of $\bar{M}_w = 3 \times 10^5$, these values correspond to $E_b = 600$ to 200 kJ/mol, i.e., to the range of bond energies in organic molecules.

The mechanical degradation test for the most rapidly degrading in TCB resin, LLDPE-8, was repeated using decalin as a solvent. A systematic decrease of the efflux time was again observed, with $S = 0.0128$. It should be noted that for the same resin in TCB this parameter was about three times larger. It is evident that the type of solvent plays an important role in the degradation process.

SUMMARY

1. The SEC/LALLS data indicated absence of long chain branching.

2. The SEC and solution viscosity $\bar{M}_w$ showed a good agreement. The reproducibility of SEC results was the best for $\bar{M}_w$ with about ±5 percent error. The range of molecular weights was relatively narrow: $\bar{M}_w \times 10^{-3} = 111$ to 256.

3. Three types of *MWD* were found: (i) very broad, with $\bar{M}_w/\bar{M}_n = 11$ for LLDPE-8- to -10, (ii) broad with $\bar{M}_w/\bar{M}_n = 6.9$ and 4.2, for LLDPE-3 and -7, respectively, and (iii) narrow, $\bar{M}_w/\bar{M}_n = 3$ to 4 for the remaining samples.

4. The intrinsic viscosity allowed to confirm the $\bar{M}_w$ values determined in SEC. Furthermore, the large values of the Huggins and Kraemer constants indicated strong interactions between the macromolecules.

5. From ^{13}CNMR the concentration of co-monomer, the triad distribution, the average mer sequence length and the run number, R_N, were calculated. It was found that the ambient temperature resin density is a function of R_N, independent of the chemical nature of co-monomer.

6. Two types of metal contaminants were found in the gas-phase resins. The very broad *MWD* LLDPE-8 contained 2.55 ppm of V and only traces of Ti, whereas the narrow *MWD* LLDPE-3 contained 4.39 ppm of Ti and only traces of V. Smaller quantities of Cr were detected in both samples.

7. The mechanical stability of the very broad *MWD* resins LLDPE-8 to -10 in TCB or decaline solutions was found to be the poorest, that of

LLDPE-7 the best, with the remaining resins forming an intermediary group.

ACKNOWLEDGMENTS

The authors wish to express their gratitude to Professor A. Rudin and Dr. V. Grinshpun from University of Waterloo, Ontario for SEC/LALLS data and to Dr. S. K. Brownstein from the Division of Chemistry, National Research Council of Canada, Ottawa, Ontario for carrying out the ^{13}CNMR measurements.

NOMENCLATURE

A, B	= viscometer constants; *Eq 1.*
a	= exponent of Mark-Houwink-Sakurada; *Eq 11.*
^{13}CNMR	= carbon-13 Nuclear Magnetic Resonance.
c, c_k	= concentration, that of the k-th dilution in the viscometer.
GPC	= gel permeation chromatography.
D	= density correction factor; *Eqs 5, 6, 7, 8.*
E_b	= bond energy.
K	= Mark-Houwink-Sakurada coefficient; *Eq 11.*
k_H, k_K	= Huggins, Kraemer constants; *Eqs 2, 3, 6, 7.*
k_{Hi}, k_{Ki}	= Huggins and Kraemer uncorrected interaction constants; *Eq. 6, 7.*
LALLS	= low angle laser light scattering.
LCB	= long chain branching.
LDPE, LLDPE	= low density and linear low density polyethylene.
$\bar{M}_n, \bar{M}_v, \bar{M}_w, \bar{M}_z$	= number, viscosity, weight, and z-average molecular weights, respectively in kg/mole.
MI	= melt index.
MW	= molecular weight.
MWD	= molecular weight distribution.
SCB	= short chain branching.
SEC	= size exclusion chromatography.
UHMWPE	= Ultra high molecular weight polyethylene.
n, n_i	= number, number of the i-th pass of the solution through the capillary.
PE	= polyethylene.
PC	= plate count of GPC columns.
$S, \bar{S}$	= slope and its average value; *Eq 9.*
T	= temperature.
$t, t_0, [t], t_{sp}$	= efflux time for solution and solvent, intrinsic and specific efflux time, respectively.
t_p	= pumping time.
$\eta, \eta_r, \eta_{sp}, [\eta]$	= absolute, reduced, specific, and intrinsic viscosity, respectively.
η_0	= solvent viscosity.
ρ_0, ρ_p	= solvent and polymer density.

REFERENCES

1. L. A. Utracki, *Adv. Plast. Technol.*, **5**, 41 (1985).
2. A. A. Alim in "Panel and General Discussion," during NRCC/IMRI symposium "Polyblends-'84," Boucherville, Quebec, Canada, 17 April 1984; *Polym. Eng. Sci.*, **24**, 1359 (1984).
3. A. E. Hamielec and A. C. Ouano, *J. Liq. Chromat.*, **1**, 111 (1978).
4. L. A. Utracki and M. M. Dumoulin, *ACS Div. Org. Coat. Plastics Chem.*, **48**, 859 (1983).
5. L. A. Utracki and M. M. Dumoulin, in "Size Exclusion Chromatography," T. Provder, Ed., *A.C.S. Symp. Ser.*, **245**, 97 (1984).
6. V. Grinshpun, K. O'Driscoll, and A. Rudin, *J. Appl. Polym. Sci.*, **9**, 1071 (1984).
7. L. Letot, J. Lesec, and C. Quivoron, *J. Liq. Chromat.*, **3**, 1637 (1980).
8. V. Grinshpun, K. F. O'Driscoll, and A. Rudin, in "Size Exclusion Chromatography," T. Provder, Ed., *A.C.S. Symp. Ser.*, **245**, 273 (1984).
9. G. Samay and L. Füzes, *J. Polym. Sci. Polym. Symp.*, **68**, 185 (1980).
10. M. R. Cannon, R. E. Manning, and J. D. Bell, *Anal. Chem.*, **32**, 355 (1960).
11. L. A. Utracki, *J. Polym. Sci.: Part A-1*, **4**, 717 (1966).
12. B. A. Whitehouse, *Macromolecules*, **4**, 463 (1971).
13. E. P. Otocka, R. J. Roe, M. Y. Hellman, and P. M. Muglia, *Macromolecules*, **4**, 507 (1971).
14. H. L. Wagner and C. A. J. Hoeve, *J. Polym. Sci., Polym. Phys. Ed.*, **11**, 1189 (1973).
15. A. Barlow, L. Wild, and R. Ranganath, *J. Appl. Polym. Sci.*, **21**, 3319 (1977).
16. W. A. Dark, *Chromatogr. Sci.*, **13**, 281 (1980).
17. F. A. Bovey, R. E. Cais, L. W. Jelinski, F. C. Schilling, W. H. Stornes Jr., and A. E. Tonelli, *Am. Chem. Soc., Adv. Chem. Ser.*, **203**, 421 (1983).
18. W. Klöpffer, "Introduction to Polymer Spectroscopy," Springer-Verlag, Berlin (1984).
19. J. C. Randall, Ed., "NMR and Macromolecules," *Am. Chem. Soc., Symp. Ser.*, **247**, (1984).
20. J. C. Randall and E. T. Hsieh, Ch. 9 in Ref. 19.
21. T. E. Nowlin, *Prog. Polym. Sci.*, **11**, 29 (1985).
22. T. B. MacRury and M. L. McConnell, *J. Appl. Polym. Sci.*, **24**, 651 (1979).
23. J. D. Culter, J. L. Zakin, and G. K. Patterson, *J. Appl. Polym. Sci.*, **19**, 3235 (1975).
24. D. L. Hunston, *J. Polym. Sci., Polym. Chem. Ed.*, **14**, 713 (1976).
25. J. F. S. Yu, J. L. Zakin, and G. K. Patterson, *J. Appl. Polym. Sci.*, **23**, 2493 (1979).
26. H. G. Müller and J. Klein, *Makromol. Chem. Rapid Commun.*, **1**, 27 (1980).
27. S. Ghoniem, G. Chauveteau, M. Moan, and C. Wolff, *Can. J. Chem. Eng.*, **59**, 450 (1981).
28. H. G. Barth and F. J. Carlin, Jr., *J. Liq. Chromat.*, **7**, 1717 (1984).
29. F. N. Cogswell, *Polym. Eng. Sci.*, **12**, 69 (1972).
30. L. A. Utracki, M. M. Dumoulin, and P. Toma, paper No. 7 presented at the sixth annual NRCC/IMRI meeting, "Polyblends-'85," Boucherville, Que., Canada, 16–17 April, 1985; *Polym. Eng. Sci.*, **26**, 34 (1986).

Linear Low Density Polyethylenes and Their Blends: Part 2. Shear Flow of LLDPE's

L. A. UTRACKI *and* B. SCHLUND*

National Research Council Canada
Industrial Materials Research Institute
Boucherville, Quebec, J4B 6Y4

The steady state and dynamic shear behavior of eleven commercial linear low density polyethylenes (LLDPE) and one low density polyethylene (LDPE) resin were measured in capillary and parallel plate geometries at T = 150 to 230°C. The extrudate swell and the Bagley correction were determined. A large pressure effect on capillary flow of narrow molecular weight distribution LLDPE was observed and a new corrective procedure was proposed. After the correction the steady state viscosity was found to be equal to the dynamic (not complex) viscosity: $\eta(\dot{\gamma}) = \eta'(\omega = \dot{\gamma})$. A newly proposed four parameter relation between η and the deformation rate was found to provide a simple means for computation of the zero shear viscosity, η_0, and the primary relaxation time. Both these parameters showed a high degree of correlation. The expected relation: $\eta_0 \propto M_w^{3.4}$ was observed for low molecular weight samples with low polydispersity. The LLDPE activation energy of flow, E_a = 29.9 ± 1.8 kJ/mole, was determined.

INTRODUCTION

In this second part the steady state and dynamic shear properties of 11 linear low density polyethylene samples (LLDPE) and one low density polyethylene resin (LDPE) will be discussed.

It is a common practice to use the rotational rheometer to measure the steady state or dynamic properties of polymer melts at relatively low rates of deformation. The instrument allows determination of both the viscous and elastic parts of the stress tensor. These data are of prime interest for correlating the flow functions with molecular parameters and predicting the material behavior at the low rates of deformation in processing steps, usually outside the processing equipment.

In order to measure the melt flow properties at high deformation rates, a plunger-type capillary viscometer is used. This type of instrument in principle allows determination of the steady state viscosity, η, as a function of the rate of shear, $\dot{\gamma}$, at the capillary wall. However, it is generally accepted that: (i) the extrudate swell, B, and (ii) the entrance-exit (Bagley) correction, P_e, may provide information on the first normal stress difference, N_1. Both η and N_1 are needed to predict the processability.

On the following pages an attempt will be made to correlate the viscous and elastic measures at low deformation rates in steady state and dynamic shear flow, as well as to establish relations between those and the rheological functions extracted from the capillary measurements.

The shear flow results will be compared with the extensional data in Part 3 of this series of publications. Finally, in Parts 4 and 5, the shear and elongational behavior of LLDPE blends will be discussed respectively.

EXPERIMENTAL

Materials

Ten LLDPE resins (characterized in Part 1 (1)), one commercial LLDPE, LPX-30, and one low density polyethylene, LDPE-102, were used in this study. The characteristics of the two latter resins are provided in *Table 1*.

Molecular Characterization

The 12 resins with different melt index, density, molecular weight, and molecular weight distribution were analyzed by SEC, SEC/LALLS, solution viscosity, and ^{13}CNMR. The Waters Sci. GPC-150C instrument was used at

* Present Address: CNRS—Laboratoire des Matériaux Organiques Echangeur de Solaise, Autoroute Lyon-Vienne, BP-24 69390 VERNAISON, FRANCE.

Table 1. Characteristics of LPX-30 and LDPE-102.

No.	Parameter	LPX-30	LDPE-102
1	Manufacturer	Esso Chem. Canada	Exxon Chem.
	Density (kg/m^3)	918	922.5
	Melt Index (190°C, 2.16 kg; g/10 min)	1.0	6.5
2	Molecular Weight averages (kg/mole)		
	M_n	29 ± 2	20 ± 1
	M_z	212 ± 27	225 ± 8
	M_w/M_n	3.4 ± 0.2	4.1 ± 0.1
3	Co-monomer	Butene	—
4	Branches (C_n long per 1000 C-atoms)		
	from SEC/LALLS: $n \geq 10$	0	≤1.2[a]
	from ^{13}CNMR: $n = 2$	n.m.[b]	2.06
	$n = 3$	n.m.	0.00
	$n = 4$	n.m.	4.93
	$n = 5$	n.m.	1.52
	$n = 6$	n.m.	4.11
5	Solution viscosity results:	n.m.	
	$[\eta]$ (dl/g)		0.655
	k_H		2.48
	k_K		1.82

[a] Branching density decreases with MW, (3).
[b] n.m.—means "not measured".

140°C with 1,2,4,trichlorobenzene (TCB) as a solvent. The four columns (10^3, 10^4, 10^5, and 10^6 Å) were calibrated using 12 polystyrene (PS) standard samples (2) in TBC at 140°C. The results are listed in *Table 3* of part 1 (1) and *Table 1* of this paper. The complementary studies by the SEC/LALLS (3), carried out under the same conditions, demonstrated an absence of long chain branching (LCB) for all LLDPE's. The LCB for LDPE was found to be a decreasing function of the molecular weight, MW.

The ^{13}CNMR spectra were determined with a Brukner 100 MHz spectrometer using 10 percent solutions in o-dichlorobenzene at 120°C. From the results (4–6) for LLDPE's, the comonomer concentration, triad distribution, average sequence length, and run number were calculated (1). For LDPE the results are summarized in *Table 1*.

Sample Preparation

The samples were supplied as pellets of pure resin stabilized by addition of 0.2 weight percent of IRGANOX and IRGAFOS 1:1 mixture. Since the LLDPE's will be used in blends, for comparative purposes the neat resins were also extruded using the twin-screw Werner-Pfleiderer ZSK-30 extruder at 140 rpm. The following temperature profile was used: 158 (feeder), 192, 214, 196, and 196°C (die). The metering feeder, Incrison Model 105-C, was used. The extrusion rate for all the resins, varied from $Q = 6$ to 7.8 (kg/hr).

Rheological Testing

Instron Capillary Rheometer (Model 3211), ICR, at 190°C was used. To determine the activation energy of flow, the two samples, LLDPE-1 and LLDPE-8 having widely different z-average molecular weights, $M_z = 342$ and 936 (kg/mole) respectively, were tested at 150° and 230°C as well.

One or two series of capillaries characterized by constant diameter, either $d = 0.747$ or 1.273 mm, were used. In each series there were at least three capillary lengths, L. The ratio L/d varied from 0.6 to 60. Six crosshead speeds were used within the range of shear stress, σ_{12}, limited by onset of the melt fracture.

The extrudate swell was measured as described by Teh *et al.* (7). Briefly, the diameter, D_e, of the air-quenched extrudate about 5 cm long, was measured with a micrometer. The capillary with $d = 1.273$ mm and $L/d = 40$ was used. The range of σ_{12} varied from 18.5 to 400 MPa. The extrudate swell was calculated as:

$$B = (D_e/d)(\rho_a/\rho_{190})^{1/3} \quad (1)$$

where ρ_a and ρ_{190} represent the resin density at ambient temperature and at 190°C, respectively.

Rheometrics Mechanical Spectrometer, Model 605, RMS, was used in the dynamic mode at 150°C with the parallel plates geometry. For LLDPE-4 and LLDPE-10 the tests at 190 and 230°C were also carried out. To examine the thermal stability of the resins, first the time sweep at strain $\dot{\gamma} = 15$ percent and frequency = $\omega = 10$ rads/s was performed. At 150, and at 190 or 230°C the time sweep was respectively 120 and 60 min. Judging by stability of the shear storage modulus, G', the samples were stable in air at 150°C for at least one hour. However, at higher temperatures to ascertain similar stability the tests had to be carried out under a blanket of dry nitrogen.

The frequency sweep at $\gamma = 15$ percent was performed in two directions: for two samples from $\omega = 0.1$ to 100 (rads/s) and for two others from 1 to 0.01 (rads/s). Two diameters of platens were used: 25 and 50 mm. The results were accepted if the maximum difference between the results of these four sweeps in the common range: $\omega = 0.1$ to 1.0 did not differ by more than

5 percent (the observed error of measurement was ±2 percent).

On the basis of the experience with similar resins (8–10) the strain level was selected as γ = 15 percent. This provided a strong enough signal within the range of linear viscoelastic behavior. The measurements were recorded using the RMS Columbia terminal, Model 964, then the data were transferred to a Hewlett-Packard, HP-85, mini-computer for analysis and mathematical manipulation, viz.. calculation of two zero shear viscosities, η_0.

RESULTS

Capillary Flow

The following three rheological functions were determined: steady state shear viscosity $\eta = \eta(\dot{\gamma}, T)$, the entrance-exit pressure drop, otherwise known as the Bagley correction, $P_e = P_e(\dot{\gamma}, T)$ and the extrudate swell, $B = B(\dot{\gamma})$.

To calculate η and P_e the Bagley and Rabinowitsch corrections were applied (8, 9). It has been observed that at $T \geq 190$°C the Mooney correction was not necessary. For $L/d \geq 40$ at higher crosshead speeds a systematic deviation from that postulated by the Bagley linear correlation between the pressure and L/d was observed. The effect was treated as due to the pressure variation of the shear viscosity. A new method of data correction will be proposed in the *DISCUSSION*.

In *Table 2* the capillary results at 190°C are presented. In addition in *Figs. 1* to *3* the η versus $\dot{\gamma}$ are shown.

Dynamic Tests

For most polymeric samples the total time for loading, trimming, and relaxing does not exceed 10 min. Since it takes 24 min to scan the lower three decades of frequency, the samples should be stable for at least 34 min. It was observed that the samples LLDPE-8, 9, and 10 relaxed very slowly; $t_R > 20$ min at 230°C. Since the thermo-oxidative degradation in air was observed to become noticeable after six min at exposure to 230°C, it was necessary to test these samples in dry nitrogen. Under these conditions, both G' and G'' (in time sweep test) remained stable for at least 80 min.

It is known that G' is more sensitive than G''. During a thermooxidative degradation of polyolefins, chain scission and grafting may lead to branching and partial crosslinking. It has been observed (10) that during such a process G' systematically increases even while G'' decreases. As mentioned before, four specimens were tested in two directions in frequency sweep, using two different pairs of platens with the diameters of 25 and 50 mm. At 150°C an excellent superposition of all four sets of data was observed. However, at 190° and 230°C the data for LLDPE-10 indicated a systematic difference in G' for the two geometries. The storage modulus at the lowest frequency, 10^{-2} rad/s, from the smaller platens was higher by 18 and 36 percent and 190° and 230°C respectively than that obtained from larger ones. The difference vanished at $\omega > 2$ rads/s. It was postulated that the effect originated in a thin layer of thermo-oxidated material formed during the brief moments while the sample was exposed to air for loading and trimming. Since the area-to-volume ratio is inversely proportional to diameter, the effect should be more apparent in small than large platen tests.

The summary of dynamic test results is presented in *Figs. 1, 2* and *4* as frequency dependent dynamic, η', and complex, η^*, viscosities.

Temperature Effect on Shear Viscosities

As indicated in *Table 3*, four LLDPE's were examined at 150°, 190°, and 230°C either in dynamic or in steady state shearing mode. In *Figs. 3* and *4* η/a_T versus $\dot{\gamma}a_T$ and η'/a_T versus ωa_T are shown respectively. From the experimental values of the shift factor, a_T (determined by a horizontal shift of σ_{12} versus $\dot{\gamma}$ or G'' versus ω) the activation energy of flow:

$$E_a = R\delta \ln a_T/\delta(1/T)|_{\sigma_{12}=\text{const}} \qquad (2)$$

was calculated (see *Table 3*). Since there is no correlation with either the method of measurements or molecular parameters, the observed variation should be considered as a reflection of experimental uncertainty, i.e., $E_a = 29.9 \pm 1.8$ (kJ/mole) for LLDPE's in good agreement with the literature values: $E = 29.1$ to 34.1 (7).

The values calculated from *Eq 2* were determined at constant shear stress. Similarly, one can define the activation energy at constant rate of deformation, E_γ. By writing η as a function of σ_{12} and T and as that of $\dot{\gamma}$ and T, and by equating the total differentials, the exact general relation between E_a and E_γ can be readily obtained. Furthermore, assuming that locally σ_{12} is proportional to $\dot{\gamma}^n$ and treating $\dot{\gamma}$ as the independent variable the relation:

$$E_\gamma = nE_a; \qquad 0 \leq n \leq 1 \qquad (3)$$

is obtained, where n is the local "power-law" exponent. For $\dot{\gamma} \to 0$, $n \to 1$, and the two activation energies are equal. Experimentally E_a is nearly constant, close in its numerical value to the zero-rate-of-shear, E_0, i.e., as $\dot{\gamma}$ or σ_{12} increases causing a decrease in n, the E_γ decreases toward 3 to 4 times smaller values than E_a. The E_γ and n values are also presented in *Table 3*. It can be seen that *Eq 3* proves to be a surprisingly good description of the observed behavior.

DISCUSSION

Correction of the Capillary Viscosity Data

In *Figs. 5* and *6* the experimental data of LLDPE-8 and 2 are presented. It is evident that

Table 2. Capillary Flow Data for Polyethylene Resins at 190°C.

Polymer	V_s (cm/min)	σ_{12} (kPa)	$\dot{\gamma}$ (s^{-1})	η (kPa·s)	P_e (MPa)	B (–)	N_{1e} (kPa)
LLDPE-1	0.06	27.30	3.714	7.350	0.2932	1.24	123
	0.2	63.95	13.64	4.689	0.3061	1.26	306
	0.6	117.8	47.85	2.463	0.8619	1.32	693
	2.0	170.2	239.5	0.7105	3.462	1.44	1330
LLDPE-2	0.06	21.65	3.737	5.792	0.3294	1.22	90
	0.2	54.03	13.17	4.102	0.4475	1.31	299
	0.4	84.01	28.13	2.986	0.7020	1.33	499
	0.6	102.8	44.85	2.292	1.277	1.36	655
	1.2	137 2	108.3	1.267	2.937	1.42	10307
LLDPE-3	0.06	18.07	4.441	4.069	0.4245	1.33	107
	0.2	33.48	14.80	2.262	0.7887	1.40	237
	0.4	48.12	29.60	1.625	1.026	1.43	370
	0.6	56.86	44.41	1.280	1.446	1.47	482
	1.2	78.30	88.81	0.8816	2.058	1.52	756
	2.0	105.8	148.0	0.7148	3.551	1.58	1131
LLDEP-4	0.06	19.16	3.837	4.993	0.009899	1.20	74
	0.2	46.97	13.13	3.578	0.07401	1.28	237
	0.4	73.22	27.29	2.683	0.2665	1.31	409
	0.6	91.88	42.55	2.159	0.4885	—	—
	2.0	153.9	198.5	0.7756	2.043	1.37	1017
	4.0	172.3	2867.0	0.06009	4.808	—	—
LLDPE-5	0.06	19.46	3.769	5.163	0.3206	1.18	69
	0.2	46.09	13.17	3.501	0.5947	1.23	232
	0.4	78.06	27.75	2.813	0.9220	1.31	438
	0.6	90.43	43.57	2.075	1.415	1.34	557
	1.2	126.9	98.95	1.283	2.152	1.41	933
	2.0	151.0	196.9	0.7668	3.708	1.43	1155
LLDPE-6	0.06	23.97	3.862	6.208	0.01997	1.23	104
	0.2	56.43	13.52	4.179	0.1482	1.30	305
	0.4	80.34	28.54	2.815	0.9977	1.33	478
	0.6	104.3	44.88	2.325	1.290	1.33	621
	1.2	138.2	102.2	1.352	2.439	1.44	1093
	2.0	161.0	203.6	0.7909	4.641	1.48	1379
LLDPE-7	0.06	21.10	4.039	5.224	0.1654	1.35	132
	0.2	44.48	13.72	3.241	0.3586	1.39	308
	0.4	67.73	28.21	2.401	0.3607	1.41	498
	0.6	83.54	43.40	1.925	0.5674	1.46	694
	2.0	145.0	170.8	0.8489	1.571	1.53	1415
	4.0	176.1	452.4	0.3893	3.228	—	—
LLDPE-8	0.06	67.39	4.698	14.35	0.6997	—	—
	0.2	114.4	16.00	7.146	0.6844	1.25	539
	0.4	147.9	33.45	4.421	0.9247	1.25	678
	0.6	169.6	52.78	3.213	1.113	1.30	916
	1.2	214.0	127.9	1.673	1.612	1.31	1216
	2.0	229.9	328.4	0.7002	4.295	1.34	1272
LLDPE-9	0.06	51.52	4.532	11.37	—	1.31	290
	0.2	88.62	15.26	5.808	0.4135	1.27	440
	0.4	126.3	31.11	4.060	—	1.19	459
	0.6	146.3	47.64	3.071	0.4432	1.17	498
	1.2	192.3	101.6	1.893	0.4865	1.21	761
	2.0	230.3	185.6	1.241	1.238	1.24	1017
LLDPE-10	0.06	27.40	4.553	6.018	0.1442	1.36	—
	0.2	51.52	15.18	3.395	0.4840	1.36	334
	0.4	68.41	30.35	2.254	0.5103	1.32	393
	0.6	79.16	45.53	1.739	—	1.36	513
	1.2	117.8	91.06	1.294	0.7334	1.40	851
	2.0	141.2	151.8	0.9305	0.9530	1.43	1087
LPX-30	0.06	19.54	3.765	5.190	0.08002	1.21	78.6
	0.2	48.79	13.19	3.699	0.1361	1.22	203
	0.4	71.61	27.92	2.565	—	—	—
	0.6	95.40	44.05	2.166	0.8777	1.26	460
	1.2	126.5	101.8	1.242	2.534	1.31	713
	2.0	146.3	210.3	0.6956	4.605	1.43	1127
LDPE-102	0.06	4.534	4.212	1.076	0.1195	1.29	24
	0.2	8.972	14.04	0.6391	0.2932	1.69	119
	0.4	14.71	28.08	0.5238	0.3500	1.91	286
	1.2	26.87	84.24	0.3189	0.6167	1.96	567
	2.0	34.97	140.4	0.2491	0.8859	1.92	692
	4.0	47.87	280.8	0.1705	1.173	—	—

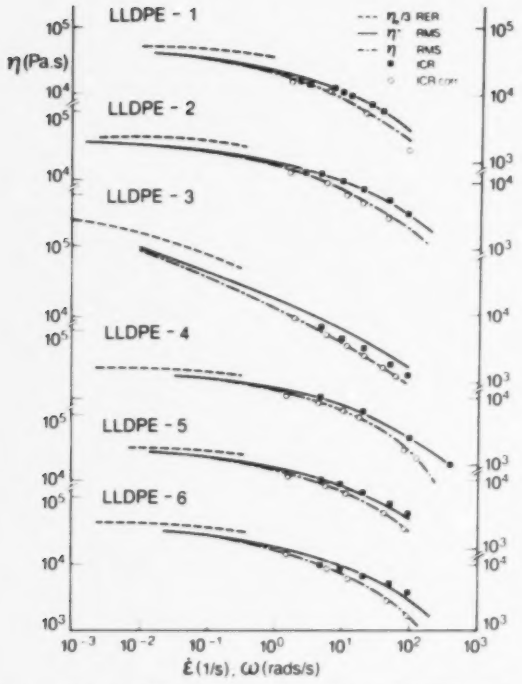

Fig. 1. The capillary shear viscosity, η, versus rate of shear, $\dot{\gamma}$, at 190°C for LLDPE-1 to 6 (points) compared with the dynamic flow results (η^*-solid line, η' broken line). Two sets of η-values are indicated: solid squares—not corrected for the pressure effect, open circles—corrected.

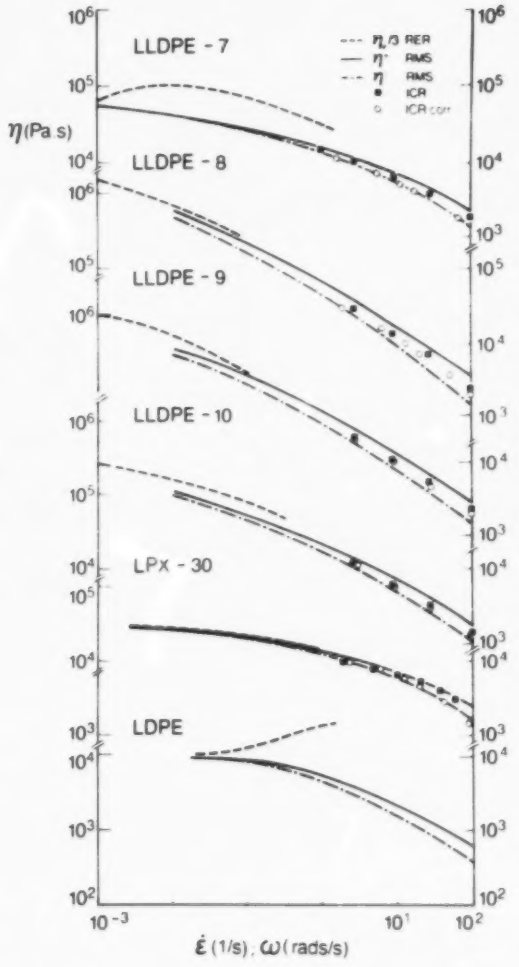

Fig. 2. The same dependence as in Fig. 1 for the remaining samples, LLDPE-6 to 10, LPX-30, and LDPE-102.

while for the first sample the Bagley linearization works very well ($r^2 \geq 0.999$), for the latter one (when F starts to exceed 100 kg) a serious deviation from linearity is observed.

The positive deviation in the Bagley plots at higher values of L/d has been discussed (11–13). The authors considered the effect to be mainly due to increase of η with pressure. Following this assumption, various methods were proposed to correct the plot and to extract the $\eta = \eta(P)$ dependence from the capillary measurements. However, since the effect is usually small and there are several sources of experimental errors in capillary measurements, the methods did not yield accurate information.

The main goal of the new method is to correct the Bagley plot in order to extract the true values of shear stress and the entrance-exit corrections.

In the recent paper on the method of computation of the pressure and temperature effects on the zero shear melt viscosity, η_0, Utracki (14) reported that η_0 can be expressed as a function of the free volume fraction, f, computed for a given system from Simha's (15) statistical thermodynamic equation of state. A linear correlation:

$$\log_{10}\eta_0 = a_0 + a_1 Y_s \qquad (4)$$

was found, where:

$$Y = Y(T, P) = 1/(f + a)$$

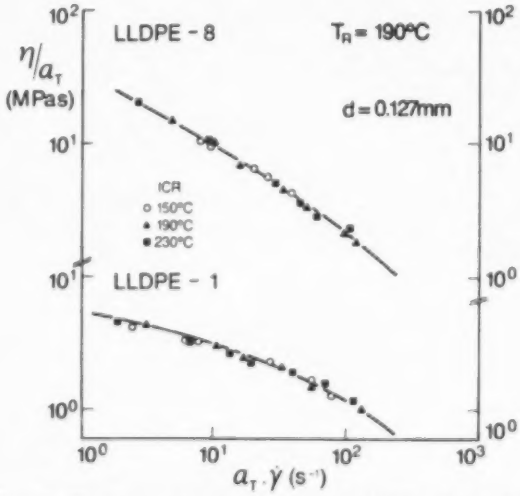

Fig. 3. Time—temperature superposition of capillary shear viscosity data for LLDPE-1 and 8. The reference temperature, T_R = 190°C was used.

Table 3. Summary of the Temperature Dependence of Shear Viscosity of LDDPE's.

No.	Property	LLDPE-# #1	#4	#8	#10
1	Function measured:	η	η^*	η	η^*
2	Shift Factor a_T at T = 150°C	2.40	2.01	2.27	2.21
	190°C	1.000	1.000	1.000	1.000
	230°C	0.57	0.57	0.615	0.55
3	Activation Energy of Flow (kJ/mol) E_a at $\sigma_{12} = G''$ = 0.8 to 1.5 × 10^4 (Pa)	31.9	27.9	29.0	30.8
	E_a at $\dot{\gamma} = \omega$ = 0.1		26.6		19.1
	0.3		23.2		18.0
	1.0		22.9		17.3
	3.0		21.8		13.2
	4.0	23.4	—	13.67	—
	10	23.2	18.9	12.8	11.2
	20	21.9	—	10.5	—
	30	20.1	15.5	9.8	10.4
	40	17.7	—		
	100		10.8		
4	The local "power law" exponent n (from ICR)				
	at $\dot{\gamma}$ = 10	0.672	0.716	0.422	0.467
	100	0.321	0.400	0.268	—

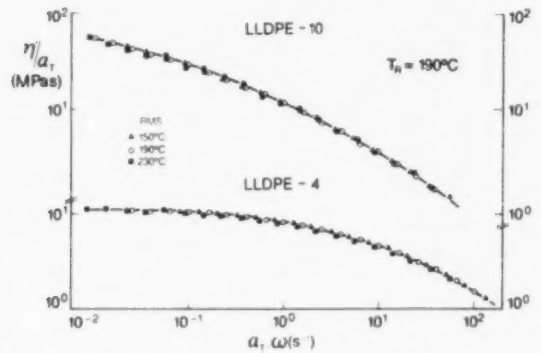

Fig. 4. Time-temperature superposition of dynamic viscosity, η', for LLDPE-4 and 10. T_R = 190°C.

(a_i's are parameters). In the most recent publication in that series (16) for n-paraffins, $5 \leq n \leq 18$, and their mixtures a_0 was found to be determined by the iso-free volume viscosity; $\eta_0^* = \eta_0^*(n)$, while both $a_1 = 1.82$ and $a_2 = 0.07$ were constant, independent of the system. For polymer melts a similar observation was made (16): for a series of samples of a given polymer the rate of viscosity increase, a_1, was observed to be similar, provided the molecular structure and the molecular weight distribution, *MWD*, of the samples were similar. Furthermore, as the M_w/M_n decreased, a_1 increased. In short, the sensitivity of η_0 to P and T increases with narrowing of *MWD*. It should be noted that LLDPE-8, which obeys the Bagley's linearity, has the broadest, while LLDPE-2 has the narrowest *MWD* of all the samples. It is important to recognize that $Y_s = Y_s(P, T)$ is the same for all samples of the same polymer (the thermodynamics is insensitive to MW and *MWD*), i.e. under given P and T there is as much free volume in LLDPE of $M_w = 10$ as in $M_w = 1000$ (kg/mol). The higher viscosity of the latter is due to entanglement-affected molecular dynamics. However, if the *MWD* of these two samples are identical, the slope a_1 in *Eq 4* should be the same.

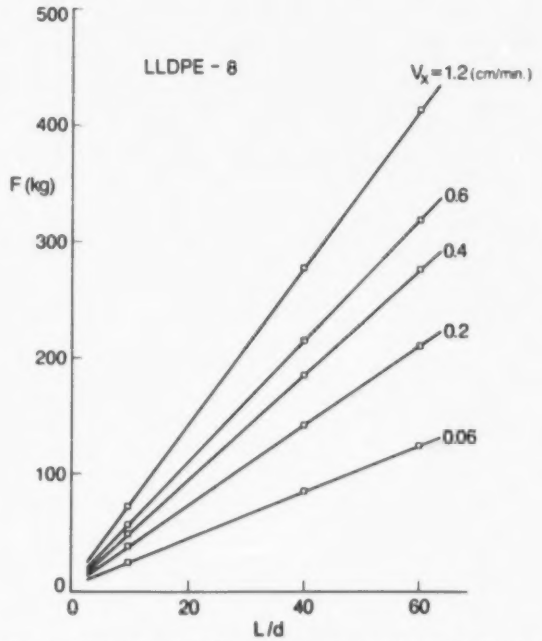

Fig. 5. Bagley's plot: force, F, versus L/d at indicated crosshead speeds, V_x (in cm/min), at 190°C for LLDPE-8.

At 190°C, using the reducing parameters listed for HDPE (*Table 5* (14)) the theory permits the following pressure dependence of the free volume:

$$1/f = 6.1657 + 0.01298\ P\ (\text{MPa}); \qquad r^2 = 0.9999 \tag{6}$$

For ICR with 9.5 mm diameter barrel *Eq 6* can be written as:

$$1/f = 6.16657 + 1.7864\ F\ (\text{Mg})$$

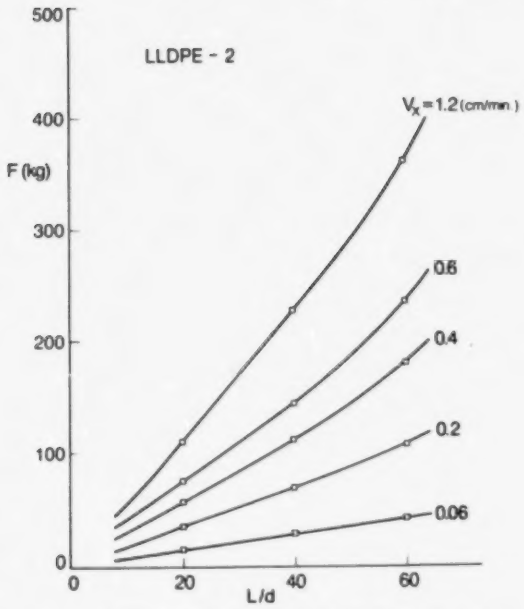

Fig. 6. Same plot as in Fig. 5 but for LLDPE-2.

Equations 6 and *7* are strictly valid for HDPE fractions investigated by Christmann (17) (viz., Fig. 24 in (14)). It is expected that the thermodynamic reducing parameters, P^*, V^*, and T^* for LLDPE are similar to those of HDPE, and the use of *Eq 7* is justified. Two additional assumptions were made: (i) the data $\eta = \eta(\dot{\gamma}, P, T)$ can be superimposed on a master curve by a two step, a_T and a_P, shift procedure, and (ii) the pressure drop along the capillary length is linear.

With these assumptions the correcting factor of the pressure effects is given by:

$$K_p \equiv F_{corr}/F_{obs} = (a_1/(f_0 + a_2))(1 - (f_0 - a_2)/(f - a_2)) \quad (8)$$

where F_{corr} and F_{obs} are the corrected and observed values of the force, f_0 and f are the free volume fractions calculated from *Eq* (7) for $F = 0$ and $F = F_{obs}/2$, respectively.

In the calculation, in order to avoid complications due to the shear heating effects only data with crosshead speed $V_x \leq 0.6$ (cm/min) were used. Within this range the average pressures in the capillary $\bar{P} \leq 14$ MPa and the $\ln\eta$ versus $1/f$ can be approximated by a straight line, i.e., $a_2 = 0$.

The following interactive procedure was used. Starting with the $V_x = 0.2$ (cm/min) data, K was calculated from the deviation from linearity of the highest F-point. From *Eq 8* a_1 was calculated and the *all* data points were corrected. If linearization has not been obtained, the procedure was repeated until a minimum in the standard deviation was found. It was noted that while for some systems the initial values of P_e (obtained prior to correcting for the pressure effect) were negative, after the correction they became positive, (shown in *Table 2*).

The plot of a_1 versus M_w/M_n is presented in *Fig. 7*, where the data computed for HDPE from Christmann's (17) results are also shown. For $M_w/M_n < 8$, good agreement is observed, but above this value there is a divergence. It is highly probable that a_1 depends not only on polydispersity, but also on branching. If so, the increase in a_1 with polydispersity observed for two Christmann samples may indicate that these high molecular weight, polydispersed resins were partially branched.

It is worth mentioning that the adopted procedure resulted in high values of the correlation coefficient squared, ranging from $r^2 = 0.999$ to 1.000. The correction factor, K_p, for the least and the most pressure sensitive samples (LLDPE-8 and 2) at $V_x = 0.6$ cm/min are respectively 1.030 and 1.248, resulting in decrease of shear stress by 4.1 and 35 percent. More significant is the change in P_e: for LLDPE-2 at $V_x = 0.6$ P_e changed from −1.25 to +1.28 MPa.

The data in *Fig. 7* suggest that compressibility should decrease with polydispersity.

Extrudate Swell, *B*

The values listed in *Table 2* were converted to N_1 using Tanner's (18) Equation:

$$S_R^2 = 2(B^6 - 1.13) \quad (9)$$

where the recoverable shear strain:

$$S_R = J_e^0\sigma_{12} = N_1/2\sigma_{12} \quad (10)$$

(J_e^0 is the steady state compliance), and the numerical constant in parenthesis of *Eq 9* has been adjusted to provide the correct kinetic swelling value for Newtonian liquids. These relations were found to provide the best fit to the experimental data (19). Theoretically (20) J_e^0 is a characteristic parameter of a system, observed at small stresses:

$$J_e^0 = a\, M_e/\rho\, RT \quad (11)$$

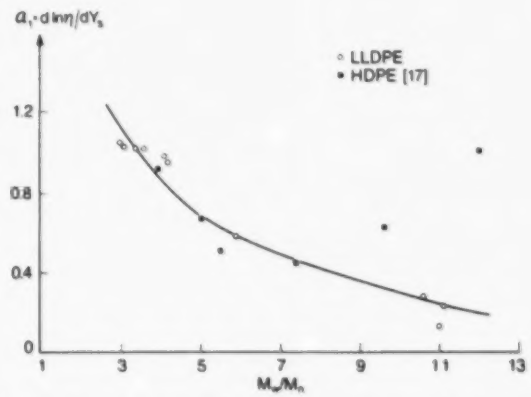

Fig. 7. Pressure sensitivity of the shear viscosity versus polydispersity for LLDPE 1 to 10 circles and the high density polyethylenes, HDPE (17) black squares.

where a is a numerical constant ($a = 1.798$ or 3/2), M_e is the entanglement molecular weight, and ρ is the melt density at temperature T. Using a mechanistic model J_e^0 is a measure of the total energy stored in the springs. From *Eq 10* it is evident that for J_e^0 to be constant N_1 should increase with σ_{12}^2.

The recoverable shear strain, S_R, is a measure of the distribution of energy stored to energy dissipated. S_R expresses the ultimate, free strain recovery and as such has been used as a measure of relative elasticity. An excellent discussion on the subject can be found in Lodge's monography (21). For S_R to be constant, N_1 must be proportional to σ_{12}.
Experimentally:

$$N_1 = K\sigma_{12}^b \qquad (12)$$

where K and b are parameters. For polymer solutions and low viscosity melts at low deformation rates $b \simeq 2$ and $J_e^0 = \text{const}$ is obtained. For numerous commercial polymers $b \simeq 1$ and $S_R = \text{const}$ are observed. For most melts of polydispersed resins $1 \leq b \leq 2$ (51).

Using the values of B listed in *Table 2* from *Eqs 9* and *10* the apparent first normal stress difference, N_{1a}, was computed. The results are listed in the *Table*. For all LLDPE's the correlation can be approximated by a straight line with $r^2 = 0.990$ to 1.000. Only for the high molecular weight samples LLDPE-8 and 9 was the slope $b \simeq 1$ found ($N_{1a}/\sigma_{12} = 4.7 \pm 0.8$). LLDPE − 1, 2, 4, 5, 6 and LPX-30 superimpose on a single line with $K = 1.533$ and $b = 1.31$. Similar slope ($b = 1.33$) but higher K (= 2.175) was calculated for LLDPE-3. The dependence observed for LLDPE-7 is less steep: $b = 1.23$, $K = 2.99$. Finally, for LDPE-102 two regions were obtained. For $\sigma_{12} < 20$ kPa: $b = 2$, $K = 1.32 \pm 15$, which gives $J_e^0 \simeq 661$ (1/Pa), and using *Eq 11* a very reasonable value of $M_e = 1.29 \pm 0.15$. For $\sigma_{12} > 20$ kPa $N_{1a}/\sigma_{12} = 20.4 \pm 0.5$, i.e., a much higher value than that observed for LLDPE-8 and 9.

Entrance-Exit (Bagley) Correction

The other capillary measure of melt elasticity is P_e. According to Bagley (22)

$$P_e = 4\ \sigma_{12}(n_v + S_R) \qquad (12)$$

where n_v is a measure of viscous dissipation, usually considered a geometric parameter. Frequently, experimental values of P_e/σ_{12} increase linearly with $\log\dot{\gamma}$ (23), which may indicate that $n_v \ll S_R$. Under these circumstances P_e should be proportional to N_1. However, recent computer simulations (24, 25) indicate that increase of N_1 causes a reduction of P_e. It seems that P_e is rather due to a complex velocity rearrangement at the entrance to capillary in which not only σ_{12} and N_1 but also the extensional properties of the melt play an important role (26). It has been shown (27, 28) that energy loss due to free convergence equals one half of that in shear, $\sigma_{12}\dot{\gamma}$. The transient character of the convergent flow and the unknown value of the stress growth function which determines P_e add to the complications.

When P_e is plotted versus σ_{12}, a dependence similar to (N_1 versus σ_{12}) emerges. Considering data at constant shear stress, P_e for LDPE-102 is the largest, those for LLDPE-8, 9 the lowest, LLDPE-3 values are close to LDPE's and the samples LLDPE-1, 2, 4, 5, 6 form a cluster in between, also absorbing the points of LLDPE-7.

An alternative way of analyzing the data is to plot P_e versus N_{1a}. It should be noted that both these quantities obtained from capillary flow suffer from large errors. In particular B represents relative nonequilibrium values. Nevertheless, a clear correlation emerges. For six samples $P_e = K_1N_1$ with the proportionality factor $K_1 = 1$ for LLDPE-7, 8, 9, and 10 and $K_1 \simeq 3$ for LLDPE-3 and 5. A steeper dependence $P_e = K_2N_1^2$ is obtained for LLDPE-4, 6 and LPX-30. The data for LLDPE-1 and 2 fall between two groups (slope = 1.55), while P_e of LDPE shows a weakest dependence on N_1 with the slope = 0.55.

Dynamic Test Data

The plot of G'' versus G' provides the dynamic equivalence of the steady state estimate presented in *Table 2*. However, when N_{1a} is an apparent measure of the first normal stress difference in a steady state flow, the data in *Fig. 8* are direct and precise to ±2 percent. Since at $\dot{\gamma} = \omega\ \eta = \eta'$ and $N_1 = 2\ G'$ (29) the low stress data in *Table 2* should only be shifted by a factor of two in relation to high stress values in *Fig. 8*. As indicated in the figure the data can be discussed in terms of four groups of samples: No. 1 for LDPE-102, No. 2 for LLDPE-3, 8 to 10 No. 3 for LLDPE-7, and No. 4 for LLDPE-1, 2, 4 to 6 and commercial LLDPE grade LPX-30. Within groups Nos. 2 and 4 at low stress values there is a "fine structure;" e.g., in group No. 2

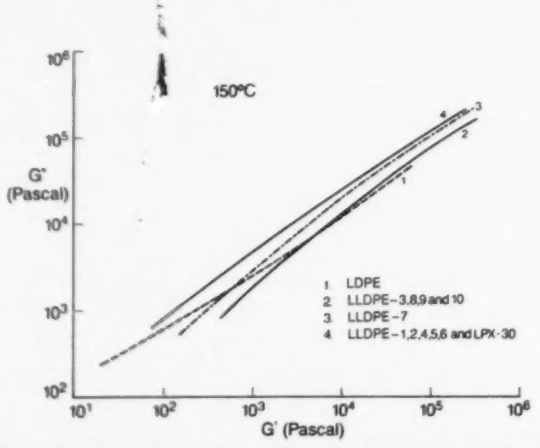

Fig. 8. Summary of the dynamic tests at 150°C for LLDPE-1 to 10, LPX-30, and LDPE-102. Curves: No. 1—LDPE, No. 2—LLDPE—3 and 8 to 10, No. 3—LLDPE-7, No. 4—LLDPE-1, 2, 4 to 6 and LPX-30.

LLDPE-10 is about 5 percent above the other samples, whereas in group No. 4 sample LLDPE-4 lies about 20 percent above that of LLDPE-6 with the others in between. There is a very important difference in the curve shapes for LLDPE and LDPE resins; the loss versus storage modulus is concave in the first and convex in the second case. This means that while at high frequency the slope $g \equiv \partial \ln G'/\partial \ln G'' \simeq 1.6 \pm 0.2$ is common for all PE's at low frequency g decreases toward 1.1 for LLDPE, whereas for LDPE it increases toward 1.8.

Comparing the steady state and dynamic data, a qualitative agreement is obtained; within the comparable shear stress range there is similar gradation of elasticity from LDPE to LLDPE-1. Quantitatively there is a large difference: at $\sigma_{12} = G'' \simeq 20$ kPa $N_{1a} = 80$ to 430 kPa but $2G' = 14$ to 38 kPa. The difference may be due to large extensional effects at the entrance to capillary or the "shear modification" of PE's (7, 30–32). Note that plots of N_1 versus σ_{12} and G' versus G'' should be independent of temperature.

Comparing the information on melt elasticity with the molecular parameters (1), it is evident that the short chain branching, introduced by different co-monomers, does not seem to be important. Two parameters seem to efficiently increase elasticity: the long chain branching, as in LDPE, and broadening of *MWD*. The latter factor can be readily illustrated by comparing G' at G'' = const for LLDPE-1, 7 and 3, all having similar values of M_z but different $M_w/M_n = 3.4$, 4.2, and 6.9; e.g., at $G'' = 50$ kPa $G' =$ 29, 32, and 70 kPa, respectively.

The data in *Fig. 8* allow determination of the coordinates of the crosspoint, defined as $G_x \equiv G' = G''$ at the frequency ω_x. Zeichner and Patel (33) reported that for polypropylene, G_x is related to *MWD* and ω_x to the zero-shear viscosity, η_o.

The values of G_x and ω_x are listed in *Table 4* and presented in *Figs. 9* and *10*. The data follow the power law relation:

$$y = Ax^B \qquad (13)$$

with the least-squares parameters listed in *Table 5*. Drawing the lines in *Fig. 10* the slope $B = -1$ was assumed. The assumption was based on two observations: (i) as shown in *Fig. 5*, master curves were obtained plotting η'/a_T versus ωa_T, where $a_T \propto \eta_o$; (ii) the two lines in *Fig. 10* represent well the dependence for samples polymerized with the same catalyst, i.e., having a similar *MWD*.

In both figures the point for LLDPE-3 is apart. The sample has been specially treated by the manufacturer to broaden the *MWD*. The divergence can be explained by the presence of a small amount of very high molecular weight fractions, undetected by SEC. However, before continuing this discussion the methods of η_o evaluation should be presented.

Zero-shear Viscosity

Three methods were used to determine η_o: I.

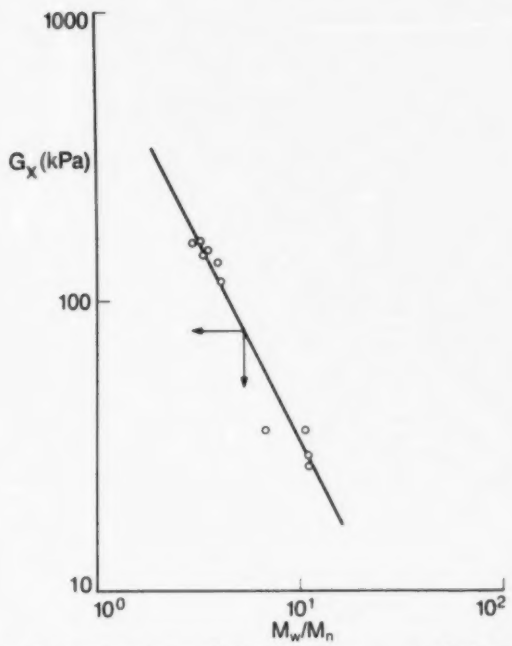

Fig. 9. Cross-point modulus, G_x, versus the polydispersity parameter, M_w/M_n for LLDPE-1 to 10.

Table 4. The Rheological Parameters of Polyethylene Resin.

No.	Sample No.	G_x (kPa)	ω_x (rads/s)	η_o (kPa·s) I	II	III	τ(ms)	m_1	m_2	α	β
1	LLDPE-1	146	32.0	45	51.6	47.5	19.0	0.336	3.95	0.754	2.48
2	LLDPE-2	157	46.0	32	34.8	35.4	12.8	0.348	3.83	0.760	2.97
3	LLDPE-3	36.8	7.80	150	144.5	143.1	49.1	0.152	5.69	0.924	8.17
4	LLDPE-4	161	58.5	27	27.0	25.8	6.71	0.364	4.31	0.712	2.48
5	LLDPE-5	137	44.5	30	31.3	31.1	13.4	0.363	3.82	0.741	3.02
6	LLDPE-6	150	41.8	39	40.5	33.6	12.7	0.321	4.80	0.701	2.11
7	LLDPE-7	117	43.0	60	64.5	75.2	22.3	0.244	5.03	0.847	5.03
8	LLDPE-8	27.0	0.265	1700	10495	10495	10,220	0.181	5.63	0.920	7.86
9	LLDPE-9	29.5	0.700	790	3709	3679	3,260	0.179	5.80	0.919	8.37
10	LLDPE-10	36.5	4.60	210	645	656	308	0.181	6.34	0.904	6.74
11	LPX-30	155	68.6	25	33.7	32.3	9.39	0.280	5.27	0.789	3.33
12	LDP-102	22.6	25.0	9.5	9.29	—	6.99	0.270	3.46	—	—

Graphical extrapolation of dynamic and extensional (see Part 3) data to limiting rate of deformation; II. The least-squares curve fitting procedure using the generalized equation (34):

$$\eta'/\eta_o = [1 + (\omega\tau)^{m_1}]^{-m_2} \quad (14)$$

where τ is the average relaxation time, and m_i's are parameters; and III. The least-squares fit to the Havriliak and Negami (35) equation in which the dielectric constants were replaced by their viscoelastic equivalents:

$$(\eta^* - \eta_\infty)/(\eta_o - \eta_\infty) = [1 + (i\omega\tau)^{(1-\alpha)}]^{-\beta} \quad (15)$$

(α and β are parameters).

Equation 14 was recently proposed (36) for polydispersed samples; for $m_1 = 2$ and $m_2 = (1 - n)/2$ it converts back to Carreau's model A relation, derived for systems with a single relaxation time. The relation (*Eq 14*) has been found very successful in describing observed dependencies for numerous polymeric systems. The exponent m_1 varied from 0.3 to 2.0.

Equation 15 was proposed as a generalization of the Cole-Cole equation (37) for dielectric constants. The later dependence has been used to determine η_o for neat resins, polymer alloys, blends, and composites (38–40). When η'' is plotted versus η', there are two values of η' corresponding to $\eta'' = 0$: $\eta' = \eta_\infty \simeq 0$ and $\eta' = \eta_o$.

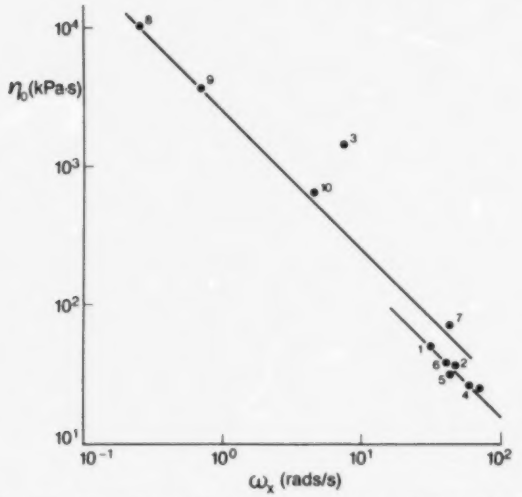

Fig. 10. Zero-shear viscosity, η_o, versus cross-point frequency, ω_x, for LLDPE-1 to 10.

Substituting the first value into *Eq 15* simplifies the calculations. The developed computer program makes use of the separated functions of the real and imaginary parts of the dynamic function:

$$\eta' = H^{-\beta/2}\cos\beta\theta \quad (16)$$

$$\eta'' = H^{-\beta/2}\sin\beta\theta \quad (17)$$

$$H \equiv [1 - (\omega\tau)^{1-\alpha}\sin\alpha\pi/2]^2 + [(\omega\tau)^{1-\alpha}\cos\alpha\pi/2]^2 \quad (18)$$

$$\tan\theta \equiv [(\omega\tau)^{1-\alpha}\cos\alpha\pi/2]/\cdot[1 + (\omega\tau)^{1-\alpha}\sin\alpha\pi/2] \quad (19)$$

Results of the calculations are shown in *Table 4*. For LLDPE-1 to 7, the extrapolation and computations lead to similar η_o-values. However, as the polydispersity increases so does the difference between η_o(I) and η_o(II) $\simeq \eta_o$(III). To test the accuracy of the computational procedure, the isothermal data as well as the master curve data, with the frequency range extended by nearly two decades, were used with virtually identical results.

Graessley *et al.* (41, 42) reported that η_o varies with the relaxation time, τ, according to the semi-empirical formula:

$$\tau = k_1(\eta_o M_w/\rho T)/(1 + k_2 E) \quad (20)$$

where k_1, and k_2 are constants and $E = M_w/M_e$ is the entanglement density. For $E \geq 50$, *Eq 20* can be simplified to read:

$$\tau = (k_1/k_2)(\eta_o M_e/\rho T) \propto \eta_o \quad (21)$$

Since for linear polyethylenes $M_e = 1.29$ and $M_w \geq 99$, *Eq 21* should be obeyed. The parameters of the least-squares fit are listed in *Table 5*. High correlation coefficient squared, $r^2 = 0.996$, was obtained, but the exponent $B = 1.19$ instead of 1.0 was found.

The last item to discuss is the correlation between zero-shear viscosity, η_o, and molecular weight. It is accepted that for the narrow *MWD* polymers:

$$\eta_o = KM_w^a \begin{cases} a \simeq 1 \text{ for } M_w < 2M_e \\ a \simeq 3.4 \text{ for } M_w \geq 2M_e \end{cases} \quad (22)$$

where for linear polymers $a = 3.4 \pm 0.3$ (43–46).

For polydispersed systems *Eq 22* is not ade-

Table 5. Least Squares Parameters for Rheological Functions of LLDPE's; see *Eq 13*.

No.	y	x	A	B	r^2	Comments
1.	M_w/M_n	G_x (kPa)	129	−0.722	0.986	LDPE, LLDPE-3 do not follow
2.	η_o (kPa)	ω_x (rads/s)	1466	−1.0	—	LLDPE-1 to 6
			2841	−1.0	—	LLDPE-7 to 10
3.	η_o (kPa)	M_w (kg/mole)	$1.64\ 10^{-6}$	3.4	—	LLDPE-1, 2, 4 to 6
			$6.19\ 10^{-5}$	3.4	—	LLDPE-3, 8 to 10 only approximately
4.	τ(ms)	η_o (kPa)	0.164	1.19	0.996	LLDPE's 1 to 10 and LPX-30
			0.230	1.14	0.982	all samples
5.	η_o (kPa)	S	7.68×10^9	1.45	0.982	LLDPE's
6.	η_o	M_s	2.35×10^{-6}	3.50	0.974	all samples

quate (47–49). Depending on the assumed type of the *MWD* and the adopted blending rule, different dependencies were proposed (49). The two simplest ones are:

$$\eta_o = KM_w^a(M_w/M_n)^b \quad (23)$$

$$\eta_o = K_1 M_z^c \quad (24)$$

where K, a, b, k, and c are parameters. It was found that these relations do not hold for LLDPE data in *Table 4*; when in *Eq 23*, $a = 3.4$ was assumed, $b = 2.50$ and $r^2 = 0.907$ were found, whereas from *Eq 24* $c = 4.17$ and $r^2 = 0.900$ were computed. As mentioned before, to derive *Eq 23* or *Eq 24*, one must assume validity of: 1) a specific type of the *MWD*, and 2) the blending rule for given systems. Rudin and Chee (46) as well as Schausberger, Schindlauer, and Janeschitz-Kriegl (48) bypassed the first problem using experimental *MWD* data and computing respectively:

$$\eta_o = A\int_o^{2M_e} M_w(M)dM + B\int_{2M_e}^{\infty} M^{3.4}\, w(M)dM, \quad (25)$$

and:

$$\eta_o = K\sum n_i M_i^{3.4} \quad (26)$$

where: $w(M)$ is the normalized weight distribution function and n_i is the mole fraction of component i. It is immediately apparent that while these authors agreed on the direct use of *MWD* data, they disagreed on the type of valid blending rule. It should be noted that it is unlikely that one type of blending rule is valid for all polymers. The latter aspect was recently discussed by Staverman (47).

Since in SEC characterization of the MWD a lower integration limit $M = 2$ (kg/mol) was imposed, while M_e(PE) $\simeq 1.29$, in the following computation only the second integral in *Eq 25* was computed as $S = \sum w_i M_i^{3.4}$. The error introduced by this truncation will be more pronounced at low MW end. The least-squares parameters are given in *Table 5* (see No. 5); an excellent correlation was obtained ($r^2 = 0.982$) but the computed exponent $B = 1.45$ significantly higher than expected $B = 1$ value. If the truncation is responsible for the difference, then use of a full *MWD* curve should help.

It has been reported (e.g., see ref. 50) that *MWD* of linear polyethylenes follows the log-normal distribution:

$$w(M)dM = (1/\beta\pi^{1/2})\exp\{-x^2/\beta^2\}dx \quad (27)$$
$$x = Ln\ M/M_o$$

with β and M_o being the distribution parameters. Various moments of the molecular weight distribution may be calculated from *Eq 27* using the following definition:

$$M_a = \left[\int_o^{\infty} M^a\, w(M)dM\right]^{1/a} \quad (28)$$

and substituting $y = x/\beta - a\beta/2$. The integration leads to the general formula

$$M_a = M_o\exp\{a\beta^2/4\} \quad (29)$$

from which the molecular weight averages can be calculated:

$$M_n = M_o\exp\{-\beta^2/4\} \quad (30)$$

$$M_w = M_o\exp\{\beta^2/4\} \quad (31)$$

$$M_z = M_o\exp\{3\beta^2/4\} \quad (32)$$

$$M_\eta = M_o\exp\{3.4\beta^2/4\} \quad (33)$$

The "melt viscosity average", M_η, can be expressed in terms of the three other averages:

$$M_\eta = M_z(M_w/M_n)^{1/5} \quad (34)$$

Equation 34 is a generalization of *Eqs 23* and *24* which should be valid for polymers with monomodal log-normal *MWD*. The plot of $\ln\eta_o$ versus $\ln M_\eta$ should have the slope $B = 3.4$. A relation of this type was derived by Staverman, assuming that the resistance to flow is an additive property of molecules.

The plot of η_o versus M_η for all polyethylenes is presented in *Fig. 11* and the least-squares parameters are listed in *Table 5*. The relation seems to hold quite well for all samples, including LDPE. This may be due to the fact that molecular weights of all samples were expressed in terms of linear equivalent MW as determined by the hydrodynamic volume in SEC.

CONCLUSIONS

1. A simple correlation $E_e = E_\gamma/n$ was derived. The value $E_e = 29.9 \pm 1.8$ kJ/mole was found for LLDPE, independent of MW, *MWD*, or comonomer.

2. A new method of correcting the capillary data for pressure effects was proposed. Corrected shear viscosity versus $\dot\gamma$ dependence superimposes on η' versus ω, i.e., Cox-Mertz rule does not apply. The pressure affects the samples with narrow *MWD* much more than those with broad *MWD*.

3. Both the apparent extrudate swell, B, and the entrance-exit correction, P_e, can be used to rate the relative elasticity of the melt, but the expected correlation $N_{1a} = 2G'$ at $\sigma_{12} = G''$ was not observed.

4. The melt elasticity (as measured by G') increases with LCB and *MWD*, but seems to be independent of comonomer.

5. The cross-point correlations observed for polypropylene by Zeichner and Patel (33) seem to be obeyed by LLDPE polymerized under similar conditions. Change of catalyst or post-reaction treatment causes deviation from Z-P plots.

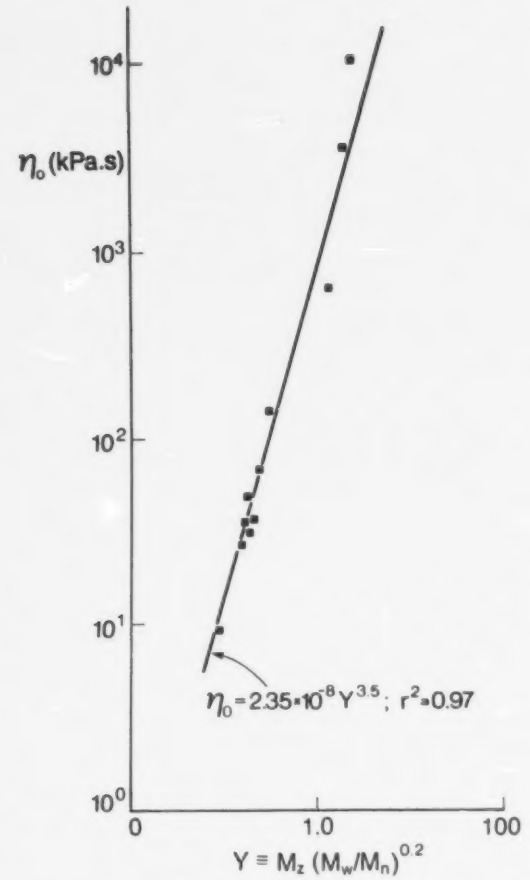

Fig. 11. Molecular weight dependence of the computed zero-shear viscosity of polyethylenes at 190°C.

6. A new four-parameter equation between the dynamic viscosity and frequency was found to provide a simple method of extrapolation to obtain consistent values of the zero-shear viscosity, η_o, and the primary relaxation time, τ, from data away from the Newtonian plateau.

7. The computed η_o and τ show a high degree of correlation for all samples.

8. The expected relation $\eta_o \propto M_w^{3.4}$ was only approximate, observed separately within the two groups of samples with narrow and broad *MWD*. By contrast good general dependence was found when M_w in that equation was substituted by $M_\eta = M_z(M_w/M_n)^{1/5}$.

9. As expected there is higher correlation between the rheological functions than between any of them and the SEC data (M_w, M_w/M_n).

ACKNOWLEDGMENTS

The authors wish to thank Mr. Dave Donald from ESSO Chemicals Canada for preparation of the samples and measurements of their behavior during the capillary flow and Dr. A. A. Alim from the same company for supplying the samples and his excellent cooperation during execution of this work. Thanks are also due to Mr. P. Sammut from NRCC/IMRI for outstanding work in collecting the dynamic shear data.

NOMENCLATURE

a, a_i	=	equation constants; *Eqs 4, 5, 11.*
a_T	=	temperature shift factor.
A	=	power law constant, *Eq 13.*
b	=	exponent in *Eq 12.*
B	=	extrudate swell or exponent in *Eq 13.*
d	=	capillary diameter.
D_e	=	extrudate diameter.
E_σ, $E_{\dot\gamma}$, E_o	=	activation energy of flow under constant stress constant shear rate and its limiting value at $\dot\gamma \to 0$.
f, f_o	=	free volume fraction at P and $P = 0$, respectively.
F, F_{obs}, F_{corr}	=	load in capillary test; its average (in the capillary), observed and corrected value, respectively.
G', G''	=	storage and loss shear modulus.
H	=	function defined in *Eq 18.*
J_e^o	=	steady state shear compliance.
k_i, K	=	equation parameters; *Eqs 12, 20, 21.*
L	=	capillary length.
LALLS	=	low angle laser light scattering.
LCB	=	long chain branching.
LDPE	=	low density polyethylene.
LLDPE	=	linear LDPE.
m_i	=	parameters of *Eq 14.*
M_e	=	entanglement MW.
M_n, M_w, M_z, M_η	=	number, weight, z-average and η-average MW.
MW	=	molecular weight.
MWD	=	MW distribution.
n	=	power law exponent in $\sigma_{12} \propto \dot\gamma^n$; number of C in n-paraffins.
n_v	=	viscous dissipation parameter in *Eq 12.*
N_1, N_{1a}	=	first normal stress difference and its apparent value calculated from B.
P	=	total pressure loss in capillary flow.
P_e	=	capillary end effects pressure loss.
P^*	=	thermodynamic reducing pressure.
Q	=	extrusion rate.
R	=	gas constant.
S_R	=	recoverable shear strain.
SCB	=	short chain branching.
SEC	=	size exclusion chromatography.

t_r = time for sample to relax in RMS.
T = temperature.
T_R = reference temperature.
T^* = thermodynamic reducing temperature.
V_x = crosshead speed.
V^* = thermodynamic reducing volume.
$w(M)$ = weight fraction of polymer.
x = independent variable in *Eq 13*.
y = dependent variable in *Eq 13*.
Y_s = packing parameter defined by *Eq 5*.
α, β = parameters in *Eq 15*.
γ = shear strain in dynamic tests.
$\dot{\gamma}$ = shear rate.
η = steady state shear viscosity.
η', η^* = dynamic, complex shear viscosity.
η_o = zero-shear viscosity.
η_∞ = viscosity at the lower Newtonion plateau, $\dot{\gamma} \rightarrow \infty$.
η_δ^* = iso-free volume value of η_o.
θ = function defined by *Eq 19*.
ρ = density.
σ_{12} = shear stress.
τ = primary relaxation time.
ω = angular frequency.

REFERENCES

1. B. Schlund and L. A. Utracki, *Polym. Eng. Sci.*, **27**, 359 (1987).
2. A. E. Hamielec and A. C. Ouano, *J. Liq. Chromat.*, **1**, 111 (1978).
3. V. Grinshpun, K. F. O'Driscoll, and A. Rudin, in "Size Exclusion Chromatography," T. Provder, Ed., A.C.S. Symp. Ser., **245**, 273 (1984).
4. F. A. Bovey, R. E. Cais, L. W. Jelinski, F. C. Schilling, W. H. Stornes, Jr., and A. E. Tonelli, *Am. Chem. Soc., Adv. Chem. Ser.*, **203**, 421 (1983).
5. W. Klöpffer, "Introduction to Polymer Spectroscopy," Springerverlag, Berlin (1984).
6. J. C. Randall, Ed., "NMR and Macromolecules," *Am. Chem. Soc., Symp. Ser.*, **247** (1984).
7. J. W. Teh, A. Rudin, and H. P. Schreiber, *Plast. Rubber Process. Appl.*, **4**, 149 (1984).
8. L. A. Utracki and M. M. Dumoulin, *Polym.-Plast. Technol. Eng.*, **23**, 193 (1984).
9. L. A. Utracki and R. Gendron, *J. Rheol.*, **28**, 601 (1984).
10. P. Sammut and L. A. Utracki, Report on the rheological behavior of commercial polyethylenes, submitted to the IUPAC Working Party, Dunblane, Scotland, Sept. 16–19, 1985.
11. R. C. Penwell and R. S. Porter, *J. Appl. Polym. Sci.*, **13**, 1049, 1069 (1969).
12. R. C. Penwell, R. S. Porter, and S. Middleman, *J. Polym. Sci.*, **A2**, 731 (1971).
13. M. R. Kamal and H. Nyun, *Polym. Eng. Sci.*, **20**, 109 (1980).
14. L. A. Utracki, *Polym. Eng. Sci.*, **25**, 655 (1985).
15. e.g. see: R. Simha, *Polym. Eng. Sci.*, **22**, 74 (1982).
16. L. A. Utracki, Paper presented during the 57th Annual Meeting of the Society of Rheology, Ann Arbor, Michigan, Oct. 13–17, 1985; *J. Rheology*, *30*, 829 (1986).
17. L. Christmann, Dr. rer. nat.—Thesis, Technischen Hoschschule Darmstadt, 1977.
18. R. I. Tanner, *J. Polym. Sci., A-2*, **8**, 2067 (1970).
19. L. A. Utracki, Z. Bakerdjian, and M. R. Kamal, *J. Appl. Polym. Sci.*, **19**, 481 (1975).
20. J. D. Ferry, "Viscoelastic Properties of Polymers," J. Wiley and Sons Inc., New York, 3rd Ed., Chaps 10 and 13, (1980).
21. A. S. Lodge, "Elastic Liquids," Academic Press, London, Ch. 7 (1964).
22. E. B. Bagley, *Trans. Soc. Rheol.*, **5**, 355 (1961).
23. K. Murata and S. Kobayashi, *Kobunshi Kagaku*, **26**, 738 (1969).
24. J. S. Vrentas and C. M. Vrentas, *J. Non-Newtonian Fluid Mech.*, **12**, 211 (1983).
25. E. Mitsoulis, J. Vlachopoulos, and F. A. Mirza, NRCC/IMRI Symposium "Modeling—'84," Boucherville, Que., Canada, Jan 24, 1984; *Polym. Eng. Sci.*, **25**, 677 (1985).
26. G. Ghauvetau, M. Moan, and A. Maguer, *J. Non-Newtonian Fluid Mech.*, **16**, 315 (1984).
27. F. N. Cogswell, *Polym. Eng. Sci.*, **12**, 69 (1972).
28. L. A. Utracki, M. M. Dumoulin, and P. Toma, NRCC/IMRI Symposium "Polyblends—'85," Boucherville, Que., Canada April 16–17, 1985; *Polym. Eng. Sci.*, **26**, 34 (1986).
29. L. A. Utracki and A. M. Catani, *Polym. Eng. Sci.*, **25**, 690 (1985).
30. M. Rokudai, *J. Appl. Polym. Sci.*, **23**, 3289 (1979).
31. A. Rudin and H. P. Schreiber, *Polym. Eng. Sci.*, **23**, 422 (1983).
32. H. P. Schreiber, A. Ajji, Y. Li, and A. Rudin, Paper 09E07 presented at 1984 Intl. Chem. Congr., Honolulu, Hawaii, Dec. 16–21, 1984; in "Current Topics in Polymer Science," Hanser V., Münich; R. M. Ottenbrite, L. A. Utracki and S. Inoue, Eds., (1987).
33. G. R. Zeichner and P. D. Patel, Proceed. 2-nd World Congress Chem. Eng., **6**, 333 (1981).
34. P. J. Carreau, *Trans. Soc. Rheol.*, **16**, 99 (1972).
35. S. Havriliak and S. Negami, *Polymer (London)*, **8**, 161 (1967).
36. L. A. Utracki, paper presented at the PAC-CHEM meeting Honolulu, Hawaii, Dec. 16–21, 1984; in "Current Topics in Polymer Science," Hanser Verlag, Münich; R. M. Ottenbrite, L. A. Utracki, and S. Inoue (1987).
37. K. S. Cole and R. H. Cole, *J. Chem. Phys.*, **9**, 341 (1941).
38. B. Fisa and L. A. Utracki, *Polym. Compos.*, **5**, 36 (1984).
39. M. M. Dumoulin, L. A. Utracki, and J. Lara, NRCC/IMRI symposium "Polyblends—'83," Montreal, Que., Canada, April 12, 1985; *Polym. Eng. Sci.*, **24**, 117 (1984).
40. M. M. Dumoulin, C. Farha, and L. A. Utracki, NRCC/IMRI symposium "Polyblends—'84;" *Polym. Eng. Sci.*, **24**, 1319 (1984).
41. W. W. Graessley and L. Segal, *Macromolecules*, **2**, 49 (1969).
42. W. C. Uy and W. W. Graessley, *Macromolecules*, **4**, 458 (1971).
43. M. M. Cross, *J. Appl. Polym. Sci.*, **13**, 765 (1969).
44. N. J. Mills, *Europ. Polym. J.*, **5**, 675 (1969).
45. W. M. Prest Jr. and R. S. Porter, *Polym. J.*, **4**, 154 (1973).
46. A. Rudin and K. K. Chee, *Macromolecules*, **6**, 613 (1973).
47. A. J. Staverman, *Europ. Polym. J.*, **19**, 973 (1983).
48. A. Schausberger, G. Schindlauer, and H. Janeschitz-Kriegl, *Rheol. Acta*, **24**, 220, 231 (1985).
49. N. G. Kumar, *J. Polym. Sci., Macromol. Rev.*, **15**, 255 (1980).
50. L. A. Utracki and M. M. Dumoulin, Ch. 6 in "Size Exclusion Chromatography," T. Provder, Ed., ACS Symposium Series No. 245, New York (1984).
51. C. D. Han and M. S. Jhon, *J. Appl. Polym. Sci.*, *32*, 3809 (1986).

Linear Low Density Polyethylenes and Their Blends: Part 3. Extensional Flow of LLDPE's

B. SCHLUND* *and* L. A. UTRACKI

National Research Council Canada
Industrial Materials Research Institute
Boucherville, Quebec, J4B 6Y4

The uniaxial extensional flow at 150°C of 11 linear low density polyethylenes (LLDPE) and one low density polyethylene was measured in a Rheometrics Extensional Rheometer. The presence of silicone oil did not affect the results. However, large effects of the molding time were observed. For specimens molded for 14 min, strain hardening was not observed for any gas-phase polymerized LLDPE. As the molding time was increased to 40 min, the strain hardening was quite apparent, the elongational viscosity nearly doubled, the equilibrium plateau vanished, and the maximum strain at break increased by about 20 percent. Explanation for the molding time effects can be found in the concept of low entanglement density in the virgin gas-phase resins. The entanglement increases with time at temperatures above the melting point. The specimens molded for longer time show strain hardening.

INTRODUCTION

The molecular parameters of the ten commercial linear low density polyethylenes (LLDPE) were presented in Part 1 (1). In Part 2 additional resins were characterized and the shear flow data were reported (2). In this Part 3 the uniaxial, isothermal flow will be discussed.

A comprehensive review up to 1978 was published by Petrie (3). During the last few years the extensional flow seems to enjoy increasing popularity, caused on one hand by availability of commercial rheometers (4, 5) and on another, demand for better understanding and control of polymer processing. Extensional flow plays an important role in any process in which streamlines are not parallel (6–8): fiber spinning, film blowing, die flow, injection and blow molding, stretch and squeeze flows, etc. An extensive collaborative study was carried out on the processibility and rheology of polyethylenes by IUPAC Working Party 4.2.1 (9–11).

The literature on the extensional flow of polyethylenes is particularly voluminous. For example, since 1979 (ante-Petrie (3) era) in several papers (12–19) the flow behavior of low density (LDPE) and high density polyethylenes (HDPE) were compared. In addition, the extensional properties of LLDPE have been also discussed (12, 16–19). The elongational flow of LDPE (20–27) and of HDPE (28–30) have been studied as well.

As this incomplete list of references indicates, there are quite a few papers dedicated to LLDPE (12, 16–19, 31, 32). In addition, the rheological properties of LLDPE, including the elongational, have been discussed in several publications on polymer blends (33–39). The vivid interest in properties of LLDPE is motivated by the growing commercial interest. In Canada, by 1985 LLDPE already have taken 50 percent of the film market (40). Furthermore, there is a growing variety of these resins. LLDPE is being manufactured in solution, in a slurry, and in the gas phase. There are several catalysts in each process allowing for modification of molecular and particulate structures, the molecular weight (MW) and the molecular weight distribution (*MWD*). In addition, since 1984 more and more resins contain higher olefins (mainly hexene or octene) (1, 2).

The aim of this paper is to compare the extensional flow behavior of 11 LLDPE's containing three types of co-monomer (butene, hexene, and octene) polymerized either in the gas phase (with Ti-based are W-based catalyst) or in solution. In particular it is of interest to find out if replacement of butene by higher olefins changes the flow behavior in a similar manner as it does the mechanical properties of the product.

* Present Address: CNRS-Laboratoire des Matériaux Organiques Echangeur de Solaise, Autoroute Lyon-Vienne, BP-24 69390 VERNAISON, FRANCE.

EXPERIMENTAL

Resins

Eleven LLDPE's and one LDPE-102 were used. Their molecular characteristics, determined by size exclusion chromatography (SEC), low angle laser light scattering (LALLS), solution viscosimetry, ^{13}C nuclear magnetic resonance (^{13}CNMR), and atomic absorbance (AA), were reported in Part 1 (1). The steady state (capillary) and dynamic shear flows data were presented in Part 2 (2).

Rheometers

Rheometrics Extensional Rheometer, Model 605 (RER) was used at 150°C in a constant strain rate ($\dot{\epsilon}$) mode. The principles of RER were presented by Münstedt (41) and the commercial design and operation by Au-Yeung and Macosko (42). The instrument has also been described in several recent papers (17, 18, 33–39, 43–46) on flow of polymers, polymer blends, and composites.

In the present study, to facilitate storage and manipulation of data the RER was interfaced with Hewlet-Packard Model HP-85 micro-computer. For the test the samples were transfer molded under vacuum, annealed, and then affixed with epoxy (24 hours curing) to the aluminum ties. Prepared in this manner, specimens did not show any shape change on immersion in hot ($T \leq 150$°C) silicone oil. For the test, the samples were mounted in the instrument and immersed in Dow 200 silicon oil at 150°C. The test started after a 7 to 10 min temperature equilibration period. During the measurements, the maximum temperature difference, as read by three thermocouples placed at different heights in the sample chamber, did not exceed 0.5°C. For each sample the uniformity of the cylindrical shape was verified at three different heights; in all cases the average diameter was found to be $d = 5.55 \pm 0.05$ mm. The sample length used in this study was $L_0 = 22$ mm $\pm$ 0.1 mm.

The shear properties of the samples at 150°C were determined in the steady state mode using the Rheometrics Mechanical Spectrometer, RMS, model 605. The transient measurements were made at the lowest shear rate, $\dot{\gamma} = 0.01$ s^{-1}, using two samples in four steps: (i) stress build-up during 1 s, (ii) relaxation during 9 s, (iii) stress build-up during 1000 s, (iv) relaxation during 500 s. A micro-computer (Hewlett-Packard HP-85), stored the 75 data points of each zone. The signal was averaged in such a way as to obtain 10 points by decade between $t = 10^{-2}$ to 10^3 s for stress build-up and between $t = 10^{-2}$ and 5×10^2 s for stress decay.

RESULTS

First, the effects of the suspending oil and of the transfer molding procedure (preparation of specimens) must be discussed.

To eliminate the effects of gravitational pull on polymer melt, as well as to secure good thermal conductivity during the test, the specimens were immersed in stationary silicon oil. The effect of liquid media on uniaxial flow of 1,2-polybutadiene was discussed by Kurbanaliev *et al.* (47), and the effect on HDPE, LDPE, and LLDPE by Utracki and Lara (17). Both papers demonstrated that the effects can be significant, especially as far as the ultimate properties: the maximum stress and strain at break (σ_b and ϵ_b respectively) are concerned. For this reason, in the present work the effect of silicon oil was carefully examined. As before (17), the samples were immersed in the oil at 150°C for various periods of time, dried, and weighed. Confirming the previous results it was found that within the normal test time, $t \leq 30$ min, LLDPE was not affected by the oil.

Koyama and Ishizuka (48) reported that the method of pretreatment seriously affected the elongational melt flow of polypropylene; the specimens prepared from dilute solution showed lower extensional viscosity than those prepared from the melt. In that case the observed differences may be related to lower degree of chain entanglement in the samples prepared from solution. The effects of the degree of entanglement on polymer properties enjoys a revival (49).

During the work on LLDPE's reported in this paper, it was observed that the type of stress growth function, η_e^+, depends on the method of sample preparation. In *Fig. 1*, η_e^+ versus time, t, is shown for LLDPE-8 and LLDPE-10. For each polymer, there are two sets of curves indicated by the solid and broken lines. The solid lines represent the results obtained for samples heated at 180°C for 14 min. The broken lines represent samples heated for 40 min. Apparently, during the longer heating, a significant increase of chain entanglement takes place. It is evident that change in the sample preparation procedure affects only the high strain response; the basic stress growth function within

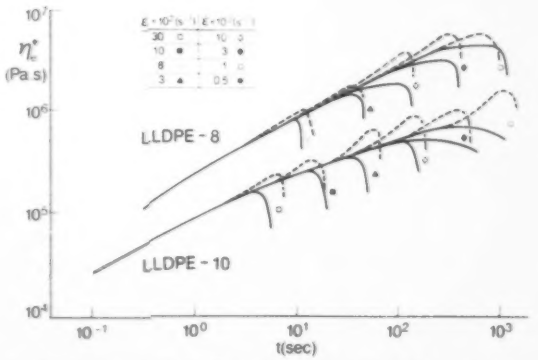

Fig. 1. Stress growth functions in uniaxial extension at 150°C for LLDPE-8 and 10. Solid lines—specimens molded for 14 min, broken lines—for 40 min. The strain rates are indicated.

the range of linear viscoelastic region remains largely unchanged. The high strain behavior depends strongly on the extent of entanglement. It is known that addition of a small amount of LDPE to LLDPE has a pronounced effect on the high strain behavior (46). There is no clear evidence that the longer heating of LLDPE-8 or 10 (see *Fig. 2*) caused any chemical modification, leading to long chain branching (LCB). The SEC as well as the dynamic flow tests of the specimens prepared from the 40 min molded samples did not indicate any change in respect to unmolded material. It is also worth recalling that under nitrogen the dynamic time sweep test indicated that the samples were stable for at least 80 min at 230°C. If LCB was created during prolonged molding, its level was far below the detection limit of SEC or RMS.

The data reported in the following text refer to specimens prepared by transfer molding conducted as follows. The polymer granules were heated for 7 min from ambient temperature to 180°C, then kept at this temperature for another 7 min before transferring the melt to the cavities and cooling under pressure P = 81 (MPa). To anneal, the samples were reheated at a rate 5°C/min back to 180°C and then allowed to slowly cool without excess pressure.

The stress growth functions of LLDPE-1 to 10 are presented in *Fig. 3*, and those of LDPE-102 in *Fig. 4*. The results for LLDPE's are separated into three groups: samples Nos. 1, 2, 4, 5, and 6 forming the lowest group, samples Nos. 3 and 7, the second (the η_e^+ is multiplied by 10), and samples Nos. 8, 9, and 10, the top one (data multiplied by 100). The following observations can be made:

1. LLDPE-2 and 6, copolymers of, respectively, butene (C_4) and hexene (C_6) show nearly identical behavior. Both these samples contained 11.1 co-monomer units per 1000 carbon atoms.

2. LLDPE-3 and 7 are the only ones showing strain hardening.

3. In spite of broad *MWD* ($M_w/M_n \simeq 11.0$), LLDPE-8 to 10 do not show strain hardening.

4. Qualitatively the samples with broader *MWD* show steeper initial slope of the stress growth function:

$$S = d\ln\eta_e^+/d\ln t \qquad (1)$$

In *Fig. 5* the experimental values of S, taken within t = 0.1 to 1 s, are plotted versus M_z/M_n. In spite of the uncertainty in determining both these variables, the correlation is quite evident.

5. The LDPE-102 shows a large strain hardening, quite remarkable considering the relatively low values: M_w = 225 (kg/mol) and M_w/M_n = 4.1.

The stress growth functions in steady state

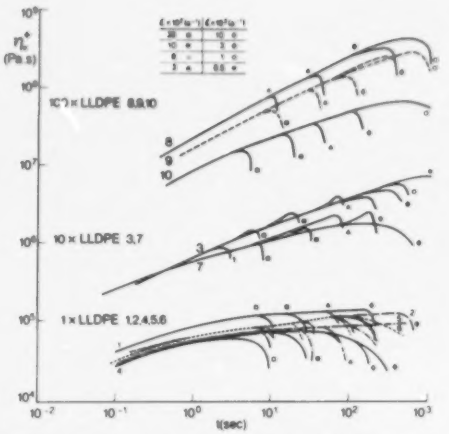

Fig. 3. Summary of the extensional behavior of the ten LLDPE's; top curves—polydispersed LLDPE-8 to 10 (data shifted vertically by two decades), middle curves—LLDPE-3 and 7 with strain hardening effects (data shifted vertically by one decade), bottom curves for the remaining, relatively narrow MWD polymers.

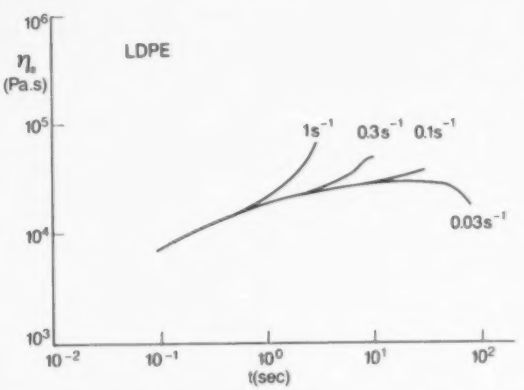

Fig. 4. Stress growth function for LLDPE-102 at 150°C; the strain rates are indicated.

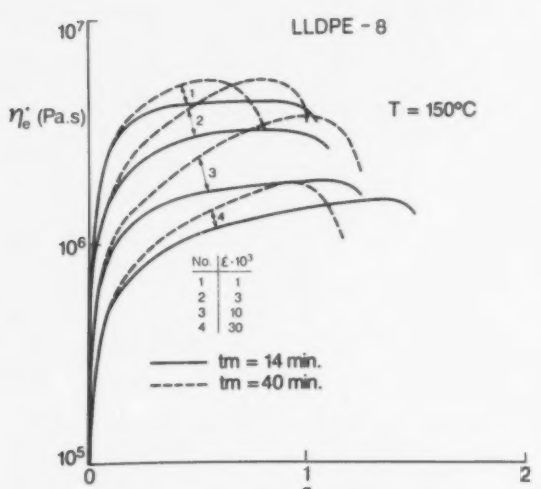

Fig. 2. Effect of molding condition on the stress growth for LLDPE-8; solid and broken lines are for 14 and 40 min molded samples, respectively. Four strain rates were used: $\dot{\epsilon} \times 10^3$ = 1, 3, 10, and 30 (s^{-1}) from top.

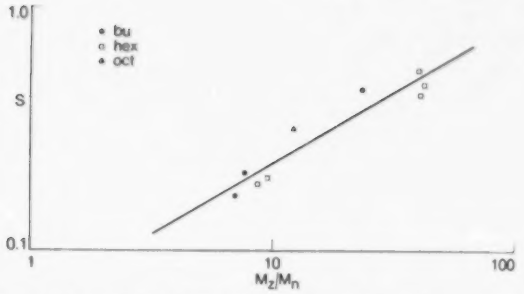

Fig. 5. The initial slope of the stress growth function of LLDPE's versus polydispersity index M_z/M_n.

shear, η^+, and uniaxial extension, η_e^+, for LLDPE-4, 3, and 8 are compared in *Fig. 6*. M_w/M_n of these resins is respectively: 3.3, 6.9, and 11.1. The values of η^+ in the figure are multiplied by three. As it can be seen only for LLDPE-8 a superposition was obtained. For LLDPE-3 and 4 the η_e^+ is systematically larger than $3\eta^+$ by about 10 percent. To confirm veracity of these observations, both instruments, RER and RMS, were thoroughly checked, calibrated, and several sets of samples used. Furthermore, the RMS discs were also prepared from the transfer molded RER specimens. All the tests indicated about 10 percent difference between the shear and extensional stress growth functions.

Three types of the deformation were observed during the extensional flow. They are illustrated in *Fig. 7* for LLDPE-4, 3, and 8. The MW and *MWD* of the samples (1) are: $M_w = 134$, 111, and 256, and $M_z/M_n = 7.7$, 23, and 41, respectively. These are: (i) uniform thinning of specimens leading to large value of the maximum strain at break, $\epsilon_b > 3$, and an equilibrium plateau value of $\eta_e = \eta_e(\dot{\epsilon})$—example, LLDPE-4, (ii) necking, or non-uniform deformation, usually associated with strain hardening within an appropriate range of deformation rates—example, LLDPE-3; and (iii) brittle fracture associated with a severe, sharp necking and localized deformation of the specimen—example LLDPE-8 at the highest rate of straining, $\dot{\epsilon} = 0.3\ s^{-1}$. It should be noted that in all cases at low enough $\dot{\epsilon}$ an equilibrium plateau was obtained. There are no sharp boundaries between the three types of deformation. For all specimens the initial straining seems to be uniform. The necking is associated with the pre-fracture mechanism.

The data in *Fig. 7* also illustrate correlation between the molecular parameters and η_e as well as ϵ_b. It is obvious that η_e of LLDPE-3, 4, and 8 does not depend on M_w. It very well may be that this is rather due to differences in the polymerizing method, but if all these resins are linear as ^{13}CNMR indicates, then η_e should be a function of a certain moment of *MWD*—it is obvious that moment higher than M_w should be used. It is also evident that as *MWD* broadens, ϵ_b decreases. This is also evident from data presented in *Table 1*; there is a linear relation between $\epsilon_b = \epsilon_b$ ($\dot{\epsilon}$ = const) and M_z/M_n obeyed by all LLDPE resins, independently of the co-monomer or the polymerization process. Another interesting aspect illustrated in the Table is the effect of molding time on ϵ_b; it can be seen that increasing the molding time, systematically increases ϵ_b. One could explain this phenomenon by thermal degradation, but as discussed in Part 2 (2) the resins were stable for more than 1 hr even at 230°C (RMS scan under nitrogen). Furthermore, the specimens molded for 40 min show systematically higher values of η_e (see *Fig. 2*), i.e., one could suspect increases in MW and *MWD*, not decreases. It seems that only a change in the level of entangelement may explain this behavior.

The extensional viscosity, η_e, versus rate of straining, $\dot{\epsilon}$, was presented in *Figs. 2* and *3* of Part 2 (2). As the equilibrium value of η_e either the plateau value or the maximum value of the stress growth function was taken. In the past

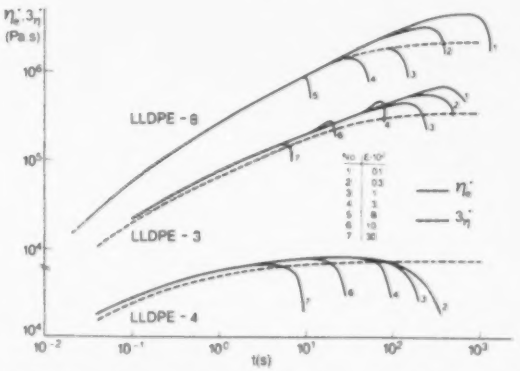

Fig. 6. Comparison between stress growth functions in extension, η_e^+, (solid lines) and shear, η^+ ($\dot{\gamma} = 0.01$), (broken lines), for LLDPE-8, 3, and 4 (from the top) at 150°C. The strain rates are indicated.

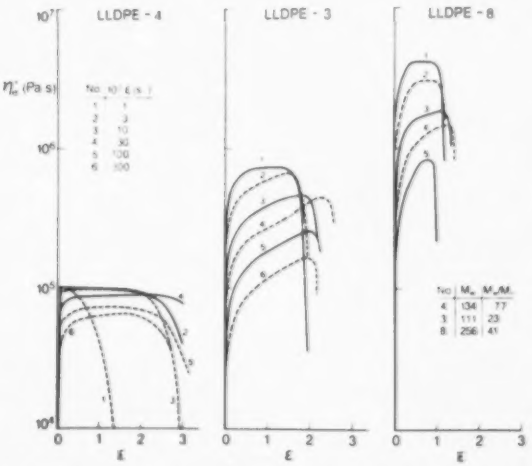

Fig. 7. Illustration of the polydispersity effect on the stress growth functions in uniaxial extension. Data η_e^+ of LLDPE-4, 3, and 8 are plotted versus Hencky strain, ϵ.

Table 1. Molecular Parameters and Maximum Strain at Break for LLDPE.

Property	LLDPE-1	2	3	4	5	6	7	8	9	10
M_w (kg/mol)	150	142	111	134	135	144	127	256	232	180
M_z/M_n	7.8	7.0	23	7.7	9.6	8.7	12	41	42	42
ϵ_b at $\dot{\epsilon}$ = 5E-4										>1.15 —
E-3	>2.20	1.70	1.94	1.31		2.34	0.83 —	1.17 —	>1.35 —	>1.50 (>1.50)
3E-3	>2.69	2.37	1.99	e	2.57	2.92	1.89 (>1.5)	1.19 (1.23)	1.14 (>1.5)	1.66 (1.65)
E-2	2.89	2.97	2.24	e	e	e	2.67 (e)	1.37 (1.49)	1.20 (1.73)	1.61 (1.87)
3E-2	2.99	e	2.57	e	e	e	2.77 (e)	1.40 (1.40)	1.28 (1.66)	1.56 (2.20)
E-1	e	e	2.27	e	e	e	e (e)	1.05 (1.77)	1.40 (1.69)	1.93 (1.98)
3E-1	e	e	2.19	e	e	e	2.71 (e)			1.69 (2.16)
E0	e	e								

e — indicates ϵ_b > 3.0; values in parentheses for samples transfer molded 40 min, the others for the specimens molded in 14 min.

(17–19) it was observed that this assumption is reasonable and the η_e-values determined in that manner coincide with those obtained from the constant stress experiment, in which the steady state is easier to achieve.

It is worth noting that in accord with Trouton's rule on decrease of the rate of deformation, $\omega = \dot{\epsilon} \rightarrow 0$, the dynamic viscosity, η', tends to coincide with $\eta_e/3$. However, for the rule to be obeyed, the deformation rates must be less than 10^{-2} s^{-1}. In *Fig. 3* (2) η_e's of LLDPE-10 molded for 14 and 40 min are shown. The ratio: $\eta_e(40)/\eta_e(14) \simeq 1.9$ was obtained. A smaller ratio of about 1.7 can be calculated for LLDPE-8 from data presented in *Fig. 2*. It is worth recalling that the dynamic viscosity for specimens molded 14 and 40 min was found to be within the usual experimental error of ±2 percent. This means that for the Trouton rule to be obeyed, η_e for samples molded 40 min must decrease on lowering the deformation rates. The zero-deformation rate viscosities were listed in *Table 4* of Part 2 (2).

DISCUSSION

Within the limit of linear viscoelastic behavior, it is expected that the basic stress growth functions $\eta_e^+ = 3\eta^+$. Presence of the non-linearity (e.g., indicated by the broken-line loops in *Fig. 1*) is known as strain hardening (SH). The strain hardening is probably the most important characteristics of the film blowing resins. During the work on this project it was observed that the rheological parameter that best correlated with the "processability index" for pure polyethylenes and their blends was the degree of SH (50). Presence of SH has a "self healing" effect on any local film thinning, thus it improves the bubble stability, allowing to increase the production rate and/or decrease the film thickness. The SH behavior can be observed only at large strains and within a certain range of the rates of straining; at very high rates a brittle fracture can be observed before SH, at too low rates the macromolecules can disentangle during the test.

The SH can best be explained as due to the presence of a transient network structure produced by mechanical entanglement of polymeric chains or transient crosslinks due to strong inter chain interactions, (e.g., $\pi - \pi$ bonding between the aromatic rings in polystyrenes (51)). The fact that the network models predict the SH and in general provide a good description of the rheological behavior of entangled systems (52, 53) can serve as an indirect proof.

The extensional flow data reported in this paper can be summarized as follows:

1. The initial slope of the stress growth function correlates with M_z/M_n as measured by SEC.
2. With exception of LLDPE-3 and 7, the LLDPE's show no strain hardening, even for high MW and broad *MWD*.
3. The theoretically expected equality: $\eta^+ = \eta_e^+/3$ is not always observed.
4. The Trouton rule is obeyed, but there is a poor correlation between $\eta_0 \simeq \eta_{e0}/3$ and M_w (2).
5. There is no difference between melt flow of butene and hexene copolymers.

Koyama and Ishizuka (29) already observed that broadening of *MWD* increases the slope of the stress growth function. However, their observation was qualitative, applied to the magnitude of the ratio $\eta_e^+(t_1)/\eta_e^+(t_2)$, where $t_1 = 100$, $t_2 = 1$ s were taken as constant, independent of polymer system. The empirical correlation presented in *Fig. 5* is quantitative and it refers to the *initial* slope, i.e., it allows for the differences in the inherent relaxation times between samples.

As mentioned before (1, 2) LLDPE-3 is a post-reaction treated sample, whereas LLDPE-7 is the sole representant of the solution resins. All the other polymers were prepared in the fluidized-bed reaction process. The specimens prepared in 14 min molding process do not show any SH. This seems to be in conflict with prior observations by Münstedt and Laun (13) that increase of MW and *MWD* leads to SH even in HDPE. The lack of SH especially for high MW, polydispersed resins LLDPE-8 to 10 is probably the most important observation of this work. It indicates a fundamentally different behavior of the gas-phase polymerized resins.

It is worth recapitulating: (i) SH should be observed for LLDPE-8 to 10, (ii) SH was not

observed for 14 min molded specimens, (iii) SH was observed for 40 min molded specimens, (iv) Increasing the molding time from 14 to 40 min caused increase of η_e by nearly a factor of two, (v) There was no evidence of any chemical difference between 14 and 40 min molded polymers, and (vi) The maximum strain at break increased with molding time. The most plausible explanation for these observations is based on the concept of non-equilibrium entanglement in polymer melts.

Teh, Rudin, and Schreiber (54) observed that the degree of entanglement of LLDPE (as measured by the plateau modulus) systematically increases for as long as 18 hrs at 190°C, but the SEC did not detect any chemical change in the sample.

For polyethylenes the self diffusion coefficient at 200°C is given by (55):

$$D_s(\mathrm{m^2/s}) = 1.367 \times 10^{-10} M_w^{-2} \qquad (2)$$

(M_w expressed in kg/mol). Correcting the equation constant for the temperature difference and substituting M_w's for LLDPE-8 to 10 allows to calculate the diffusion distance of about 30 radii of gyration in 40 min. Considering previous observation (54), it seems that the entanglement process is controlled by much higher moment of the distribution function than M_w.

The reported non-equilibrium, low entanglement in gas phase polymerized LLDPE's may be advantageous in some processes where low level of extrudate swelling is desired (56, 57). However for film blowing, highly entangled melts with SH are required. This means that processors should develop reliable methods of compounding the resins as the first step in film extrusion.

Another observation that should be discussed is the lack of expected equality: $\eta_e^+ = 3\eta^+$ within the linear viscoelastic range of variables. As shown in *Fig. 6*, only for the broad MWD sample LLDPE-8 the equality is obeyed. However, for LLDPE-3 and 9 $\eta_e^+ \simeq 3.3\eta^+$. In the recent paper Leblans *et al.* (52) reported a similar behavior for high density polyethylenes (HDPE), concluding that an extra strain rate dependence of the strain tensor should be postulated.

ACKNOWLEDGMENTS

The stress growth functions in shear have been determined by Mr. P. Sammut. The resins were supplied by Esso Chemical Canada.

NOMENCLATURE

(additional symbols, not used in Parts 1 and 2)

a, b = exponents.
D_s = self diffusion coefficient (m^2/s).
Q = $(M_w/M_n)^a$.
SH = strain hardening.
S = slope, defined by *Eq 1*.
ϵ, ϵ_b = Hencky strain, strain at break.
$\dot{\epsilon}$ = strain rate (1/s).
η_e, η_{e0} = uniaxial extensional viscosity at $\dot{\epsilon}$ and $\dot{\epsilon} \to 0$, respectively (Pa-s).
η_e^+, η^+ = stress growth function in uniaxial extension and shear.
σ_b = extensional stress at break.

REFERENCES

1. B. Schlund and L. A. Utracki, *Polym. Eng. Sci.*, **27**, 359 (1987).
2. L. A. Utracki and B. Schlund, *Polym. Eng. Sci.*, **27**, 367 (1987).
3. C. J. S. Petrie, "Elongational Flows," Pitman, London (1979).
4. J. M. Dealy, "Rheometers for Molten Plastics," Van Nostrand Reinhold Co., N.Y. (1982).
5. J. Meissner, *Ann. Rev. Fluid Mech.*, **17**, 45 (1985).
6. T. H. Kwack and C. D. Han, *J. Appl. Polym. Sci.*, **28**, 3419, 3399 (1983).
7. T. Kanai and J. L. White, *Polym. Eng. Sci.*, **24**, 1185 (1984).
8. F. N. Cogswell, *Plast. Polym.*, **36**, 109 (1968); *Trans. Soc. Rheol.*, **16**, 383 (1972).
9. J. Meissner, *Pure Appl. Chem.*, **42**, 553 (1975).
10. H. H. Winter, *Pure Appl. Chem.*, **55**, 943 (1983).
11. J. L. White, *Pure Appl. Chem.*, in preparation.
12. G. Attalla, G. Corrieri, and D. Romanini, in "Rheology," G. Astarita, G. Marrucci, and L. Nicolais, Eds., Plenum Press, New York, **2**, 407 (1980).
13. H. Münstedt and H. M. Laun, *Rheol. Acta*, **20**, 211 (1981).
14. M. T. Shaw, *Rheol. Acta*, **20**, 231 (1981).
15. H. Münstedt and Middleman, *J. Rheol.*, **25**, 29 (1981).
16. G. Attalla and D. Romanini, *Rheol. Acta*, **22**, 471 (1983).
17. L. A. Utracki and J. Lara, Paper presented at the "Table ronde internation. Ecoulement élongationnels," La Bresse, France, Jan. 23–28, 1983.
18. L. A. Utracki, A. M. Catani, J. Lara, and M. R. Kamal, Proceedings of European Meeting on Polymer Processing and Properties, Capri, Italy, June 13–16, 1983.
19. L. A. Utracki, *Adv. Polym. Technol.*, **5**, 41 (1985).
20. T. Raible and J. Meissner, in "Rheology," G. Astarita, G. Marrucci, and L. Nicolais, Eds., Plenum Press, New York, **2**, 425 (1980).
21. H. M. Laun, ibid., **2**, 419 (1980).
22. H. Münstedt, ibid., **2**, 413 (1980).
23. A. V. Prokunin, *Intern. J. Polym. Mater.*, **8**, 303 (1980).
24. T. Raible, S. E. Stephenson, J. Meissner, and M. H. Wagner, *J. Non-Newt. Fluid Mech.*, **11**, 239 (1982).
25. K. Koyama and O. Ishizuku, *Polym. Process. Eng.*, **1**, 55 (1983).
26. A. I. Leonov and A. N. Prokunin, *Rheol. Acta*, **22**, 137 (1983).
27. S. A. Montes, *Polym. Eng. Sci.*, **24**, 259 (1984).
28. A. Garcia-Rejon, J. M. Dealy, and M. R. Kamal, *Can. J. Chem. Eng.*, **59**, 76 (1981).
29. K. Koyama and O. Ishizuka, *Sen-i Gakkaishi*, **38**, 41 (1982).
30. F. P. La Mantia and D. Acierno, *Polym. Eng. Sci.*, **25**, 279 (1985).
31. G. Attala and F. Bertinotti, *J. Appl. Polym. Sci.*, **28**, 3503 (1983).
32. D. Constantin, *Polym. Eng. Sci.*, **24**, 268 (1984).
33. M. M. Dumoulin, L. A. Utracki, and J. Lara, NRCC/IMRI mini-symposium, "Polyblends-'83," Montreal, Que., Canada, April 12, 1983; *Polym. Eng. Sci.*, **24**, 117 (1984).
34. L. A. Utracki, M. R. Kamal, and N. M. Al-Bastaki; *SPE ANTEC Tech. Papers*, **30**, 417 (1984).
35. M. M. Dumoulin, L. A. Utracki, and C. Farha; *SPE ANTEC Tech. Papers*, **30**, 443 (1984).
36. M. M. Dumoulin, C. Farha, and L. A. Utracki, NRCC/IMRI mini-symposium, "Polymer Blends-'84," Boucherville, Que., Canada, April 17, 1984; *Polym. Eng. Sci.*, **24**, 1319 (1984).

37. M. M. Dumoulin and L. A. Utracki, CSChE Meeting, Quebec, Que., Canada, Sept. 30–Oct. 3, 1984.
38. L. A. Utracki, Proceedings, 1984—International Chemical Congress of Pacific Basin Societies, Honolulu, Hawaii, USA, Dec. 16–21, 1984.
39. L. A. Utracki, 9th Intl. Congr. Rheology, Acapulco, Mexico, Oct. 8–13, 1984; "Advances in Rheology," B. Mena, A. Garcia-Rejon, and C. Rangel-Nafaile, Eds., Univ. Natl. Aut. Mexico Press, **3**, 567 (1984).
40. J. Nancekivell, *Can. Plast.*, **27**, Sept. 1985.
41. H. Münstedt, *J. Rheol.*, **23**, 421 (1979).
42. V. S. Au-Yeung and C. W. Macosko, *Mod. Plast.*, **58**, 84 (1981); in "Rheology," G. Astarita, G. Marrucci, and L. Nicolais, Eds., Plenum Press, New York, **3**, 717 (1980); *J. Rheol.*, **25**, 445 (1981).
43. I. K. Park and D. W. Riley, *J. Macromol. Sci.-Phys.*, **B20**, 277 (1981).
44. L. A. Utracki and J. Lara, NRCC/IMRI mini-symposium "Composites-'82," Montreal, Que., Canada, Nov. 30, 1982; *Polym. Compos.*, **5**, 44 (1984).
45. M. R. Kamal, A. T. Mutel, and L. A. Utracki, *Polym. Compos.*, **5**, 289 (1984).
46. L. A. Utracki, *Rubber Chem. Technol.*, **57**, 507 (1984).
47. M. K. Kurbanaliev, G. V. Vinogradov, V. E. Dreval, and A. Ya. Malkin, *Polymer*, **23**, 100 (1982).
48. K. Koyama and O. Ishizuka, *Polym. J.*, **12**, 735 (1980).
49. e.g., A. Rudin and H. P. Schreiber, *Polym. Eng. Sci.*, **23**, 422 (1983)
50. A. A. Alim, private communication (1985).
51. V. D. Fikhman, B. V. Radushkievich, and G. V. Vinogradov, *Mekh. Polim.*, **6**, 1104 (1972).
52. P. J. R. Leblans, J. Sampers, and H. C. Booij, *J. Non-Newt. Fluid Mech.*, **19**, 185 (1985).
53. R. K. Upadhyay and A. I. Isayev, *Rheol. Acta*, **22**, 557 (1983).
54. J. W. Teh, A. Rudin, and H. P. Schreiber, *Plast. Rubb. Proc. Appl.*, **4**, 149, 157 (1984).
55. G. Fleischer, *Macromol. Chem., Rapid Commun.*, **6**, 463 (1985).
56. B. Maxwell and A. Breckwoldt, *J. Rheol.*, **25**, 55 (1981).
57. M. Rokudai and T. Fujiki, in "Contemporary Topics in Polymer Science," W. J. Bailey, and I. Tsurutu, Eds., Plenum Publ. Corp., New York, **4**, 245 (1984).

Society of Plastics Engineers

Executive Office, 14 Fairfield Drive, Brookfield Center, CT 06805, U.S.A.
(203) 775-0471
Telex No. 643-712

MEMBERSHIP APPLICATION

I am applying for:

- ☐ Membership
- ☐ Reclassification (no charge)
- ☐ Reinstatement (initiation fee not required)

NAME: _____
First Middle Last

DATE OF BIRTH: _____
Month Day Year

ADDRESS:
Fill in both addresses and check your preferred mailing address.

☐ **COMPANY** (spell out name)

_____

_____

_____

City State (Prov.) Zip

POSITION: _____

☐ **HOME** _____

_____

City State (Prov.) Zip

Job Function
What is the *primary* end product manufactured or service performed at your company location?

Please Check your Primary job function (check one only)
- ____ 01 Production or Manufacturing Engineering
- ____ 02 Design or Design Engineering
- ____ 03 Purchasing
- ____ 04 Sales or Marketing
- ____ 05 Research or Development Engineering
- ____ 06 General or Corporate Management
- ____ 07 Other (Specify)

DIVISIONS
My free primary Division choice is _____
check (✓) others below as secondary Divisions (cost -$4 each)

- ____ 21 Color and Appearance
- ____ 22 Extrusion
- ____ 23 Injection Molding
- ____ 24 Electrical and Electronic
- ____ 25 Thermoforming
- ____ 26 Engineering Properties and Structure
- ____ 27 Vinyl Plastics
- ____ 28 Thermoset
- ____ 29 Thermoplastics Materials & Foams (Nonvinyl)
- ____ 30 Blow Molding
- ____ 31 Plastics in Automotive
- ____ 33 Plastics Analysis
- ____ 34 Decorating
- ____ 35 Moldmaking and Mold Design
- ____ 36 Medical Plastics
- ____ 37 Marketing (in formation)
- ____ 38 Polymer Modifiers & Additives (in formation)

Grade	Requirements
Senior Member	Minimum of twelve (12) experience credits and current continuous membership in the Society for a minimum of two (2) years.
Member	Minimum of six (6) experience credits.
Affiliate Member	Less than six (6) experience credits.
Student Member	Regularly enrolled FULL-TIME student in a course of study in plastics.

Check below the membership grade for which you believe details of your experience in plastics qualifies you (see grades above).

☐ Student Member ☐ Member
☐ Affiliate Member ☐ Senior Member

Statement of Fees (U.S. FUNDS ONLY)
MEMBERSHIP YEAR: 7/1 thru 6/30

$10.00 INITIATION FEE MUST BE ATTACHED IN ORDER TO PROCESS YOUR APPLICATION. INITIATION FEE IS SEPARATE FROM ANNUAL DUES.

- **SENIOR MEMBER, MEMBER, AFFILIATE**
  Annual Dues: 7/1-6/30 $55.00
  If joining after 12/31 $27.50
  If joining after 4/1 $10.00 (initiation fee only)
- **STUDENT MEMBER**
  Annual Dues: whenever joining $14.00 (no initiation fee/ not pro-rated)
- **REINSTATED MEMBER**
  Annual Dues: whenever reinstated $55.00 (no initiation fee/ not pro-rated)

I wish to join the _____ Section.

REFERENCES The Bylaws require the names of three references who are familiar with your work. One of them should be a member of the Society. Assistance in providing member-references will be given on request. Signatures are not necessary.

1. (Member-Sponsor) _____
2. _____
3. _____

STATEMENT OF COLLEGE WORK

Years attended From	Years attended To	Institution	Major	Degree	Education Credits

RECORD OF QUALIFYING EXPERIENCE IN PLASTICS

DATES From Mo.	DATES From Yr.	DATES To Mo.	DATES To Yr.	Give your title, name and location of employer. List in chronological order. Describe duties fully and state any important engineering work you have done in each position. If space is not sufficient, use separate sheet.	Time in years (a)	% in plastics (b)	Qualifying experience (a x b)
					yrs./mo.		yrs./mo.
						SUB-TOTAL	

Total education and experience credits. ▶

I certify that the statements made in this application are correct. I agree, if elected, to be governed by the Constitution and Bylaws of the Society and to promote the objectives of the Society.

_____
Signature in ink. Date

CREDENTIALS COMMITTEE APPROVAL ONLY	Approved Grade
(S)	Date
(S)	Date

Office use only:	Division
ID#	Job Class
Grade	Date Elected
Section	

If applying for Member or Senior Member, please complete *in detail:*

STATEMENT OF COLLEGE WORK

Years attended		Institution	Major	Degree	Experience Credits (see notes below)
From	To				

RECORD OF QUALIFYING EXPERIENCE IN PLASTICS

DATES				Give your title, name and location of employer. List in chronological order. Describe duties fully and state any important engineering work you have done in each position. If space is not sufficient, use separate sheet.	Time in years (a)	% in plastics (b)	Qualifying experience (a × b)
From		To					
Mo.	Yr.	Mo.	Yr.				
					yrs./mo.		yrs./mo.
						SUB-TOTAL	
						Total education and experience credits. ▶	

Grade	Requirements
Senior Member	Minimum of twelve (12) experience credits and current continuous membership in the Society for a minimum of two (2) years.
Member	Minimum of six (6) experience credits.
Affiliate Member	Less than six (6) experience credits.
Student Member	Regularly enrolled FULL-TIME student in a course of study in plastics.

CREDENTIALS COMMITTEE APPROVAL ONLY		Approved Grade
(S)	Date	
(S)	Date	

Experience Credits
Grade of Membership . . .

Membership grades are based on experience credits which are earned as follows:

1. **Experience credits earned for education.**
   Maximum credits allowable for education shall be six (6). Use highest degree credits ONLY.

Doctorate in science or engineering	**6 credits**
Masters in science or engineering	**5 credits**
Bachelors in science or engineering	**4 credits**
Any degree other than above	**2 credits**
Associate or Adjunct in Plastics	**2 credits**
Associate or Adjunct (awarded by Community College or equivalent for two-year course of studies, without specializing in plastics).	**1 credit**

When filling in the "Statement of College Work" above, place the corresponding number of credits earned in the right-hand column.

2. **Experience credits** are determined by the proportion of time involved in actual technical and engineering duties in plastics for each position held. For instance, if only three of the five years you worked for the XYZ Co. comprised technical or engineering duties, then three (3) years (60% of 5 yrs.) would constitute the "Qualifying Experience" you would enter in years and months in the right-hand column under "Record of Qualifying Experience in Plastics."

   Please detail carefully the engineering skill required for each position to help the Credentials Committee judge experience as "qualifying."

When you have determined the number of credits which you believe you have earned, consult the following member grade requirements. Indicate on the reverse side the grade of membership for which you believe you are qualified.

INFORMATION FOR AUTHORS

Submission of original and review articles is encouraged. There is no limit on length. Three copies of the manuscript should be submitted, which should be typed, one side only, double space, with at least a 1-inch margin. Submission will be taken to imply that the paper has not been previously published, that it is not being considered elsewhere for publication, and that if accepted it will not be published elsewhere in the same form, in any language, without the consent of the editor or publisher. Authors must agree to transfer copyright to the publisher when an article is accepted for publication. Unless notified to the contrary by the authors, the publisher assumes that the act of submitting the article signifies the authors' agreement to such copyright transfer to the publisher. The journal carries a voluntary page charge. Each manuscript should include:

A separate title page, headed by a concise, meaningful title (avoid abbreviations) for the paper. This page should provide:

- The name and affiliations of each contributing author at the time the paper was prepared.
- Indicate by asterisk any changes of address for each author since article preparation.
- Acknowledgment of any prior oral presentation and original source of the material.

A separate abstract page, consisting of a single paragraph of 100–200 words to include the title and the names and addresses of the authors. Define any abbreviations for substances or methods (such as ABS, SAXS, etc.).

A list of references, on a separate page at the end of the text, numbered in order of text citation. The references are to be abbreviated in the form used in Chemical Abstracts using the names of all authors preceded by initials; see Bibliographic Guide for Editors and Authors, American Chemical Society, Washington, D.C.

- Within the text, the reference citations are typed in parentheses in line with the main copy (no superscripts or subscripts), thus:

  According to Young, et al. (1)...

- In the list of references the general style is as follows:

  For periodicals:

  1. S. S. Young, J. L. White, E. S. Clark and Y. Oyanogi, *Polym. Eng. Sci.*, 20, 798 (1980).

  The journal name and volume are to be underlined and the year is placed in brackets. The issue number is given only when needed for identification. The article name is eliminated unless the reference is unclear without it.

  For books: The title to be spelled out in full.
  5. H.-G. Elias, "Macromolecules," Ch. 1, Vol. 2, Plenum Press, New York (1977). (Include the state when the city is not identifiable.)

A list of nomenclature, identifying symbols and abbreviations, commonly desirable at the end of the text. Footnotes are to be avoided.

Equations, numbered and typed in the appropriate place in the text. Where symbols cannot be typed, write them neatly in ink.

Tables, each typed on a separate page, with a heading, and numbered with arabic numerals that correspond to the order in which they are cited in the text. The tables should be inserted in the manuscript after the references and before the figures.

Figures, assembled at the end of the manuscript and preceded by a typed list of captions that explain them. Please also supply a set of original figures or sharp glossy photos thereof, on 8½ × 11 paper or attached to sheets of this size, one sheet for each figure. Each should be identified on the front edge or on the back (photographs) with the name of the first author and the figure number (e.g., Smith, Fig. 1). Originals are to be prepared with high contrast India ink and to bear uniformly stencilled notations. Line drawings and photos should be of a quality suitable for good photographic reproduction and retained legibility upon size reduction to one quarter. Manuscript transmittal letter should indicate if the figures need be returned.

Send manuscripts to:
Roger S. Porter, Editor
POLYMER ENGINEERING AND SCIENCE
% Polymer Science & Engineering
University of Massachusetts
Amherst, Massachusetts 01003

For information concerning publication dates, page charges and reprint orders contact:
Editorial Dept.
Society of Plastics Engineers
14 Fairfield Drive
Brookfield Center, Connecticut 06805